

EFFECTS OF NORMAL PRESSURE AND VELOCITY ON ICE-ICE FRICTION

by

© Zhong Wu

A Thesis submitted to the

School of Graduate Studies

in partial fulfillment of the requirements for the degree of

Masters of Ocean and Naval Architectural Engineering

Faculty of Engineering and Applied Sciences

Memorial University of Newfoundland

October 2015

St John's Newfoundland and Labrador

Abstract

Improved knowledge of ice friction influences on vessels and offshore structures is desirable when we seek to optimize designs by reducing the forces applied by impinging ice. Friction is known to be important in terms of the overall load experienced by ships or offshore structures. This includes both the direct friction between ice and structure and the friction between ice pieces themselves as they move around the structure. Traditionally, a friction coefficient is considered to be independent of velocity, pressure and temperature; however, the friction of ice has been widely studied and is known to be highly variable. Numerous tests have been performed by researchers to investigate the friction between ice and various materials such as steel, concrete and other materials under various conditions. The result shows that ice friction coefficient is not generally constant when sliding velocity, pressure and temperature change. Much is still not known about ice's frictional properties. Relatively few studies have considered the friction of ice on ice, despite the fact that this is an important factor when considering the relative movement of pack ice when it impinges on a fixed or floating structure. The ice-ice friction influences the movement of ice pieces relative to each other as pack ice "flows" around a structure and this in turn influences the load on the structure. This study examines the effect of friction of ice against ice under relatively high pressures such as those that might be experienced during full scale interactions. The objective of the study is to quantify the effects of temperature, pressure, velocity and other parameters on the ice-ice friction coefficient.

Acknowledgements

I would like to thank my supervisor Professor Bruce Colbourne, Faculty of Ocean and Naval Architectural Engineering, Memorial University of Newfoundland; thanks for his excellent supervision though the whole period of this study. Thanks also to the Research & Development Corporation of Newfoundland and Labrador for their financial support.

Table of Contents

Abstract	ii
Acknowledgements	iii
Table of Contents	iv
List of Tables	viii
List of Figures	ix
List of Abbreviations and Symbols	xviii
Chapter 1 INTRODUCTION	1
1.1 Research objective	2
1.2 Outline of Thesis Structure	2
Chapter 2 LITERATURE REVIEW	3
2.1 Ice Friction Coefficient	3
2.1.1 The properties of ice	3
2.2 Theories of Ice Frictional Lubrication	6
2.2.1 Pressure melting	7
2.2.2 Frictional heating	7
2.2.3 Disordered surface layer	8
2.3 Factors that Affect Ice Friction.....	10
2.3.1 Temperature	11
2.3.2 Velocity	16

2.3.3 Normal pressure.....	22
2.3.4 Other factors	25
2.4 Experimental Methods	26
2.4.1 Real-life experiments.....	27
2.4.2 Sliding model.....	27
2.4.3 Linear experimental devices.....	27
2.4.4 Rotational experimental devices.....	28
2.5 Testing Materials	28
2.6 Ice-ice friction study	32
2.7 Review Summary	40
Chapter 3 EXPERIMENTAL SETUP AND PREPARATIONS	41
3.1 Apparatus Choice	41
3.1.1 The Turntable.....	43
3.1.2 The Flat Circular Plate.....	44
3.1.3 The Normal force apparatus	45
3.1.4 Data Acquisition and Control System	48
3.2 Ice Sample Preparation	49
3.2.1 Water preparation.....	49
3.2.2 Making ice seeds	50
3.2.3 Mixing and Freezing the Ice.....	52
3.2.4 Sample Shaping	54
3.3 Ice plate preparation.....	55

3.3.1	Mixing and freezing the ice	55
3.3.2	Ice plate surface smoothing	55
Chapter 4	EXPERIMENTAL METHOD	57
4.1	Factors Studied	57
4.1.1	Velocity	57
4.1.2	Normal force	57
4.1.3	Tests with Changing Normal Force	58
4.2	Experimental Design	58
4.3	Testing Procedures	61
4.4	Calculations	63
4.4.1	Conversion of DAC output	63
4.4.2	Ice loss weight	64
4.4.3	Extra mass calculation	65
4.4.4	Ice sample's real normal force	65
4.4.5	Ice sample friction coefficient	66
4.4.6	Rotational velocity conversion	66
Chapter 5	RESULTS	68
5.1	Smoothing method	68
5.2	Plotting of the results	71
5.2.1	Deriving Significant Parameters	74
5.2.2	Constant force tests	81
5.2.3	Changing normal force tests	84

5.3 Summary	86
Chapter 6 DISCUSSION AND ANALYSIS	88
6.1 Plotting of Significant Parameters	89
6.1.1 Slope of the coefficient change	89
6.1.2 Peak friction coefficient.....	92
6.1.3 Settled friction coefficient	94
6.2 Mechanisms.....	96
6.3 Analysis in Design Expert.....	98
6.3.1 Diagnostics	99
6.3.2 Effects and interactions	105
6.4 Summary	115
Chapter 7 CONCLUSIONS	116
7.1 Experimental Error.....	116
7.2 Future Study.....	117
REFERENCES	119

List of Tables

Table 2.1: Test conditions with respect to temperature.	12
Table 2.2: Test conditions with respect to velocity.....	16
Table 2.3: Test conditions with respect to normal pressure.....	23
Table 4.1: Test plan.....	59
Table 5.1: The value of three derived parameters for all the tests.....	78
Table 6.1: Three sections of test correspond with parameters and assumed mechanisms.....	88

List of Figures

Figure 2.1: The structure of H₂O molecules. (From Wikipedia: http://en.wikipedia.org/wiki/Bent_molecular_geometry).....4

Figure 2.2: Phase diagram of H₂O. (Rosenberg, 2005).....5

Figure 2.3: Crystal structure of hexagonal ice. Gray dashed lines indicate hydrogen bonds. (From Wikipedia: http://en.wikipedia.org/wiki/Hydrogen_bond)6

Figure 2.4: Heating of the track behind the slider, Infrared image. (Bäurle et al, 2006)8

Figure 2.5: Surface structure of ice. (Li and Somorjai, 2007)9

Figure 2.6: Three bilayers of water ice viewed from the [001] direction, where the oxygen sub-lattice is depicted by creating bonds between oxygen atoms within 3.0 Å of one another. The external bilayer is in blue, the second bilayer is shown in red and the third bilayer towards the center of the crystal slab is shown in green. a) 250°K b)285°K (Bishop et al., 2009)..... 10

Figure 2.7: Effect of temperature on the friction coefficient using various materials. (Albracht et al., 2004) 13

Figure 2.8: Influence of temperature on the static friction of real ski. ○, ski lacquer; ●, P. T. F. E.; △, Swiss wax; ▼, paraffin wax; ■, Norwegian wax (Bowden, 1953)..... 13

Figure 2.9: The variation of coefficient of friction with air temperature for various rod materials. Velocity 3.16 m/s, total normal load is 45.4 N. △ copper rods; ■ Perspex rods; ○ mild steel rods. (Evans et al., 1976) 14

Figure 2.10: Friction coefficient vs. temperature in a velocity range of $v = 3\text{--}5$ m/s and a load range of $F_n = 52$ N to 84 N, summarized and plotted for three different apparent contact areas. (Baurle et al., 2006).....	14
Figure 2.11: Dependence of friction on temperature. ●, (01T0) single crystal ice; ○, (0001) single crystal ice. (Tusima, 1977).....	15
Figure 2.12: Temperature dependence of ice–ice friction coefficient at different sliding velocities. The normal pressure is 2.9 kPa. (Yasutome et al., 1999).....	15
Figure 2.13: The variation of coefficient of friction with velocity for various rod materials and the curved skate. Air temperature - 11.5 C; total normal load (4L) is 45.4 N. △ copper rods; ■ Perspex rods; ○ mild steel rods; × mild steel skate. (Evans et al., 1976)	17
Figure 2.14: Effect of sliding velocity on the coefficient of friction of stainless steel at different normal forces. (Albracht et al., 2004)	18
Figure 2.15: Comparison of friction coefficient as a function of speed for decreasing and increasing speed test on corroded steel sample. Mu, curve of a function of friction coefficient fit to the relations between speed and friction coefficient. (Frederking and Barken, 2002).....	18
Figure 2.16: Average value of friction coefficient as a function of speed, 65 kPa, -10° C. #1, smooth concrete; #2, painted steel; #3, corroded steel; #4, wood; #5, ice. (Frederking and Barken, 2001).....	19
Figure 2.17: Effect of speed on average friction coefficient. #1, smooth concrete. (Frederking and Barken, 2001).....	19

Figure 2.18: Dependence of friction coefficient on velocity at $T_{\text{air}} = -10\text{ }^{\circ}\text{C}$ and $F_n = 84\text{ N}$ for two different apparent contact areas. (Bäurle et al., 2006).....	20
Figure 2.19: Dependence of friction coefficient on velocity at temperatures close to the melting point (wet conditions) for $F_n = 52\text{ N}$ and $A_{\text{app}} = 10\text{ cm}^2$. (Bäurle et al., 2006)	20
Figure 2.20: Dependence of (a) friction on velocity, and (b) the width of a sliding track against load. (Tusima, 1977).....	21
Figure 2.21: Ice–ice friction coefficient plotted against the sliding velocity at different temperatures (in $^{\circ}\text{C}$). Normal stress is 2.9 KPa. (Yasutome et al., 1999)	21
Figure 2.22: The dependence of steady-state ice-ice sliding friction on slip rate. (Lishman et al., 2009)	22
Figure 2.23: Effect of normal force on the coefficient of friction of stainless steel at different temperatures. (Albracht et al., 2004).....	24
Figure 2.24: Normal stress dependence of ice–ice friction coefficient above -5°C . Sliding velocity is $4.5 \times 10^{-2}\text{ m/s}$. (Mizukami and Maeno, 2000).....	24
Figure 2.25: Normal stress dependence of ice–ice friction coefficient below -5°C . Sliding velocity is $4.5 \times 10^{-2}\text{ m/s}$. (Mizukami and Maeno, 2000).....	25
Figure 2.26: Ice friction curves for different materials. (Kietzig et al, 2010b).....	26
Figure 2.27: Thin section photographs showing the structure of several common ice types: (a) fine-grained granular ice; (b) freshwater columnar ice, showing a fine-grained seed layer at the top, transitioning into a columnar growth with increasing grain size; (c) frazil ice; (d) aligned sea ice. Scale bars are 50 mm. (Cole, 2000).....	29
Figure 2.28: Thin section of first-year ice showing the ice platelets and the brine pockets along the grain boundaries. (Timco and Weeks, 2010).....	31

Figure 2.29: Vertical thin section of multi-year ice. Note the relative absence of the salt pockets and the large variation in grain structure. (Timco and Weeks, 2010)	31
Figure 2.30: (a) Intermittent crushing with ice thickness 0.2 m and drift speed 0.05 m/s occurring 12:06:39, 30 March 2003, (b) Continuous crushing with ice thickness 0.5-0.6 m and drift speed 0.35 m/s occurring 21:23:02, 19 March 2003. (Bjerkas, 2006)	32
Figure 2.31: Example of the icebreaking pattern. (above) Observed icebreaking pattern in Aalto ice tank in Feb., 2012. (Photograph by X. Tan). (below) Simulated icebreaking pattern. (Tan, Riska and Moan, 2014).....	34
Figure 2.32: Summary of ice–ice friction coefficients vs. sliding velocity. (Maeno et al, 2003)	35
Figure 2.33: Coefficients of kinetic friction versus sliding velocity of freshwater granular ice at -10°C for nominal contact pressures of 0.007, 0.02 and 0.045 MPa (Kennedy, Schulson, and Jones, 2000).	37
Figure 2.34: Normal stress dependence of ice–ice friction coefficient above -5°C. Sliding velocity is 4.5×10^{-2} m/s. (Mizukami and Maeno, 2000)	38
Figure 2.35: Normal stress dependence of ice–ice friction coefficient below -5°C. Sliding velocity is 4.5×10^{-2} m/s. (Mizukami and Maeno, 2000).....	38
Figure 2.36: Curves shear force F_f versus displacement u for each temperature-velocity combination under an applied normal stress of $\sigma_n = 60$ kPa. The origin is (0,0). The scales, shown in the top left-hand panel, are the same for each curve. The arrow on the curve at $223 \text{ }^\circ\text{K}/5 \times 10^{-8} \text{ m s}^{-1}$ means that the load was removed before sliding was initiated. The oscillations indicate stick-slip behavior.	39

Figure 3.1: Experimental setup including: the bucket, the designed apparatus, ice sample and the ice plate.....	42
Figure 3.2: Sample pressed by the bucket against the ice plate.	43
Figure 3.3: Turntable arm and pin. (Dagenais, 2013)	44
Figure 3.4: Device attach to the turntable. (Dagenais, 2013).....	46
Figure 3.5: Device attachment. (Dagenais, 2013).....	47
Figure 3.6: Bottom part of setup including fork-shaped part (red circle) and L-shaped part (purple circle). (Dagenais, 2013)	47
Figure 3.7: Bottom setup holding an ice sample with bearing 2 (red circle) and sensor (green circle). (Dagenais, 2013).....	48
Figure 3.8: Data Acquisition and Control System. (Dagenais, 2013).....	48
Figure 3.9: Thin section of conical ice sample. (Dragt, 2013).....	49
Figure 3.10: Chipped ice prior to sieving. (Manuel, 2012).....	51
Figure 3.11: Chipped ice after sieving. (Manuel, 2012)	51
Figure 3.12: Prepared bucket. (Manuel, 2012)	52
Figure 3.13: Modified freezer cover with insulators. (Manuel, 2012).....	52
Figure 3.14: Side view of modified freezer cover and insulators (circled in red). (Manuel, 2012)	53
Figure 3.15: Bucket filled with ice seeds. (Manuel, 2012)	53
Figure 3.16: Water pouring into the bucket filled with ice seeds. (Manuel, 2012).....	54
Figure 3.17: Shaper including jack (circled in red), blade (circled in black), ice sample (circled in green) and plug (circled in orange). (Manuel, 2012).....	54
Figure 3.18: Prepared Ice Plate and Ice Sample Ready for testing.	56

Figure 4.1: Video ice contact diameter and video ice diameter.	64
Figure 4.2: Radiuses for Different Velocity Level. (Dagenais, 2013).....	67
Figure 5.1: Raw data plotting of test 9.	68
Figure 5.2: Raw data plotting of test 31.	69
Figure 5.3: Smoothed raw data plotting of test 9.	70
Figure 5.4: Smoothed raw data plotting of test 31.	70
Figure 5.5: Ice cone of test 29 at 45s (Peak stage).....	72
Figure 5.6: Ice cone of test 29 at 270s (Steady state stage).	73
Figure 5.7: Sequence picture of test 29 around peak stage.	73
Figure 5.8: The initial stage of test 9.....	75
Figure 5.9: Slope of changing fitted with a line (in blue)	76
Figure 5.10: General case of deriving Peak FC and Settled FC.....	77
Figure 5.11: Deriving of settled FC for one of irregular cases.....	78
Figure 5.12: FC of 454N normal force tests. Green, low velocity (0.47m/s); red, medium velocity (0.63m/s); blue, high velocity (0.8m/s).....	82
Figure 5.13: FC of 908N normal force tests. Green, low velocity (0.47m/s); red, medium velocity (0.63m/s); blue, high velocity (0.8m/s).....	82
Figure 5.14: FC of 1362N normal force tests. Green, low velocity (0.47m/s); red, medium velocity (0.63m/s); blue, high velocity (0.8m/s).....	83
Figure 5.15: FC of 1816N normal force tests. Green, low velocity (0.47m/s); red, medium velocity (0.63m/s); blue, high velocity (0.8m/s).....	83
Figure 5.16: FC of 454N normal force tests. Green, low velocity (0.47m/s); red, medium velocity (0.63m/s); blue, high velocity (0.8m/s).....	84

Figure 5.17: FC of 908N normal force tests. Green, low velocity (0.47m/s); red, medium velocity (0.63m/s); blue, high velocity (0.8m/s).....85

Figure 5.18: FC of 1362N normal force tests. Green, low velocity (0.47m/s); red, medium velocity (0.63m/s); blue, high velocity (0.8m/s).....85

Figure 5.19: FC of 1816N normal force tests. Green, low velocity (0.47m/s); red, medium velocity (0.63m/s); blue, high velocity (0.8m/s).....86

Figure 6.1: Slope of changing plotted against initial normal force. Green, low velocity (0.47m/s); red, medium velocity (0.63m/s); blue, high velocity (0.8m/s). Dots connected by a dashed line indicate changing normal force tests and dots connected by solid line indicate constant normal force tests.90

Figure 6.2: Slope of changing plotted against velocity. Green, 454N initial normal force; red, 908N initial normal force; blue, 1362N initial normal force; black, 1816N initial normal force. Dots connected by a dashed line indicate changing normal force tests and dots connected by solid line indicate constant normal force tests.91

Figure 6.3: Peak friction coefficient plotted against initial normal force. Green, low velocity (0.47m/s); red, medium velocity (0.63m/s); blue, high velocity (0.8m/s). Dots connected by a dashed line indicate changing normal force tests and dots connected by solid line indicate constant normal force tests.92

Figure 6.4: Peak friction coefficient plotted against velocity. Green, 454N initial normal force; red, 908N initial normal force; blue, 1362N initial normal force; black, 1816N initial normal force. Dots connected by a dashed line indicate changing normal force tests and dots connected by solid line indicate constant normal force tests.....93

Figure 6.5: Settled friction coefficient plotted against initial normal force. Green, low velocity (0.47m/s); red, medium velocity (0.63m/s); blue, high velocity (0.8m/s). Dots connected by a dashed line indicate changing normal force tests and dots connected by solid line indicate constant normal force tests.94

Figure 6.6: Settled friction coefficient plotted against velocity. Green, 454N initial normal force; red, 908N initial normal force; blue, 1362N initial normal force; black, 1816N initial normal force. Dots connected by a dashed line indicate changing normal force tests and dots connected by solid line indicate constant normal force tests.95

Figure 6.7: Ice plate after testing. Ice chips beside the sliding track in red rectangle.97

Figure 6.8: Close picture of the red rectangle in Figure 82.97

Figure 6.9: Residuals vs. run plot for Changing slope. Different colors indicate different tests.99

Figure 6.10: Residuals vs. run plot for Peak FC. Different colors indicate different tests.100

Figure 6.11: Residuals vs. run plot for Settled FC. Different colors indicate different tests.100

Figure 6.12: Normal plot of residuals for changing slope. Different colors indicate different tests.101

Figure 6.13: Normal plot of residuals for Peak FC. Different colors indicate different tests.102

Figure 6.14: Normal plot of residuals for Settled FC. Different colors indicate different tests.102

Figure 6.15: Residuals vs. predicted plot for changing slope. Different colors indicate different tests.....	103
Figure 6.16: Residuals vs. predicted plot for Peak FC. Different colors indicate different tests.	104
Figure 6.17: Residuals vs. predicted plot for Settled FC. Different colors indicate different tests.....	104
Figure 6.18: Half-normal plot for Peak FC.....	106
Figure 6.19: ANOVA table for Peak FC.....	107
Figure 6.20: Interaction between velocity and normal force on Peak FC. Red, low velocity (0.47m/s); green, medium velocity (0.63m/s); blue, high velocity (0.8m/s).	108
Figure 6.21: Interaction between normal force and if change force on Peak FC. Red, constant normal force; green, change normal force.....	109
Figure 6.22: Half-normal plot for Peak FC.....	110
Figure 6.23: ANOVA table for settled FC.....	111
Figure 6.24: Interaction between velocity and normal force on Settled FC. Red, low velocity (0.47m/s); green, medium velocity (0.63m/s); blue, high velocity (0.8m/s).	112
Figure 6.25: Half-normal plot for changing slope.....	113
Figure 6.26: ANOVA table for changing slope.....	113
Figure 6.27: Interaction of velocity and weight on initial changing slope. Red, low velocity (0.47m/s); green, medium velocity (0.63m/s); blue, high velocity (0.8m/s).	114

List of Abbreviations and Symbols

DAC	Data acquisition and control system
μ	Friction coefficient
v	Velocity
F_n	Normal force
T_{air}	Temperature of ambient air
A_{app}	Apparent area of contact
ρ	Ice density
ω	Angular velocity of turntable
r	Radius for velocity level
D_C	Real ice contact diameter
D_S	Real ice sample diameter
D_{Cv}	Video ice contact diameter
D_{Sv}	Video ice sample diameter
F_f	Frictional force
σ_n	Normal stress
m_1	Mass of camera
m_2	Mass of C-clan holding camera
m_3	Mass of railing and L-Shaped part
m_4	Mass of forklift part

Chapter 1 INTRODUCTION

The Arctic Ocean is warming up because of the global warming phenomenon, thus opening new shipping routes through the Arctic Ocean. The world economy could seemingly profit from shorter routes via the Arctic Ocean, because more than 90% of cargo transportation is sea-based and much of that travels between the Pacific and Atlantic Oceans. For example, the navigation distance between Tokyo and Rotterdam is reduced by 40% via the Arctic Ocean compared to the Suez Canal. In addition to expanding marine transportation in arctic regions, Gautier et al (2009) pointed out that the United States Geological Survey estimated that the Arctic Ocean might hold 13 percent of the world's undiscovered oil and 30 percent of undiscovered natural gas. Exploration of the Arctic for petroleum is more technically challenging than for any other environment. However, as the technology improves, the Arctic region is receiving renewed interest from the petroleum industry. The need for better understanding of ice effects on ships, offshore structures and navigation installations is increased by this potential increase in traffic and activity. Ice friction, as one component of the total ice load on such structures, is important and perhaps one of the least understood aspects of ice loading (Timco and Weeks, 2010). We do know that friction is important in ice loading scenarios, since considerable energy consumption is due to ice frictional loss (Akimoto, 2009). Ice-ice friction influences the total load of ice on vessels or structures by affecting the ice pieces around the vessels or structures. Improving the knowledge of ice friction as one component of the total load on vessels or structures can be beneficial in optimizing

designs for icebreaking ships and ice resistant structures and ice movement prediction models.

1.1 Research objective

In the present study, an experiment is designed to test ice-ice friction at temperature -10°C (263°K), aiming to understand more about how the ice friction coefficient changes at these higher velocities and pressures; and to specifically understand ice friction coefficient changes when crushing deformation is involved. The range of velocity is varied from 0.45m/s to 0.76m/s and the range of normal forces varied from 526N to 1888N , with normal pressure up to 6MPa . These parameters were somewhat set by the availability of an existing experimental apparatus, but they do provide pressure values outside the range of previous studies and velocity values that are within the full scale range expected for ship-ice and ice-structure interactions.

1.2 Outline of Thesis Structure

In this thesis, chapter 1 gives the background and the research objective for this study. Chapter 2 introduces the related previous studies. Chapter 3 shows the experimental setup for the study. In chapter 4, the experimental method for the research is introduced. The results of the study are shown in chapter 5 and they are analyzed and discussed in chapter 6. In chapter 7, the conclusions of this study and some suggestion for future study are presented.

Chapter 2 LITERATURE REVIEW

2.1 Ice Friction Coefficient

As traditionally understood, dry friction is governed by Amontons' and Coulomb's laws: The force of friction is independent of the apparent area of contact (Amontons' 1st law); the force of friction is directly proportional to the applied normal load (Amontons' 2nd law); and kinetic friction is independent of the sliding velocity (Coulomb's law). Although an ice surface is dry at low temperature, tests between ice and various materials such as steel and concrete show that ice friction coefficient is not consistent with either Amontons' laws or Coulomb's law. The behavior of ice indicates the presence of lubrication when parameters are changed. Generally speaking, increasing temperature, pressure or sliding velocity causes decreasing of ice friction coefficient even without melting. The effects due to the change of different influencing parameters on ice friction coefficient will be presented and discussed in this chapter after a brief introduction on the molecular structure of ice as a material.

2.1.1 The properties of ice

Ice is the solid form of H₂O, which is the most abundant compound on the earth's surface. The physical properties of ice are due to the unique properties of the H₂O molecule. The H₂O molecules are physically unsymmetrical. As it is shown in Figure 2.1, the H-O-H angle in H₂O is 104.5°.

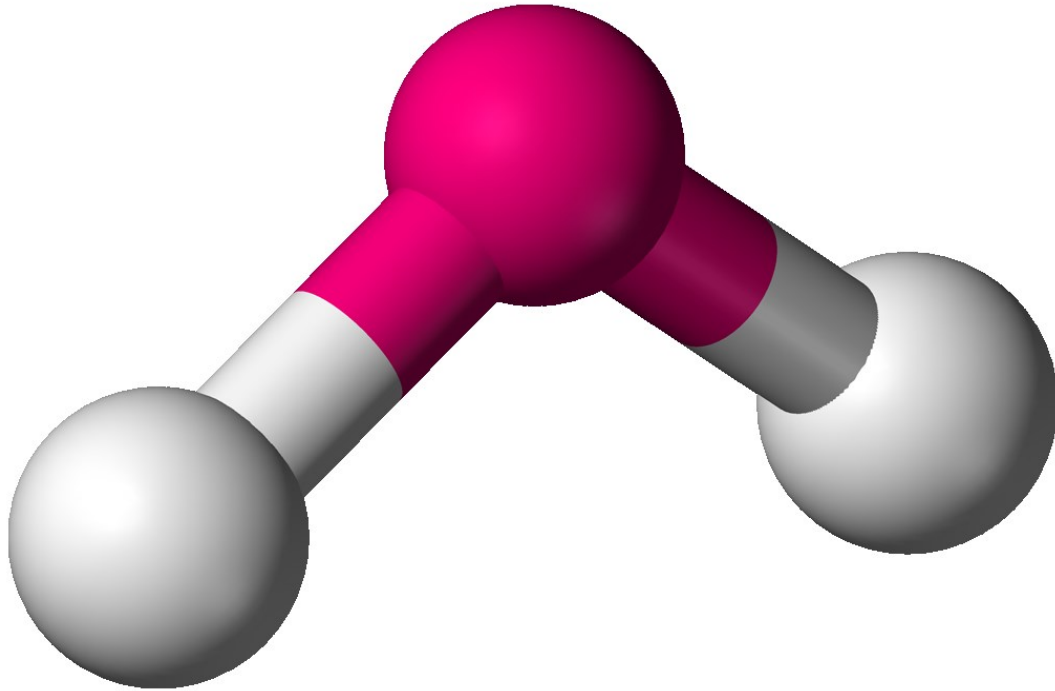


Figure 2.1: *The structure of H₂O molecules. (From Wikipedia:*

http://en.wikipedia.org/wiki/Bent_molecular_geometry)

Although the H₂O molecule is overall electrically neutral, the electrical charges are not evenly distributed within the molecule. This unbalanced charge distribution leads to a form of attraction between molecules. The positively charged hydrogen atoms are attracted to the negatively charged oxygen atoms of neighboring molecule. The phenomenon is called a hydrogen bond (see Fig. 2.3). Marechal (2008) suggested that it is crucial to understand the subtle properties of the hydrogen bond, because many unique properties of H₂O are due to it. Figure 2.2 is a phase diagram of H₂O. The most common solid phase that exists in the natural world is Ice Ih, where “h” stands for “hexagonal”.

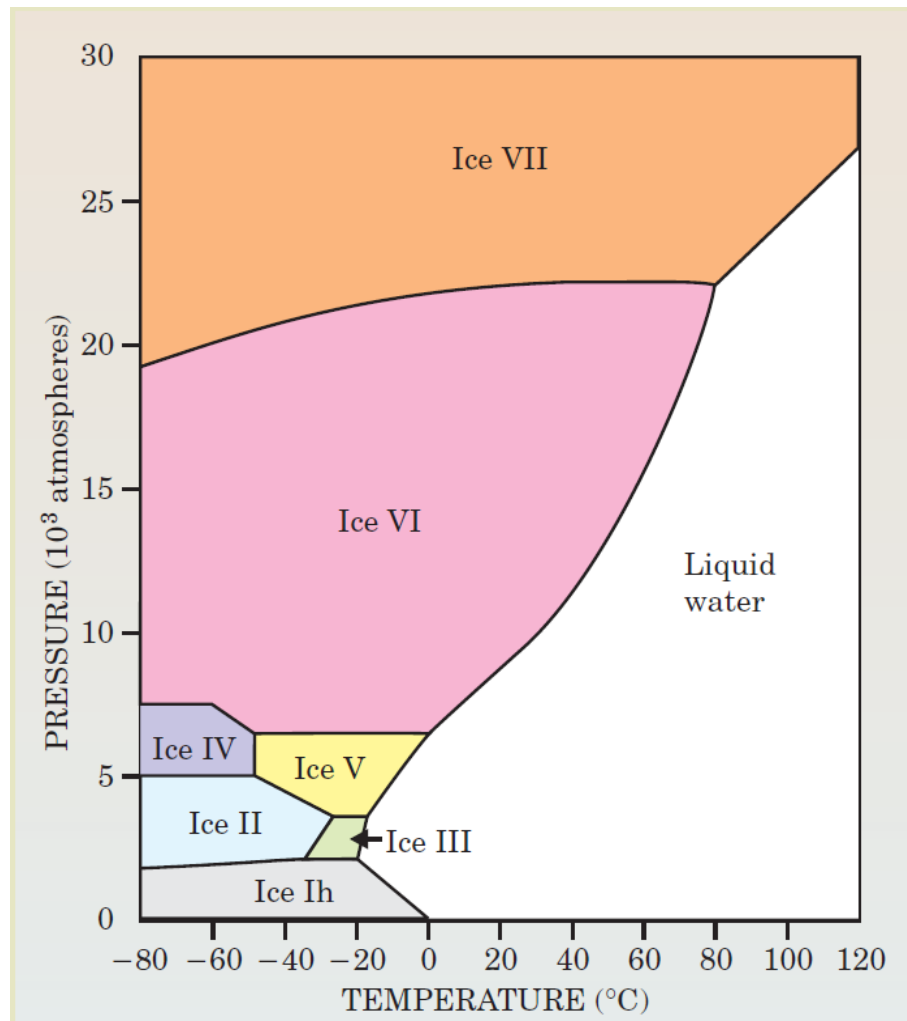


Figure 2.2: Phase diagram of H₂O. (Rosenberg, 2005)

The hydrogen bond is the cause for the crystal structure of Ih ice. As shown in Figure 2.3, hydrogen bonding, which is presented as grey dashed line, helps to create hexagonal lattices when ice is formed below the freezing point. It is important to note that the H-bonds are stable at a distance greater than the space between H₂O molecules in the liquid phase, and thus, the organized structure of solid H₂O occupies larger space than its liquid form.

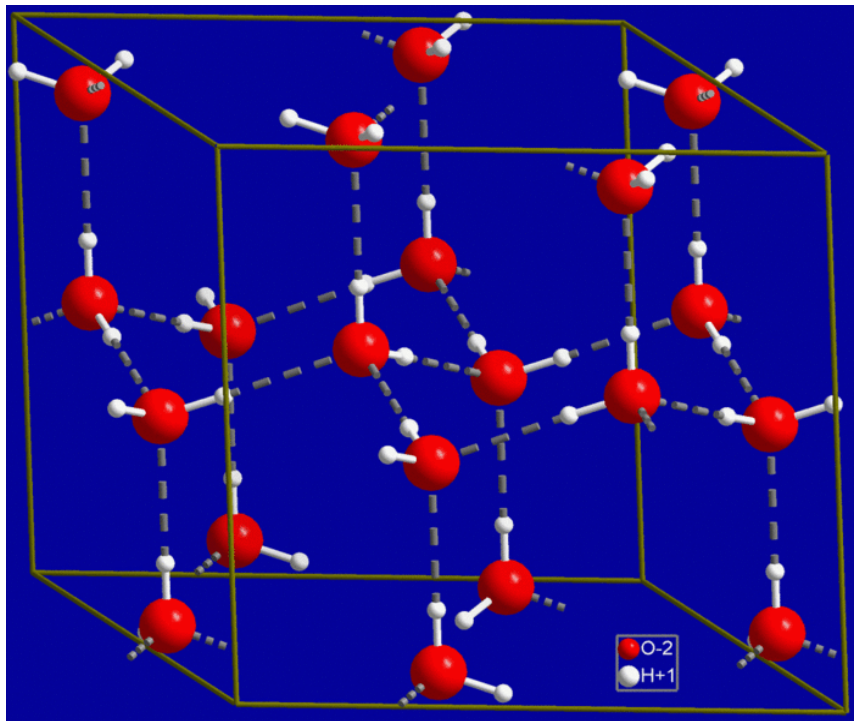


Figure 2.3: Crystal structure of hexagonal ice. Gray dashed lines indicate hydrogen bonds. (From Wikipedia: http://en.wikipedia.org/wiki/Hydrogen_bond)

2.2 Theories of Ice Frictional Lubrication

Over the years, a number of theories have been advanced to explain the frictional characteristics of ice. Most of these theories assume the presence of a liquid or liquid-like layer on the surface of the solid material (Tomas and Frank, 1983; Bowden and Hughes, 1939; Colbeck, Najarian and Smith, 1997; Coleck and Jaccard, 1978; Li and Somorjai, 2007). It is generally held that this layer provides a form of lubrication which strongly influences the frictional behavior of ice, and explains its apparent divergence from both Amontons' and Coulomb's laws. What continues to be debated is the root cause of this layer. The following sections provide the history of the three main theories.

2.2.1 Pressure melting

Pressure melting is one of the mechanisms that contribute to ice surface melting. It can be explained by the Le Chatelier's principle, which can be used to predict the effect of a change in conditions on a chemical equilibrium. For a fixed amount of water, the solid phase takes up more space when frozen into ice because the molecular arrangement in the solid-ice structure is more organized than it is in water as shown in Figure 2.3. When pressure is applied on ice, it forces ice to take up less space. Under the increased pressure, the ice has a reduced melting point and turns back to water in order to take less space. Weber and Stillinger's (1984) experiment proved that increasing pressure causes a melting point depression. However, pressure melting cannot fully explain the low friction on ice at lower temperatures convincingly. Colbeck (1995) argued that even if melting point depression occurs under pressure, the high pressure required to achieve melting point lower than -20°C would cause ice failure. There should be other mechanisms contributing to the low friction of ice.

2.2.2 Frictional heating

Bowden and Hughes (1939) suggested that frictional heating is the major mechanism that contributes to the low friction coefficient on ice. The friction between the two surfaces converts kinetic energy into heat when ice and the surface in contact move relative to each other. The water that is melted locally by the frictional heat becomes the lubricant between the surfaces and lowers the friction coefficient.

Colbeck, Najarian and Smith (1997) confirmed that frictional heating plays a more important role in low ice friction than pressure melting in their study.

Figure 2.4 is extracted from Baurle et al's work in 2006. It shows a thermal image illustrating that an increase of temperature can be observed on the sliding track.

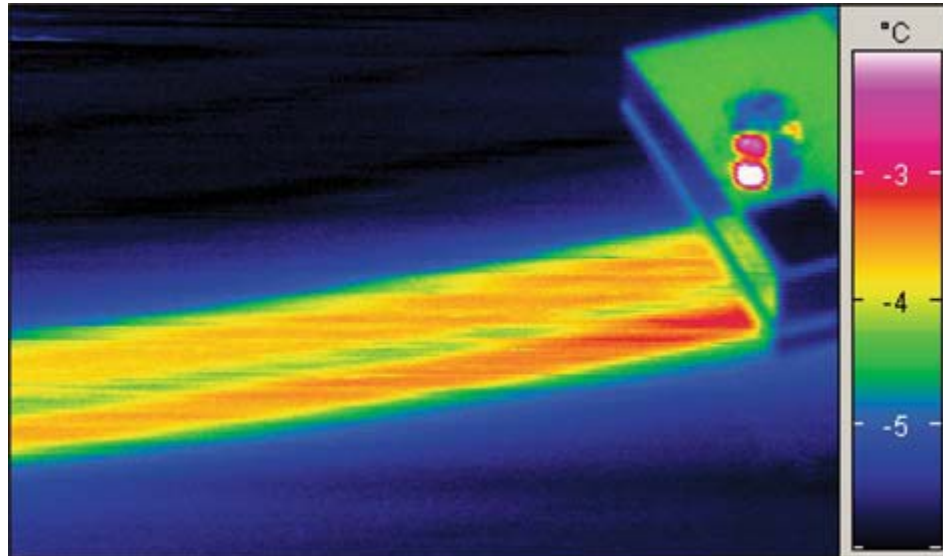


Figure 2.4: Heating of the track behind the slider, Infrared image. (Baurle et al, 2006)

However, Kietzig et al (2010) argued that frictional heating may not be the dominant contributor to low ice friction. When the temperature is low and energy is lost to heat conduction, the heat from frictional heating may just “warm” the ice, not necessarily contribute to melting the ice.

2.2.3 Disordered surface layer

Golecki and Jaccard (1978 or 2001) found that the molecular structure of ice at the ice surface is intrinsically disordered at temperatures between -30°C and the melting point. In a paper published in 2007, Li and Somorjai suggested that there is a thin water-like layer on the ice surface due to the property of the H_2O molecule below the bulk melting point. As shown schematically in Figure 2.5, ice measured with surface imaging techniques indicates that a less structured surface layer is formed in the temperature range

240°-273°K. According to “Facts on ice bergs” (Canadian Geographic) the interior temperature of icebergs off the coast of Newfoundland and Labrador is in the range of -15° to -20° C; and the surface temperature of an iceberg is close to the freezing point of sea water which is -1.9° C. Thus, the normal temperature of natural ice is in the range in which the phenomenon of surface disordered layer is relatively active.

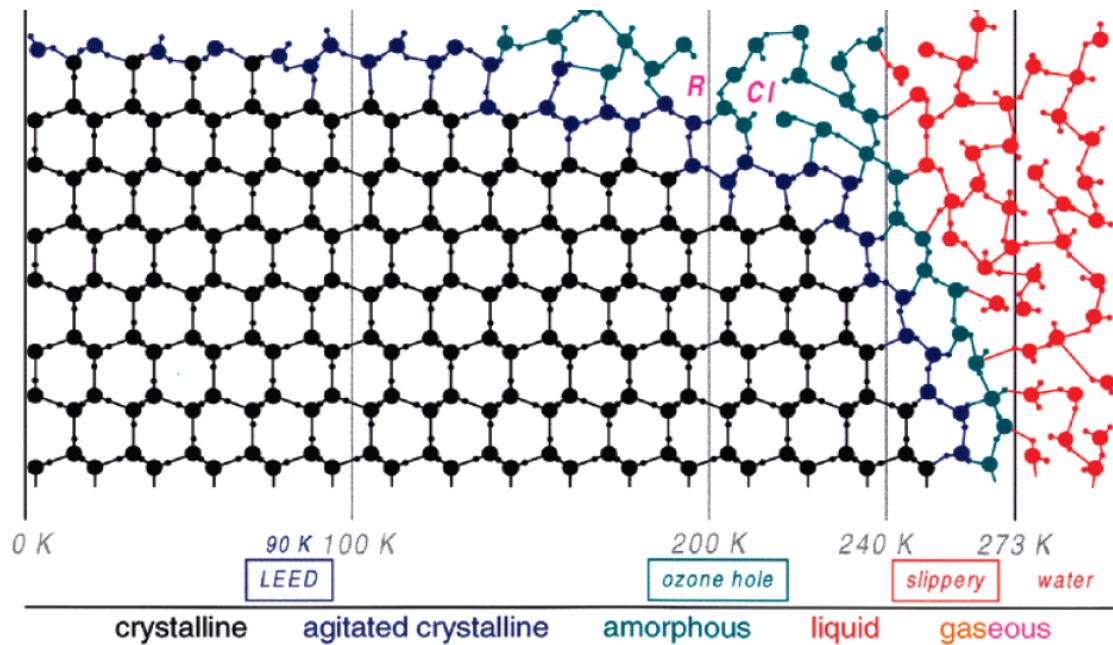


Figure 2.5: Surface structure of ice. (Li and Somorjai, 2007)

Figure 2.6 is a figure extracted from Bishop and his co-workers’ work in 2009. Figure 2.6 (a) illustrates ice structure at 250 °K, in which only the outermost layer (Blue) is interrupted whilst the sub-surface layers (Orange, Green) display a fully connected hexagonal sub lattice. Figure 2.6 (b) illustrates ice structure at 285° K. in which it is obvious that the hexagonal structure has been lost in the outermost bilayer and the second bilayer has also lost significant order. From their research, the authors pointed out that the ice surface is liquid-like above 250°K.

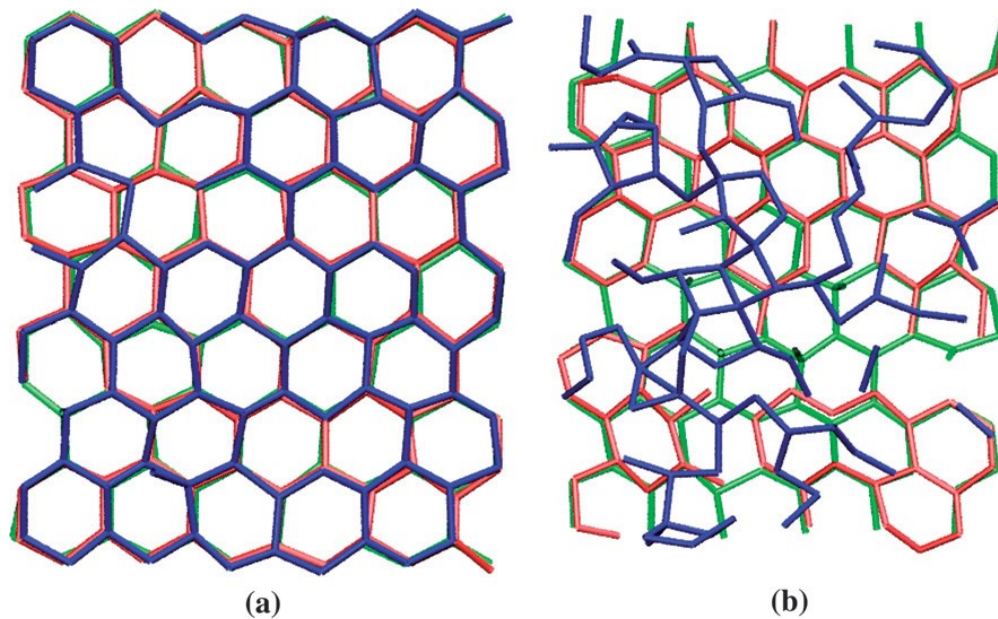


Figure 2.6: Three bilayers of water ice viewed from the [001] direction, where the oxygen sub-lattice is depicted by creating bonds between oxygen atoms within 3.0 Å of one another. The external bilayer is in blue, the second bilayer is shown in red and the third bilayer towards the center of the crystal slab is shown in green. a) 250 K b) 285 K

(Bishop et al., 2009)

2.3 Factors that Affect Ice Friction

The factors identified in the previous section lead to observations of ice friction characteristics in which the ice friction “coefficient” is known to deviate from the classical law. The changes in the apparent friction coefficient are associated with changes in temperature, sliding velocity and with changes in normal force (or pressure). These results have been widely reported from experimental studies and are discussed below.

2.3.1 Temperature

Temperature plays a significant role in the frictional characteristics of the ice surface.

Many researchers have looked into the influence of temperature on ice friction coefficient (Albracht et al., 2004; Bowden, 1953; Evan et al., 1976; Baurle et al., 2006; Tusima, 1977; Yasutome et al., 1999). (See Fig. 2.7-2.12) The results of their research generally show that the ice friction coefficient decreases as temperature increases; however, some studies show that the ice friction coefficient increases slightly when the material temperature approaches the melting point of ice (Albracht et al., 2004; Tusima, 1977; Yasutome et al., 1999). (See Fig. 2.7, 2.11&2.12) According to Kietzig, the increase of the friction coefficient around the melting point may be due to the adhesion force from the liquid layer formed from melting. (Kietzig et al., 2010b)

The test conditions of the reviewed studies with respect to temperature are shown in Table 2.1.

Table 2.1: Test conditions with respect to temperature.

Reference	Sliding Materials	Velocity(m/s)	Normal pressure(kPa)
Albracht et al., 2004	Stainless steel	0.13	500
Bowden, 1953	P.T.F.E., wax	0	2.5
Evan et al., 1976	Perspex, mild steel et al.	3.16	570
Bäurle et al., 2006	PE Block	3 – 5	52 – 420
Tusima, 1977	Steel	7.40E-005	160
Yasutome et al., 1999	Ice	0.001 – 0.1	2.9

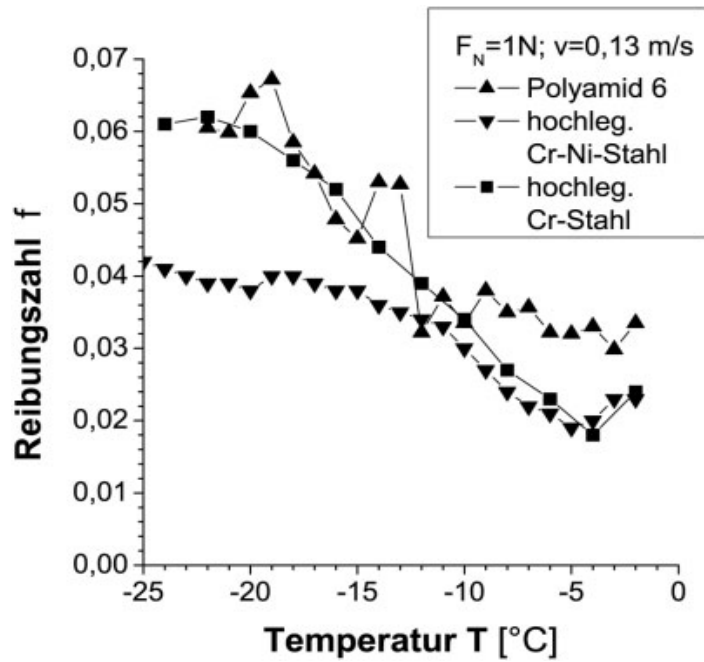


Figure 2.7: Effect of temperature on the friction coefficient using various materials.

(Albracht et al., 2004)

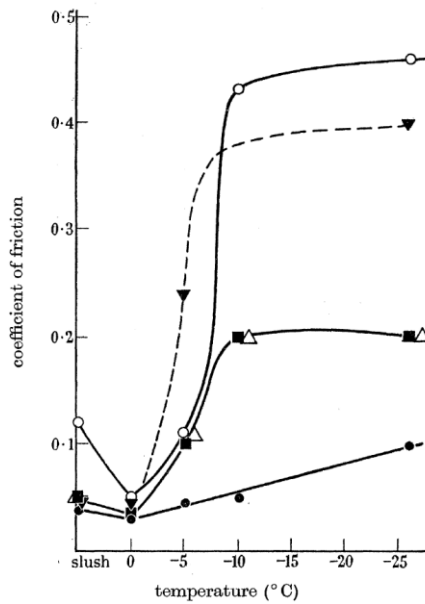


Figure 2.8: Influence of temperature on the static friction of real ski. ○, ski lacquer; ●, P.

T. F. E.; △, Swiss wax; ▼, paraffin wax; ■, Norwegian wax (Bowden, 1953)

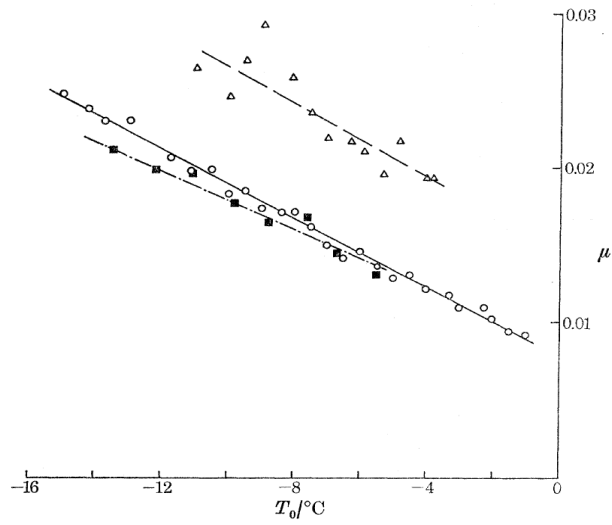


Figure 2.9: The variation of coefficient of friction with air temperature for various rod materials. Velocity 3.16 m/s, total normal load is 45.4 N. \triangle copper rods; \blacksquare Perspex rods; \circ mild steel rods. (Evans et al., 1976)

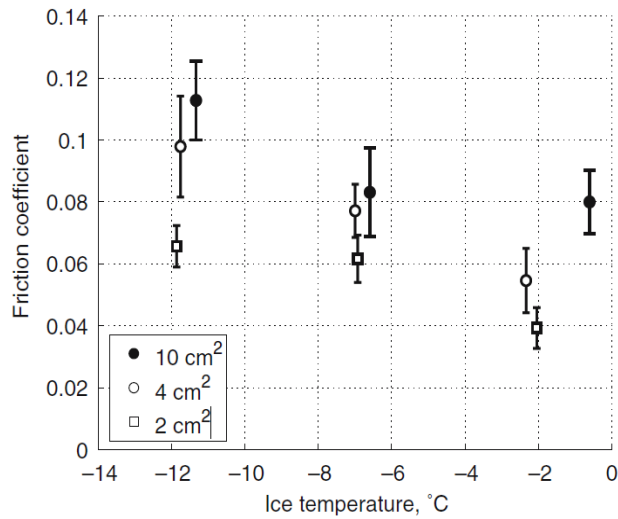


Figure 2.10: Friction coefficient vs. temperature in a velocity range of $v = 3\text{--}5$ m/s and a load range of $F_n = 52$ N to 84 N, summarized and plotted for three different apparent contact areas. (Bäurle et al., 2006)

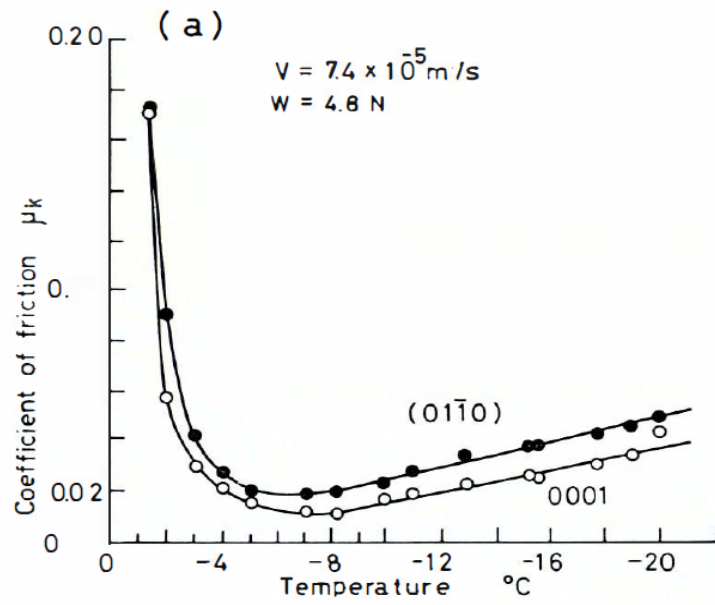


Figure 2.11: Dependence of friction on temperature. ●, (0110) single crystal ice; ○, (0001) single crystal ice. (Tusima, 1977)

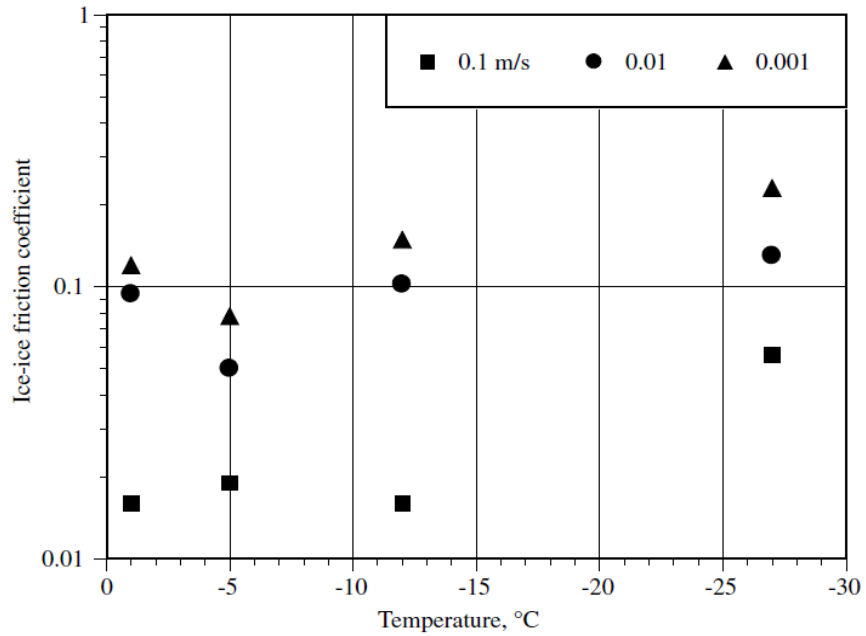


Figure 2.12: Temperature dependence of ice-ice friction coefficient at different sliding velocities. The normal pressure is 2.9 kPa. (Yasutome et al., 1999)

2.3.2 Velocity

Sliding velocity may be the most interesting parameter that influences the ice friction coefficient. There are reported wide differences in the velocity effect. In real applications, the sliding velocity could cover a wide range due to the wide range of activities that involve sliding on ice at various speeds.

The results of many researchers are shown below in Fig. 2.13-2.22, as velocity vs. ice friction coefficient under different conditions. (Evans et al., 1976; Albracht et al., 2004; Frederking and Barken, 2002; Frederking and Barken, 2001; Bäurle et al., 2006; Tusima, 1977; Yasutome et al., 1999; Lishman et al., 2009)

According to the Figures 2.13-2.22, it is evident that most studies agree that ice friction coefficient decreases as velocity increases (e.g. all figures except figure 2.14), especially in the range 0.01m/s to 0.1 m/s. However, when velocity goes higher than 1m/s, some other factors, such as normal pressure, contact area and surface wetness, appears to have a relatively larger effect on the ice friction coefficient, leading to trends that might be due to the design of the experiments. The test conditions of the reviewed studies with respect to velocity are shown in Table 2.2.

Table 2.2: Test conditions with respect to velocity.

Reference	Sliding Materials	Temperature(C)	Normal pressure(kPa)
Evans et al., 1976	Perspex, mild steel et al.	-11.5	570
Albracht et al., 2004	Stainless steel	-7	500 – 1000

Frederking and Barken, 2002	Corroded steel	-3	50
Frederking and Barken, 2001	Ice, painted steel et al.	-10	65
Bäurle et al., 2006	PE Block	-10	420 – 1050
Bäurle et al., 2006	PE Block	- 0.5 to 0.5	52
Tusima, 1977	Steel	-10	470
Yasutome et al., 1999	Ice	- 1 to - 27	2.9
Lishman et al., 2009	Ice	-10	-

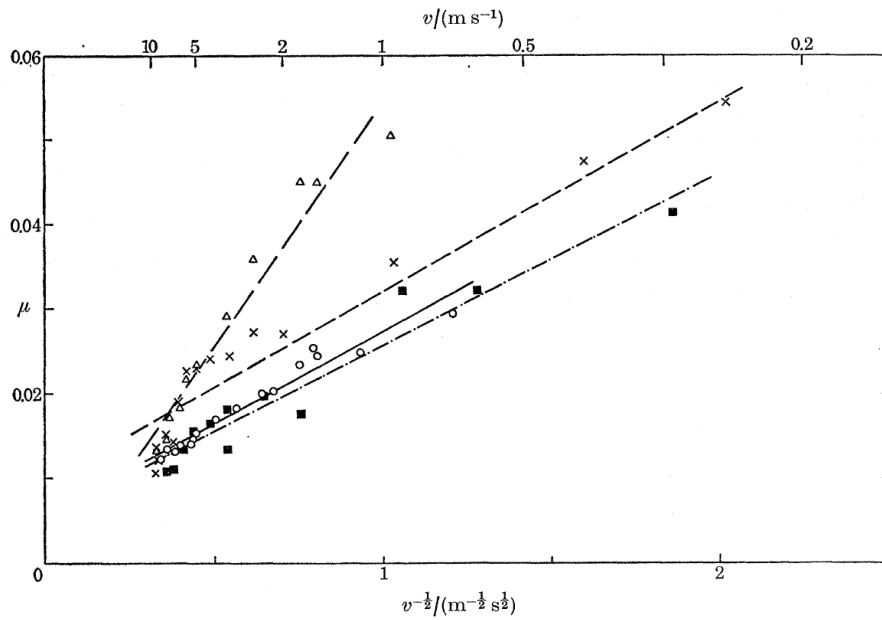


Figure 2.13: The variation of coefficient of friction with velocity for various rod materials and the curved skate. Air temperature - 11.5 C; total normal load ($4L$) is 45.4 N. Δ copper rods; \blacksquare Perspex rods; \circ mild steel rods; \times mild steel skate. (Evans et al.,

1976)

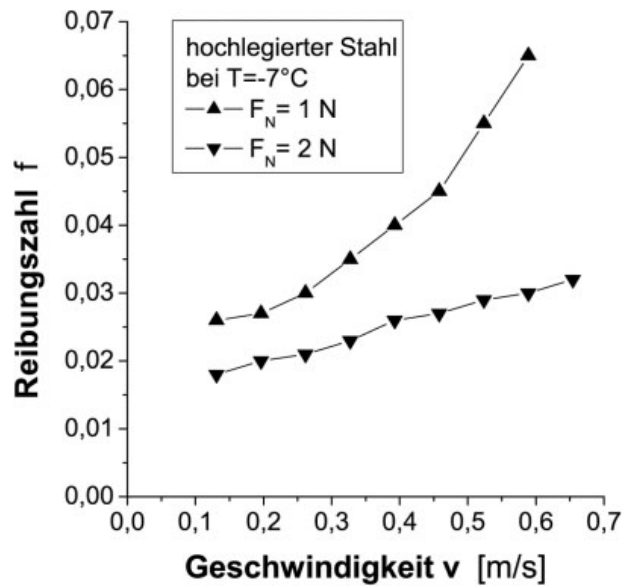


Figure 2.14: Effect of sliding velocity on the coefficient of friction of stainless steel at different normal forces. (Albracht et al., 2004)

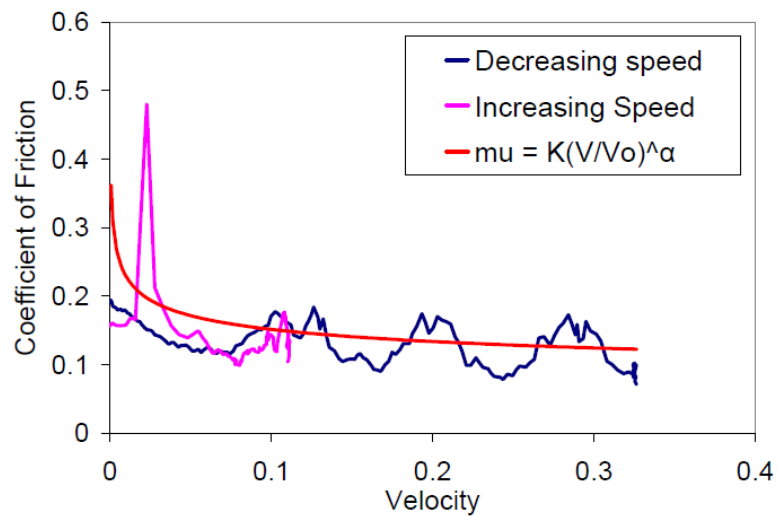


Figure 2.15: Comparison of friction coefficient as a function of speed for decreasing and increasing speed test on corroded steel sample. μ , curve of a function of friction coefficient fit to the relations between speed and friction coefficient. (Frederking and Barken, 2002)

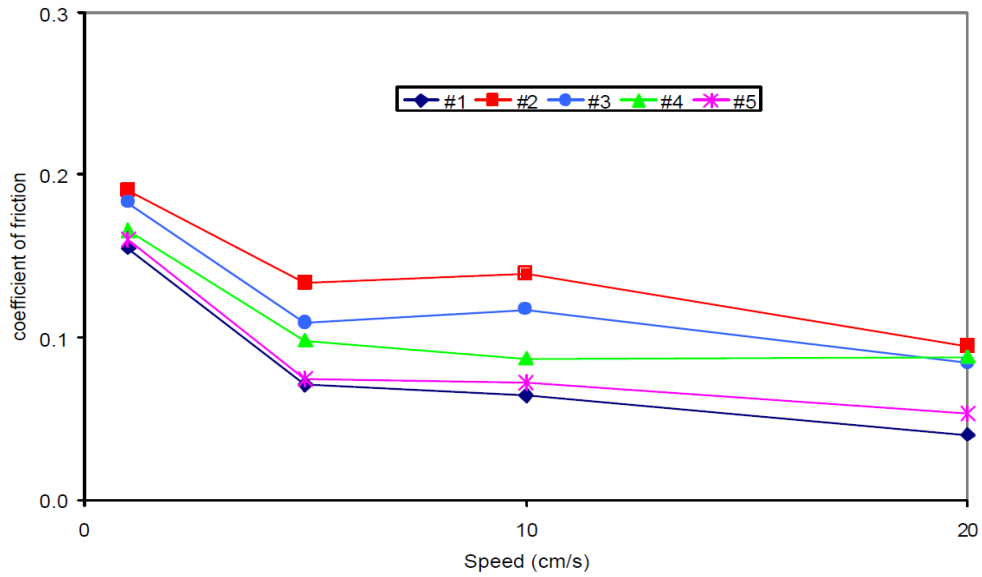


Figure 2.16: Average value of friction coefficient as a function of speed, 65 kPa, -10°C . #1, smooth concrete; #2, painted steel; #3, corroded steel; #4, wood; #5, ice. (Frederking and Barken, 2001)

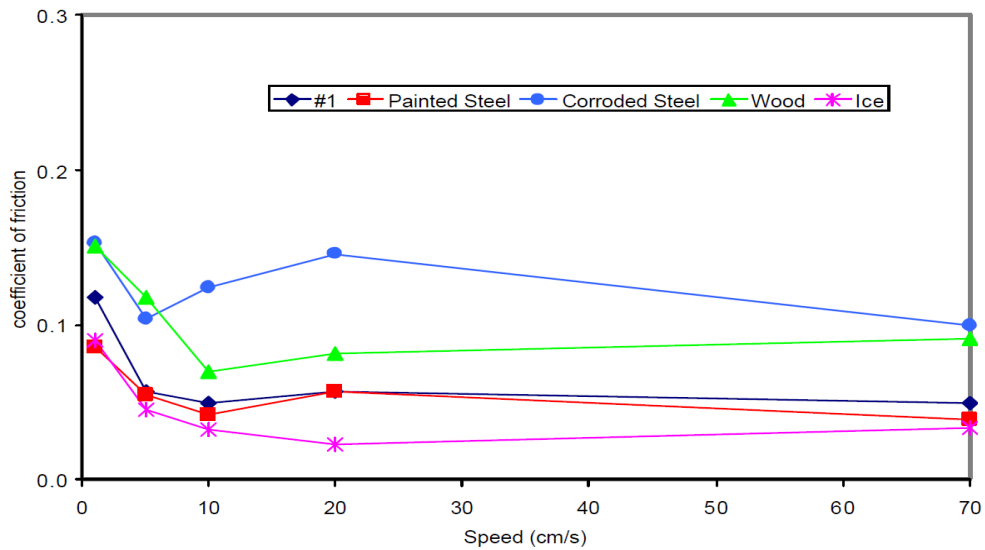


Figure 2.17: Effect of speed on average friction coefficient. #1, smooth concrete. (Frederking and Barken, 2001)

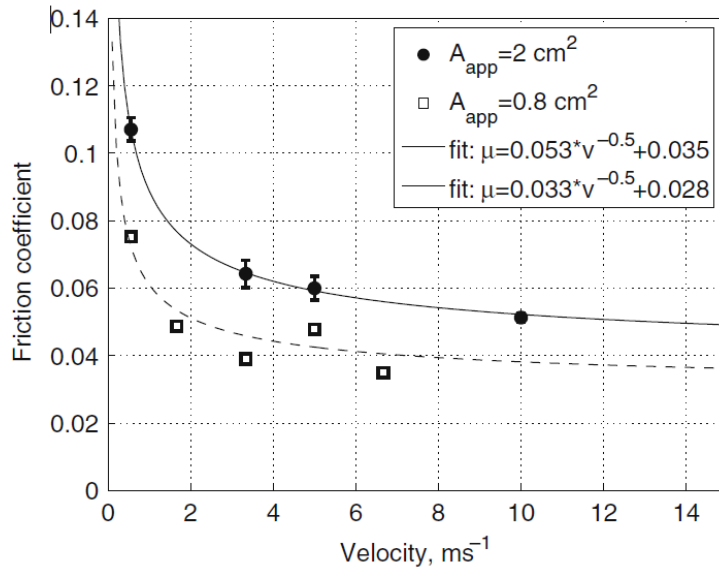


Figure 2.18: Dependence of friction coefficient on velocity at $T_{air} = -10\text{ °C}$ and $F_n = 84\text{ N}$ for two different apparent contact areas. (Bäurle et al., 2006)

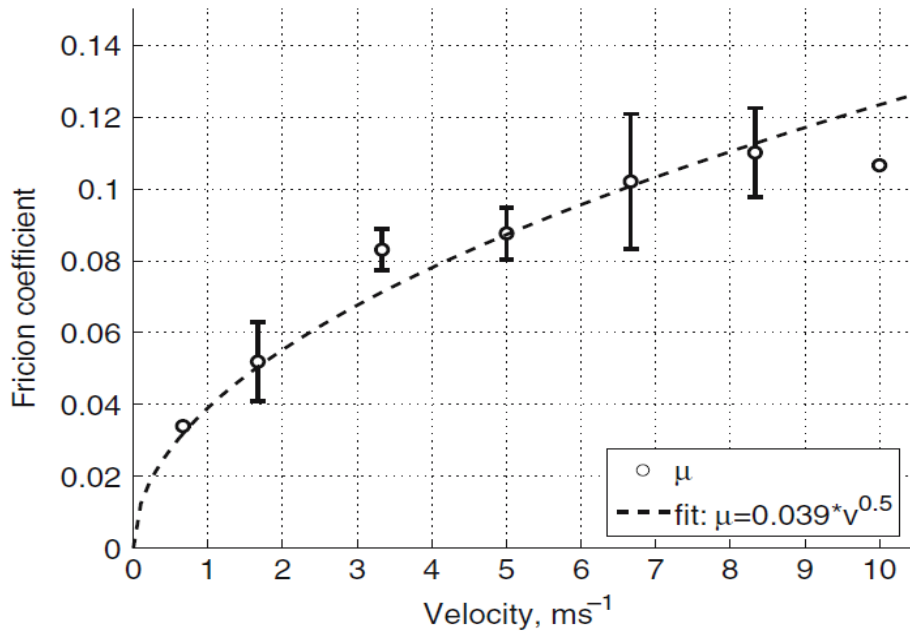


Figure 2.19: Dependence of friction coefficient on velocity at temperatures close to the melting point (wet conditions) for $F_n = 52\text{ N}$ and $A_{app} = 10\text{ cm}^2$. (Bäurle et al., 2006)

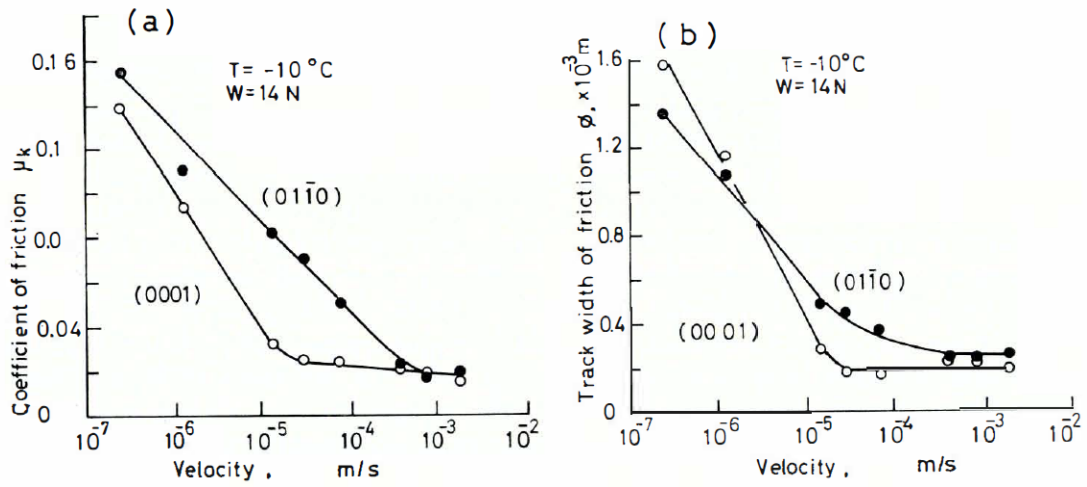


Figure 2.20: Dependence of (a) friction on velocity, and (b) the width of a sliding track against load. (Tusima, 1977)

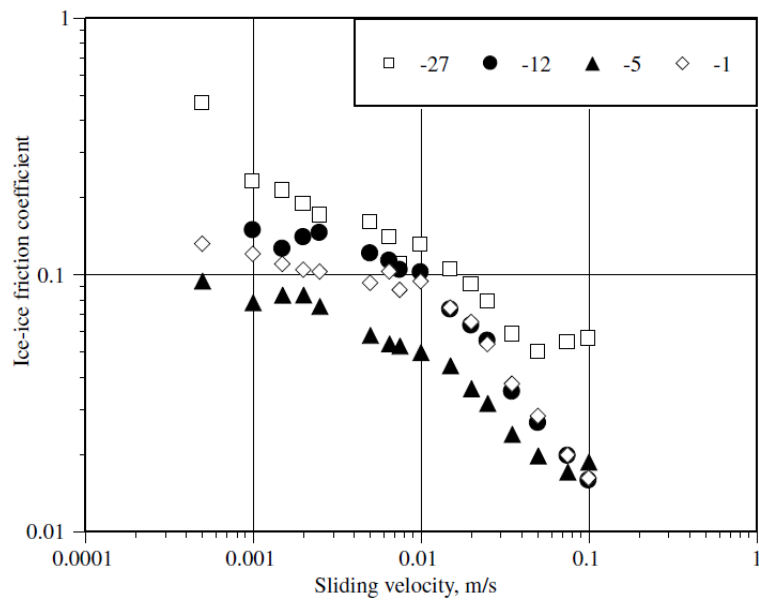


Figure 2.21: Ice-ice friction coefficient plotted against the sliding velocity at different temperatures (in $^\circ\text{C}$). Normal stress is 2.9 KPa. (Yasutome et al., 1999)

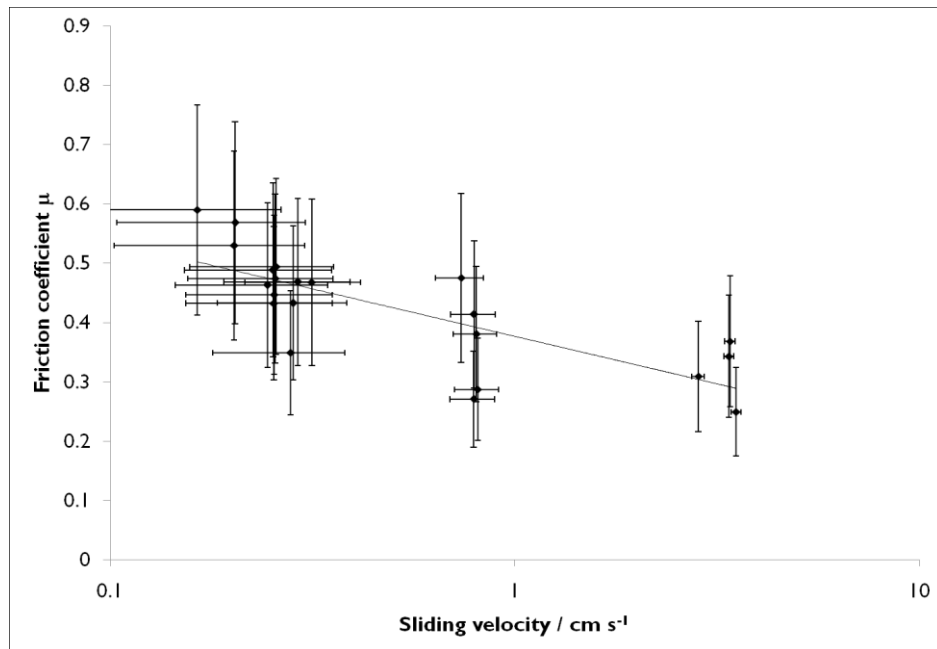


Figure 2.22: *The dependence of steady-state ice-ice sliding friction on slip rate.*

(Lishman et al., 2009)

2.3.3 Normal pressure

A summary of testing conditions of the reviewed studies with respect to normal pressure are shown in Table 2.3.

Table 2.3: Test conditions with respect to normal pressure.

Reference	Sliding Materials	Temperature(C)	Velocity(m/s)
Albracht et al., 2004	Stainless steel	-4 to - 20	0.13
Mizukami and Maeno, 2000	Ice	- 5 to - 0.5	4.50E-002
Mizukami and Maeno, 2000	Ice	- 20 to - 5	4.50E-002

When considering icebreaking ships or ice resistant structures, the forces applied to ice are relatively high. Ice crushing commonly occurs during the interaction between structures and ice. A study done by Jordaan and others (2006) suggested that in compressive failure of ice the pressure could be as high as 70 to 100 MPa. This would suggest that a study of ice friction coefficient under high pressure is where the offshore and shipping industry's interest should be. The actual range that can be tested in details may be limited due to the practicalities of experimental equipment.

The following plots (Fig. 2.23-2.25) show some results for changes in friction coefficient associated with changes in normal force. It is evident that the coefficient is not independent of the normal force and that the coefficient tends to decrease as force (or pressure) increases; however, in all the cases illustrated, the forces and pressures are well below those required to cause ice crushing.

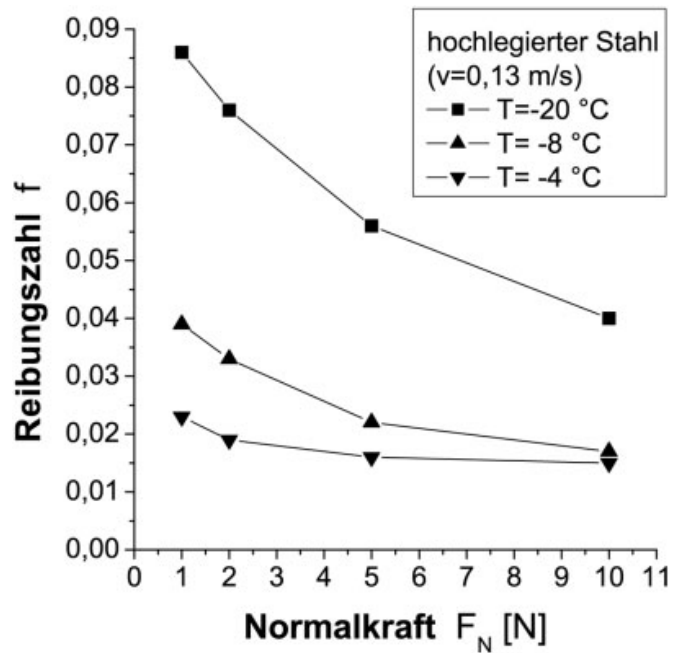


Figure 2.23: Effect of normal force on the coefficient of friction of stainless steel at different temperatures. (Albracht et al., 2004)

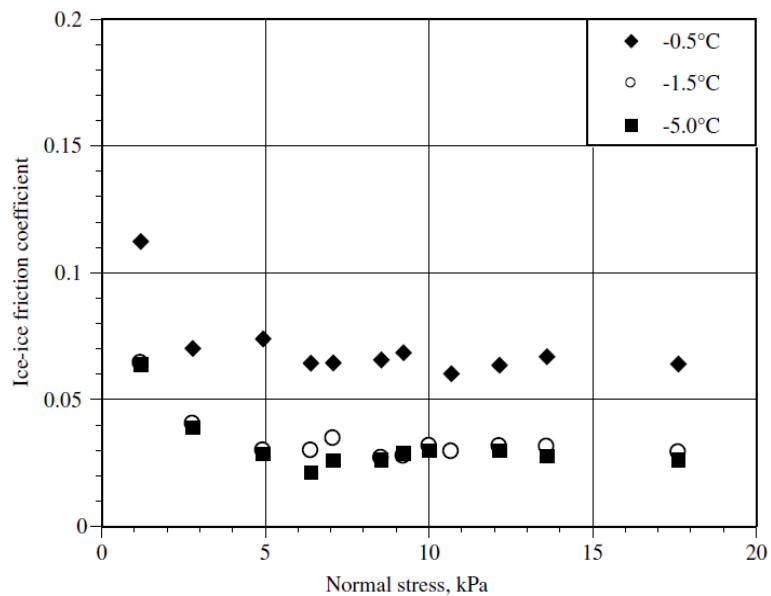


Figure 2.24: Normal stress dependence of ice–ice friction coefficient above -5 °C.

Sliding velocity is 4.5×10^{-2} m/s. (Mizukami and Maeno, 2000)

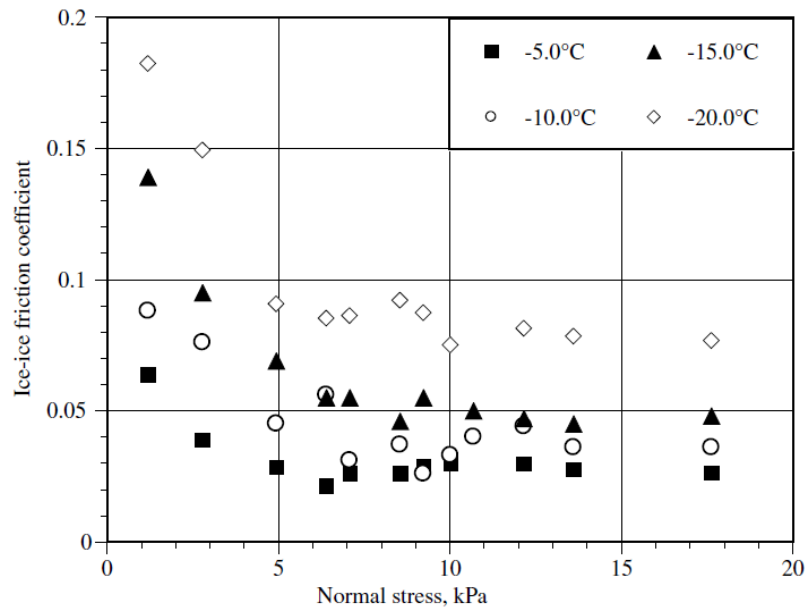


Figure 2.25: Normal stress dependence of ice–ice friction coefficient below -5°C .

Sliding velocity is 4.5×10^{-2} m/s. (Mizukami and Maeno, 2000)

2.3.4 Other factors

The energy loss which affects the ice surface condition is influenced by thermal conductivity of the sliding material. In Kietzig et al.’s study (2010), different materials are used to study how thermal conductivity influences ice friction and interacts with the heat generated through the sliding velocity. Figure 2.26 shows how ice friction changes with the sliding velocity for different materials at -7°C . From the research, the authors claimed that ice friction decreases for materials with lower thermal conductivity. However, Kietzig et al. also pointed out in another paper (Kietzig et al, 2010b) that the results cannot indicate unambiguously the influence of thermal conductivity, because other parameters such as surface wettability and hardness also changed with the materials.

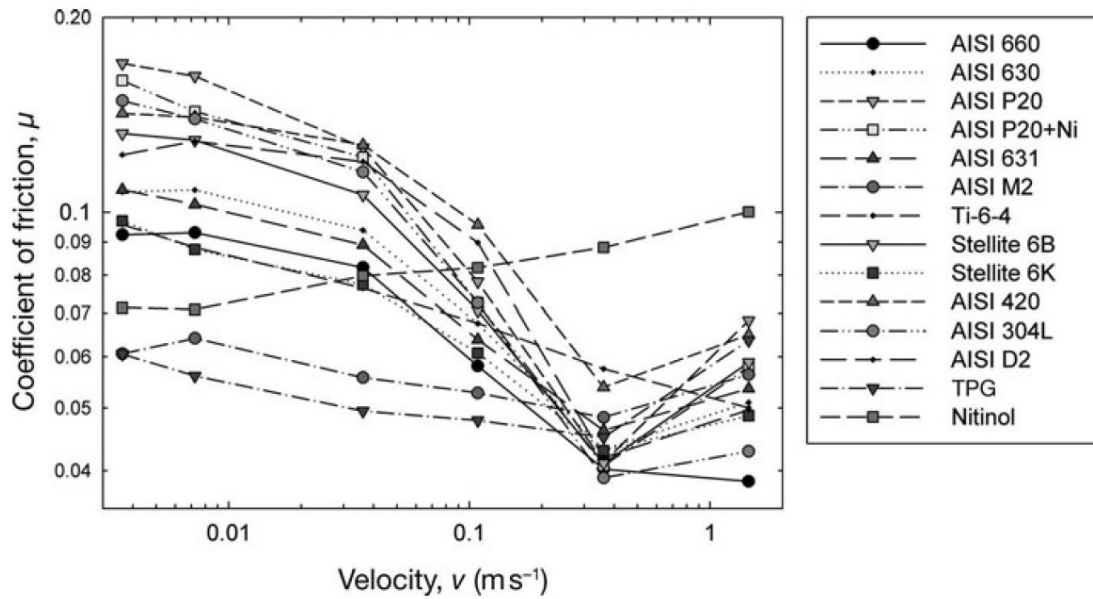


Figure 2.26: Ice friction curves for different materials. (Kietzig et al, 2010b)

There are other factors also have effects on the ice friction, such as wettability, roughness and so on. (Kietzig et al, 2010b)

2.4 Experimental Methods

There is no analytical or numerical approach that has been successfully implemented in analyzing or studying ice friction due to the complexity of ice behavior, so researchers are invariably faced with conducting experiments as a mean of studying ice frictional characteristics. There are many experimental methods used in previous studies. The advantages and disadvantages of several kinds of experimental methods on ice studies are introduced in this section.

2.4.1 Real-life experiments

In Colbeck et al's (1997) study, an instrumented skate was used to measure the temperature change at the skate surface in order to prove the frictional heating theory. The shortcoming of many real-life experiments is the limitation on controlling different variables that were not the main parameters of the given study, for instance, operating air temperature, ice making procedures of different ice rinks, water qualities and so on. As shown in previous sections, it is difficult to compare results from study to study if all the other variables which may have influenced the frictional results are unknown or uncontrolled. Additionally, some studies of sporting equipment involve the additional influence of the athletes themselves and it is expected that there is significant variability in a skaters' daily performance.

2.4.2 Sliding model

Compared to the real-life experiment method, a sliding model improves in the control of different variables, such as velocity, normal stress and the ice used in experiments. It also reduces the variability of the human performance. However, some variables like temperature are still difficult to control. Another problem of sliding model is that unpredictable sliding track adds variability to the measurement (Bowden, 1953).

2.4.3 Linear experimental devices

Linear devices were used in many studies. The problem of unpredictable sliding track is solved by using purpose-built linear experimental devices. Because one identical characteristic of different devices is that the slider on the ice is well controlled in the

experiment. Montagnat and Schulson (2003) and also Ducret et al. (2005) conducted friction experiments in cold rooms in order to control the temperature. In this case, the process of the experiment is limited by the size of the cold room.

2.4.4 Rotational experimental devices

Many prior studies employed different rotational experimental devices. In addition to improved control of certain parameters as with linear experimental devices, rotational devices allow smaller size equipment, which is more suitable to using in a closed temperature chamber. Accordingly, more parameters of an experiment can be better controlled, such as humidity. The significant advantage of longer test times and more compact apparatus is countered by the fact that the friction sample does not have a fresh track in a rotational device after the first revolution.

2.5 Testing Materials

For this research, the interest is in the friction between two ice surfaces. In an area of water when floating ice is present, ice does not only affect the vessels, but also interacts with other ice fragments and causes additional effects to the vessels. For instance, ice that is fragmented by ice-breakers is restrained and pushed back by other ice. This would also happen when a ship is travelling in an area of water with a high density of pack ice.

The micro-structure of ice differs due to how the ice is formed. Figure 2.27 shows the structures of several common types of ice.

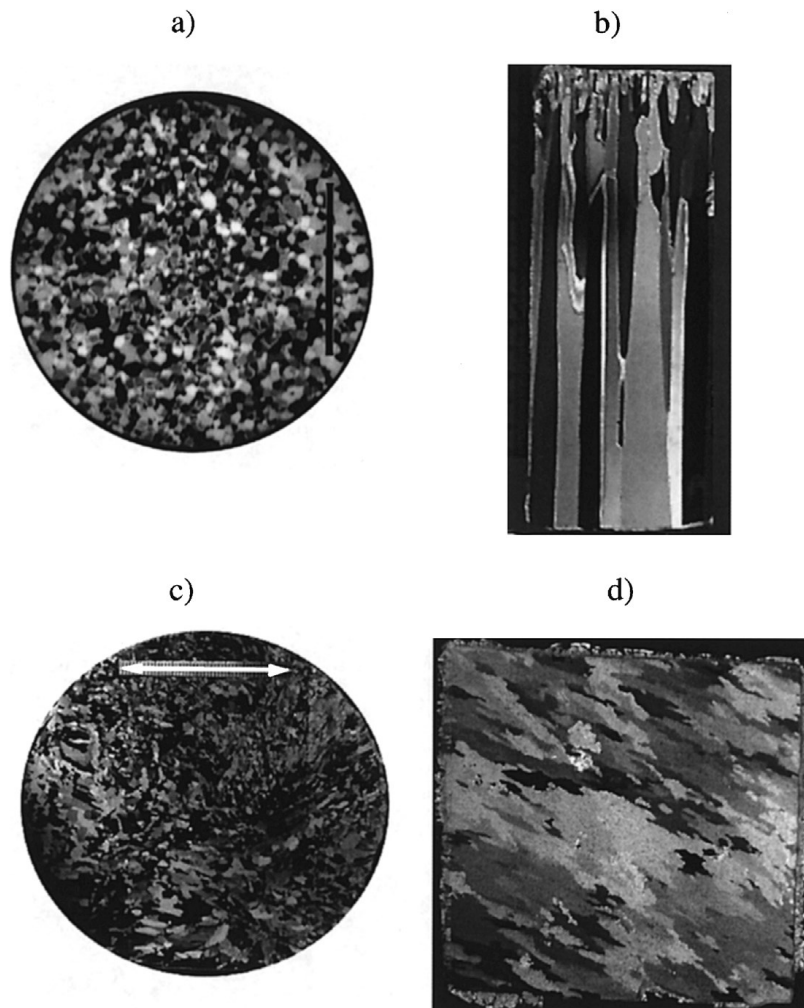


Figure 2.27: Thin section photographs showing the structure of several common ice types: (a) fine-grained granular ice; (b) freshwater columnar ice, showing a fine-grained seed layer at the top, transitioning into a columnar growth with increasing grain size; (c) frazil ice; (d) aligned sea ice. Scale bars are 50 mm. (Cole, 2000)

In nature, ice can be categorized as salt water or fresh water ice according to its salinity. Salt water ice, also called sea ice, is ice frozen from sea water. As a result, the salinity of the ice varies with the salinity of sea water. There can even be significant difference in

salinity between sea ice samples, because of the migration of salt within the ice sample through a period of time. Furthermore, if sea ice survives one melting season, its grain size will increase due to refreezing (Timco and Weeks, 2010) and its brine (salt) will drain out (Figure 2.28 & 2.29). Freshwater ice, most commonly iceberg ice in the marine environment, is more uniform in terms of impurities and micro-structure because of the way icebergs are formed.

In order to provide consistent sample properties and reduce experimental error, fresh water ice with a fine grained structure was chosen for friction testing in this case.

According to Kennedy, Schulson and Jones (2000), the effect of grain size on ice friction coefficient is not significant. A grain size of 6-8mm was chosen due to the availability of laboratory equipment and procedures to produce samples with this grain size.

The method of ice sample preparation for this research is presented in the next section.

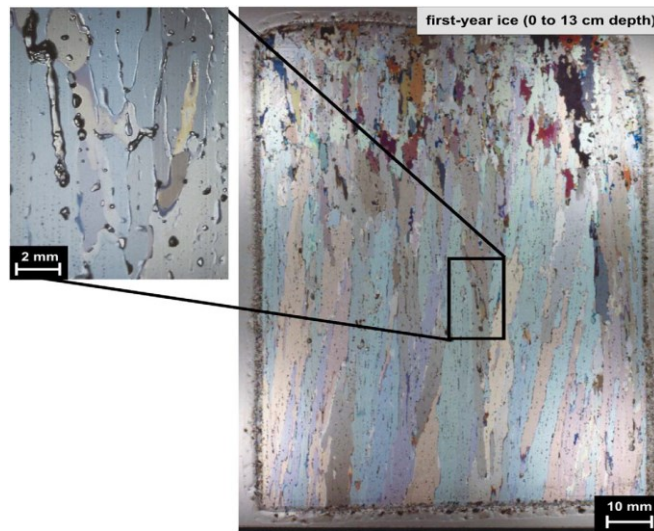


Figure 2.28: Thin section of first-year ice showing the ice platelets and the brine pockets along the grain boundaries. (Timco and Weeks, 2010)



Figure 2.29: Vertical thin section of multi-year ice. Note the relative absence of the salt pockets and the large variation in grain structure. (Timco and Weeks, 2010)

2.6 Ice-ice friction study

Studies concerning the friction of ice on ice are still relatively rare. Some fields that would involve with ice-ice friction are introduced below.

The following Figure 2.30 shows the two stages of ice crushing with vertical structure (Bjerkas, 2006). As shown in the figure, as ice is crushed and accumulated around the structure, the friction between ice and ice starts to play an indirect but considerable role in the ice loads experienced by the structure.

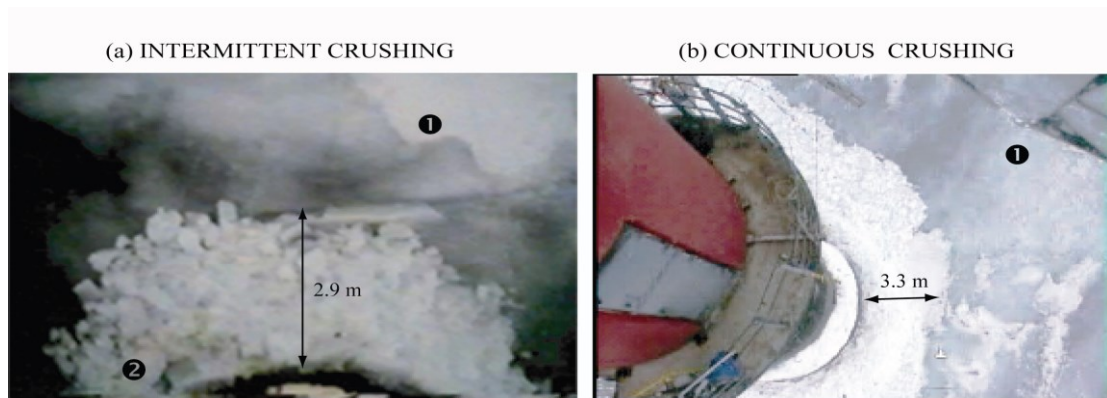


Figure 2.30: (a) Intermittent crushing with ice thickness 0.2 m and drift speed 0.05 m/s occurring 12:06:39, 30 March 2003, (b) Continuous crushing with ice thickness 0.5-0.6 m and drift speed 0.35 m/s occurring 21:23:02, 19 March 2003. (Bjerkas, 2006)

Ice-ice friction influences the total load by affecting the ability of ice rubble around the structures to clear away from the structure. The friction between ice pieces determines how easily they are able to slide over each other when confined by the impinging ice. This influences the size of the rubble area and thus the area over which pressure is applied to the structure. Ice-ice friction also influences the internal extrusion of the ice rubble

leading to higher or lower confinement forces and thus higher or lower pressures within the contact area.

Figure 2.31 shows the simulated icebreaking pattern observed in a model test tank (Tan, Riska and Moan, 2014). As a ship breaking through the ice surface proceeds, broken ice pieces are pushed against the ship hull by the outer ice sheet through intermediate pieces that have been broken off the main ice sheet. There is an ice-ice friction load between the parent ice sheet and the broken ice pieces. In many cases the ice edges are being crushed at the contact points, either with the ship or with each other. Better understanding of the ice-ice friction, particularly when the ice is at or near crushing pressures, could help predicting ice loads as a whole on ship hulls or structures.

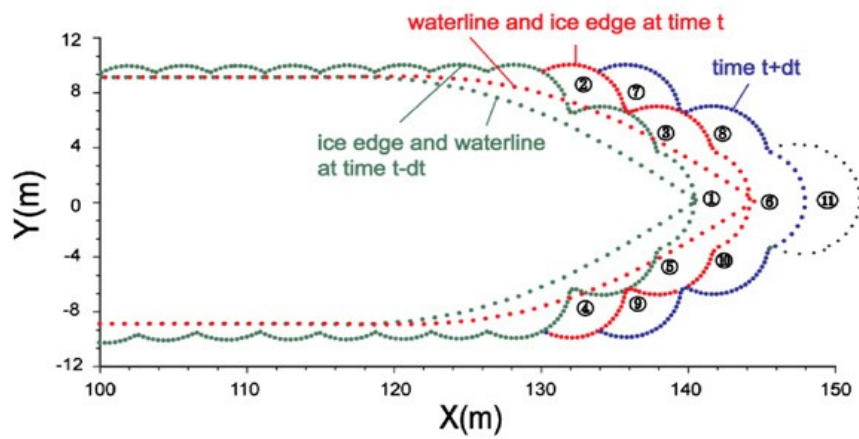
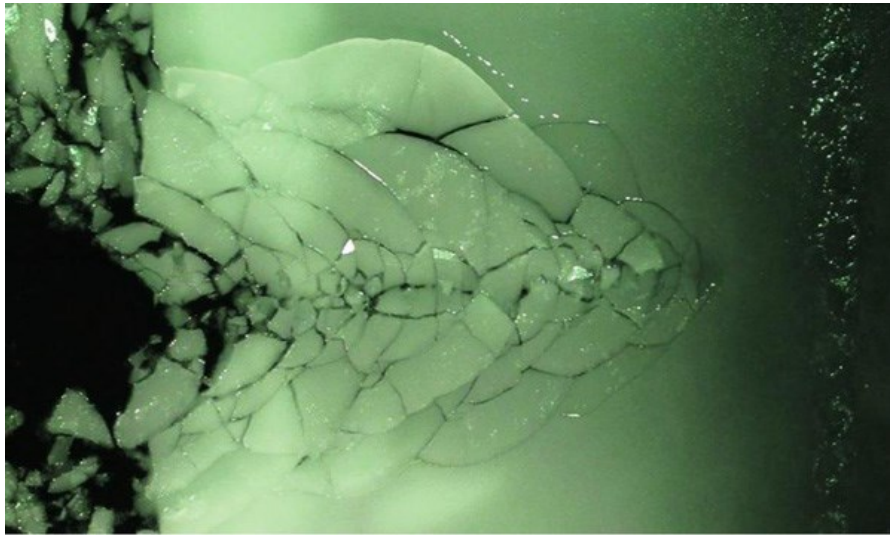


Figure 2.31: Example of the icebreaking pattern. (above) Observed icebreaking pattern in Aalto ice tank in Feb., 2012. (Photograph by X. Tan). (below) Simulated icebreaking pattern. (Tan, Riska and Moan, 2014).

According to Jiskoot (2014), ice-ice friction also plays a role in the dynamics of glaciers, although some models have not taken it into consideration. This is one area of study to which ice-ice friction study can be beneficial

Hopkins (1996) stated that, in modeling the dynamics pack ice in mesoscale (10-100km), the effect of friction between ice floes increases as the thickness of the floes increases because of the energy loss due to frictional sliding.

In Maeno et al's paper (2003), the authors gave a summary of ice-ice friction coefficient vs sliding velocity from various studies, as shown below (Fig. 2.32):

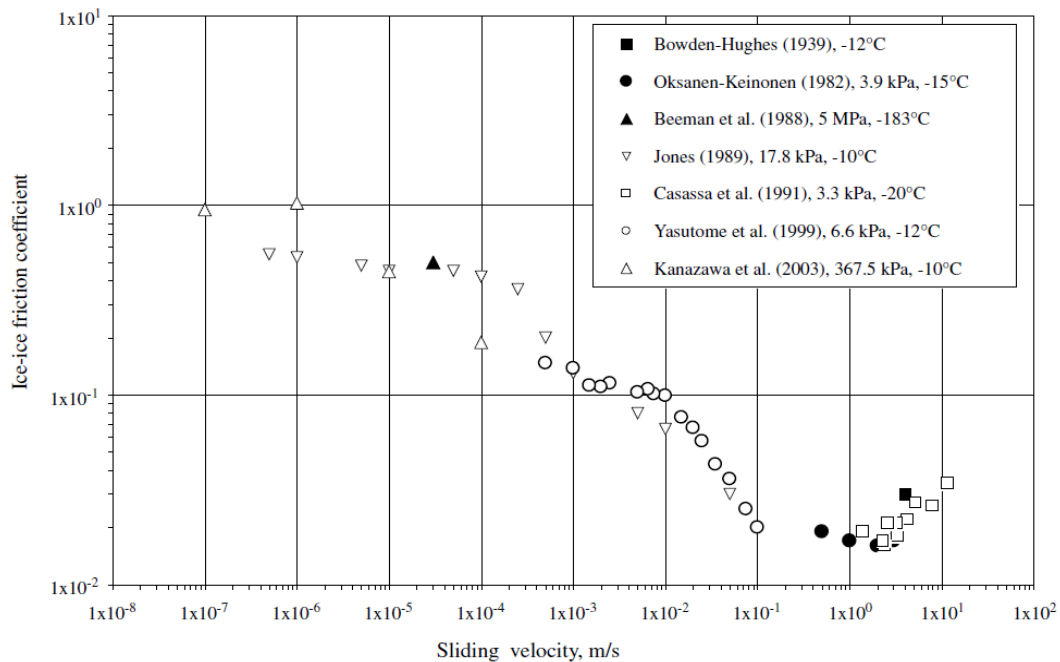


Figure 2.32: Summary of ice-ice friction coefficients vs. sliding velocity. (Maeno et al, 2003)

These data shows that the ice-ice friction coefficient has a minimum value at velocities of 0.1 to 3.0 m/s. This is the typical range of velocities covered by icebreaking ships (typically 1-2 m/s in heavy ice) and ice drift against offshore structures (0.1 – 0.5 m/s).

Maeno (2003) explained the variation of friction coefficient with velocity in terms of water lubrication mechanisms. Maeno (2003) pointed out that former studies (e.g. Bowden, 1953 and others) showed that the frictional heat at the contacting surfaces causes thin water films which lubricate the surfaces. The viscous resistance of the water film is low. As sliding velocity increases, the lubrication effect increases and results in the decrease of the friction coefficient.

Kennedy, Schulson, and Jones (2000) carried out experiments on ice-ice friction in 1999. The studied factors are ambient temperature, sliding velocity, normal pressure and grain size. The authors found that there was surface fracture associated with tests in certain ranges of velocities, and the surface fracture appeared differently at different velocities. According to the authors, normal pressure (at the test range) and grain size have insignificant effect on ice friction coefficient. Figure 2.33 cited from Kennedy, Schulson, and Jones' work shows the friction coefficient at various velocities and normal pressures at 263°K. The normal pressures on the contact surface in these tests are relatively low.

Sliding velocity (m s ⁻¹)	Friction coefficient (\pm standard deviation) for nominal contact pressure		
	0.007 MPa	0.02 MPa	0.045 MPa
5×10^{-2}	—	0.030 ± 0.005	—
10^{-2}	0.059 ± 0.008	0.066 ± 0.008	0.061 ± 0.005
5×10^{-3}	—	0.08 ± 0.01	—
10^{-3}	0.13 ± 0.02	0.13 ± 0.03	0.15 ± 0.03
5×10^{-4}	0.20 ± 0.05	0.20 ± 0.03	—
2.5×10^{-4}	—	0.36 ± 0.06	—
10^{-4}	0.42 ± 0.05	0.42 ± 0.05	0.46 ± 0.05
5×10^{-5}	—	0.45 ± 0.03	—
10^{-5}	0.50 ± 0.05	0.45 ± 0.05	0.50 ± 0.04
5×10^{-6}	—	0.48 ± 0.05	—
10^{-6}	0.55 ± 0.07	0.53 ± 0.08	0.58 ± 0.03
5×10^{-7}	—	0.55 ± 0.08	—

Figure 2.33: *Coefficients of kinetic friction versus sliding velocity of freshwater granular ice at -10°C for nominal contact pressures of 0.007, 0.02 and 0.045 MPa (Kennedy, Schulson, and Jones, 2000).*

According to Mizukami and Maeno's study in 2000, the friction coefficient, at the temperature range of -0.5 to -20°C, decreases as normal pressure increases in the range 0 – 5 kPa. In the range 5 – 20 kPa, the effect of normal pressure on ice friction coefficient is not significant (see Fig. 2.34 & 2.35). Weber and Stillinger's (1984) experiment proved that increasing pressure causes a melting point depression. However, pressure melting cannot fully explain convincingly the low friction on ice at lower temperatures.

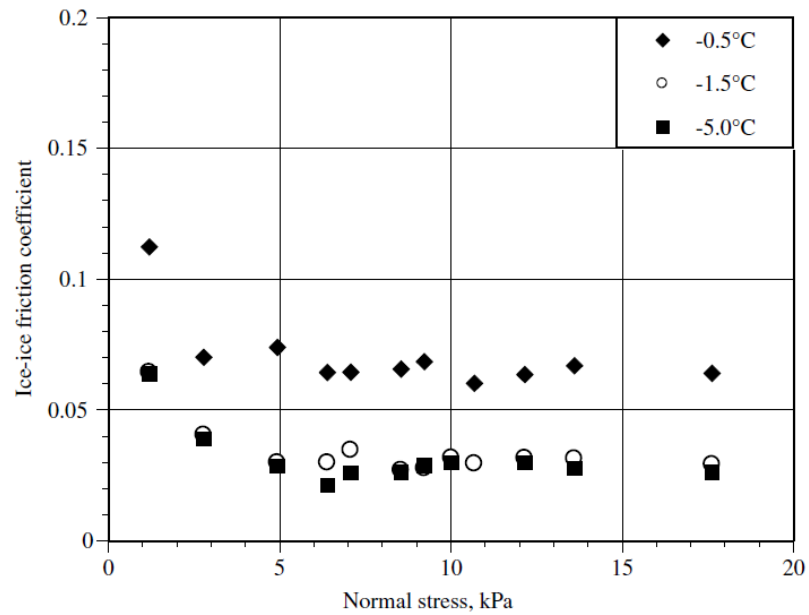


Figure 2.34: Normal stress dependence of ice–ice friction coefficient above -5°C . Sliding velocity is 4.5×10^{-2} m/s. (Mizukami and Maeno, 2000)

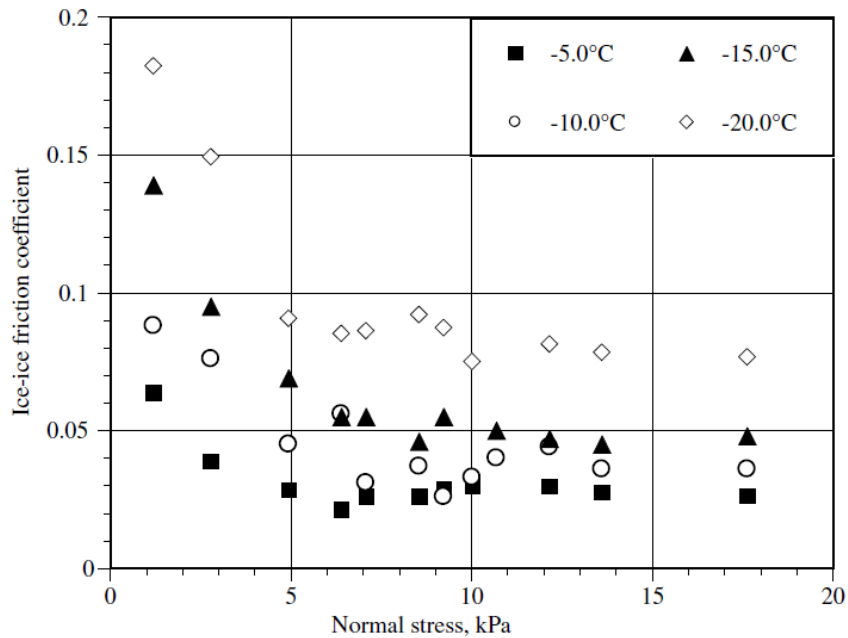


Figure 2.35: Normal stress dependence of ice–ice friction coefficient below -5°C . Sliding velocity is 4.5×10^{-2} m/s. (Mizukami and Maeno, 2000)

Schulson and Fortt (2012) did new measurements of frictional force with fresh water polycrystalline ice at low velocities and low pressure in 2012. According to the authors, frictional heating, pressure melting and deformation of the surfaces have effects on the changing of friction coefficient at temperature 223°K and above.

Stick-slip phenomenon is exhibited, when two surfaces sliding over each other, alternately stick to each other and then slide over each other for a short period as the shear stress builds up enough to break the stick bond, in a repetitive pattern. Figure 2.36 (Schulson and Fortt, 2012) shows the stick-slip behavior of ice-ice friction at different temperatures and velocities. Schulson and Fortt (2012) stated that stick-slip is an indication of dynamic instability. As the sliding velocities increases, within the relatively low range presented, the instability increases.

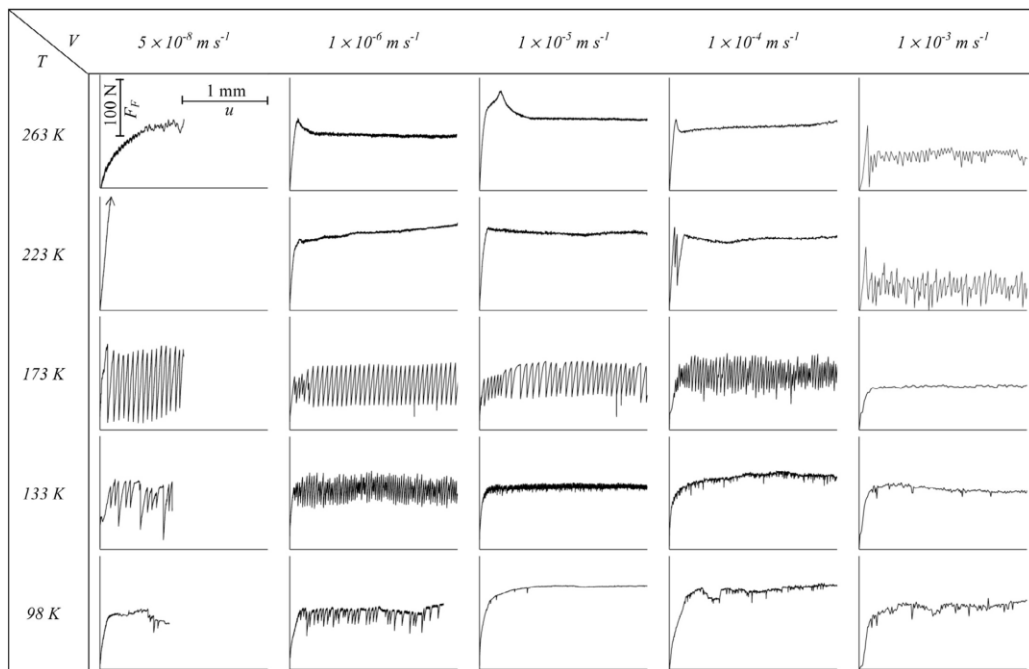


Figure 2.36: Curves shear force F_f versus displacement u for each temperature-velocity combination under an applied normal stress of $\sigma_n = 60 \text{ kPa}$. The origin is $(0,0)$. The

scales, shown in the top left-hand panel, are the same for each curve. The arrow on the curve at $223\text{ }^{\circ}\text{K}/5 \times 10^{-8}\text{ m s}^{-1}$ means that the load was removed before sliding was initiated. The oscillations indicate stick-slip behavior.

2.7 Review Summary

Many studies have been carried out on ice friction with dissimilar materials. These studies all show that the ice friction coefficient does not obey the classical dry friction laws but exhibits some characteristics of lubricated friction, even for notionally dry contact. The mechanisms that explain this are thought to be pressure melting, frictional heating and surface molecular disorder. Studies of ice-ice friction show similar conclusions. A small subset of the existing literature covers ice friction on dissimilar materials at high pressures such as those that would be experienced in ship-ice or ice-structure interactions. However there are no available studies covering ice-ice friction at very high pressures. Most of the former studies have been carried out at low normal pressures (up to $60\text{ }^{\circ}\text{kPa}$) and low velocities (up to 0.1 m/s). However, the interaction between ice in cold ocean engineering generally happens at higher pressures, with crushing at $1\text{-}10\text{ MPa}$ (but possibly up to 70 MPa); and velocities in the range of $0.1\text{ to }3\text{ m/s}$. Hence, the present study aims to improve the understanding of ice-ice friction under higher normal pressure and velocity.

Chapter 3 EXPERIMENTAL SETUP AND PREPARATIONS

Following the conclusions of the literature review, an experimental program has been developed to measure the ice-ice friction coefficient under circumstances where the ice fails initially and then comes to a steady state at relatively high pressures. Considering the pros and cons of former studies and the limitations of conducting experiments in the laboratory, this section explains the apparatus used including the reasons for choosing the method and an explanation of the workings of the apparatus.

3.1 Apparatus Choice

As introduced in the literature review section, different types of apparatus have been previously used for ice friction experiments. The aim of this experiment is to simply mimic the process where one piece of ice would come into contact with another and grind-slide along the contact face of another ice piece. The apparatus needs to provide an ice contact where the pressure is sufficient to cause some crushing failure followed by a period where the force level provides a steady state sliding friction. The study also aims to conduct ice friction experiments at relatively high speed for relatively long duration. Given that this type of experiment requires a relatively long period of contact time and due to the space and cost limit of a laboratory setup, a rotational experimental device is chosen for the tests. It is recognized that a rotational device for relatively long experiments will introduce some experimental compromises. The main one of these is that the contact zone will become worn over time by repeated passes and thus the friction will not be measured on an unblemished ice-ice surface.

Figure 3.1 shows the experimental setup from two angles, including: the bucket, the designed apparatus and ice sample and the ice plate. Figure 3.2 shows the sample pressed against the ice plate by the bucket which is ready for testing.



Figure 3.1: Experimental setup including: the bucket, the designed apparatus, ice sample and the ice plate.



Figure 3.2: Sample pressed by the bucket against the ice plate.

3.1.1 The Turntable

A turntable which was readily available from an ice sample shaper was used as the rotational device for the experiment. The turntable consists of a recessed disc attached to a motor and an arm with its end fixed to the table itself through a hinge. The arm can move in a circular arc in a direction normal to the turntable rotation. The arm is held in place with a jack and it has holes to attach the normal force apparatus, which is described in section 3.1.3. The turntable turns at a speed of 20.5 rpm and the diameter of the recessed disc is 1.156m. (See Fig. 3.3)



Figure 3.3: Turntable arm and pin. (Dagenais, 2013)

3.1.2 The Flat Circular Plate

A metallic flat plate located inside the recessed disc of the turntable to provides a uniform surface on which an ice surface can be prepared (Figure 3.2). This disc-shaped ice surface provides one side of the ice-ice contact. On the other side of the contact, cone shaped ice samples are forced against the ice disc starting with the point of the cone. This provides a contact area that increases as the point of the cone is crushed and abraded under the normal force applied by the apparatus. The ice plate was made as large as possible within the recessed disc in order to test with a range of radii which provides a range of linear velocities, according to the ice cone's radial distance from the center of rotation.

3.1.3 The Normal force apparatus

In order to measure the normal and frictional forces at the ice-ice contact, a device was used to compress the conical ice sample on to the turning plate. It can be mounted on to the radial arm of the turntable apparatus in different positions. This allows the ice samples to change positions for each test along the radial direction. On the other side of the attachment (opposite to the arm), there is a vertical linear bearing. The bearing holds a linear carriage at a fixed distance away from the center of the turntable, while permitting its movement up and down. This allows vertical movement while applying a constant normal force as the ice sample is crushed shorter and shorter on the ice plate as the experiments proceed (Figure 3.5).

On the top of the linear carrier is a metal bucket in which steel pebbles can be placed to generate several weights, up to 1958 N (approx. 200kg or 440lb) including the weight of the bucket (Figure 3.4). The bucket can be lifted by a crane when adding weight to the bucket or installing the ice sample on the bottom of the carriage. A sensor is placed between the bucket and the linear carrier in order to measure the weight of the bucket for calculation of the normal force applied on ice samples.

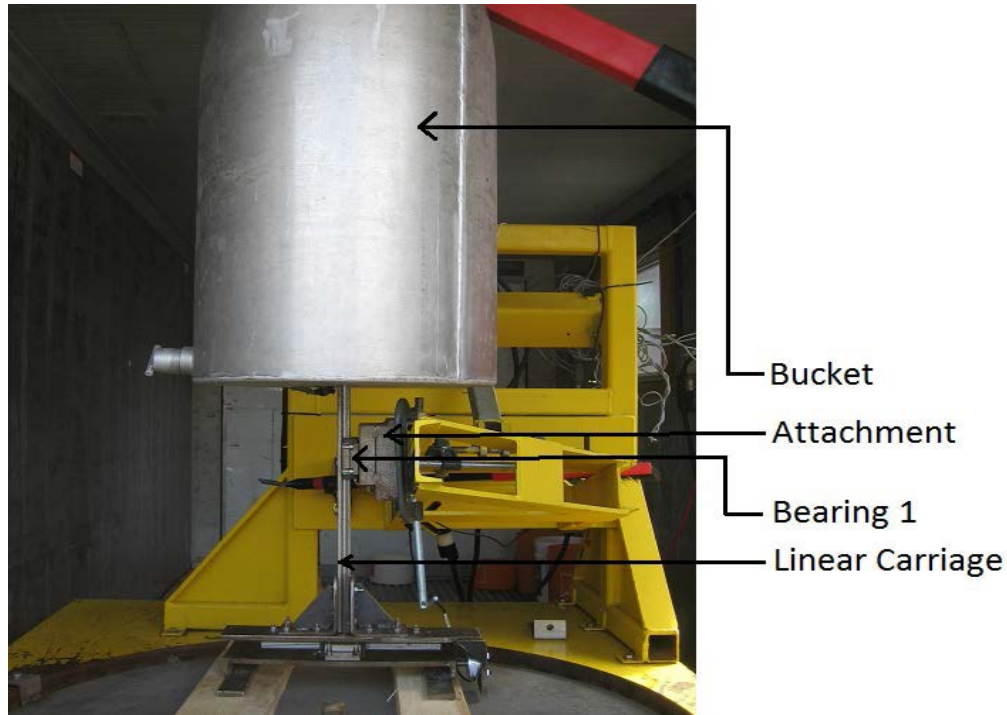


Figure 3.4: Device attach to the turntable. (Dagenais, 2013)

At the bottom of the vertical linear carrier, ice samples are attached to the bottom of the normal force apparatus to be pressed on the ice plate. As shown in Figure 3.4, at the bottom of the linear carrier is an L-shaped part and a fork-shaped part. The L-shaped part has a horizontal linear carriage attached at the bottom and a sensor at the bent end. The fork-shaped part, on which ice samples are fixed, has a linear bearing on the top. The linear bearing holds the carriage to the bottom of the L-shaped part to keep the ice sample at a fixed radial distance away from the center of the turntable while allowing it to move tangentially with the rotational motion. The sensor on the bent end of the L-shaped part restrains the tangential motion and records the frictional force when the ice sample is pushed horizontally by the turning ice plate (Figure 3.6, 3.7). A camera is set up on the L-shaped part to record the test for the calculation of the ice sample weight loss and the contact area during the tests.



Figure 3.5: Device attachment. (Dagenais, 2013)

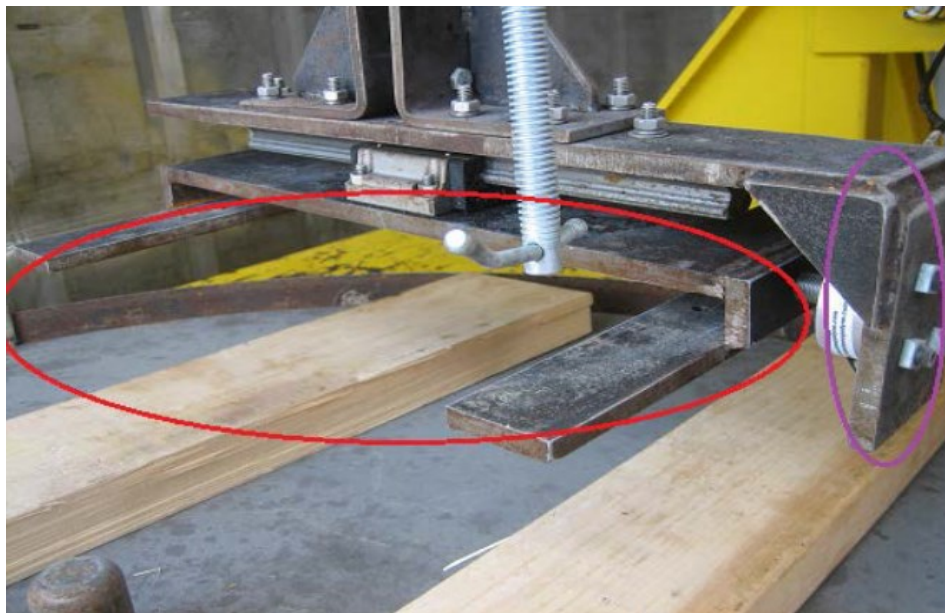


Figure 3.6: Bottom part of setup including fork-shaped part (red circle) and L-shaped part (purple circle). (Dagenais, 2013)

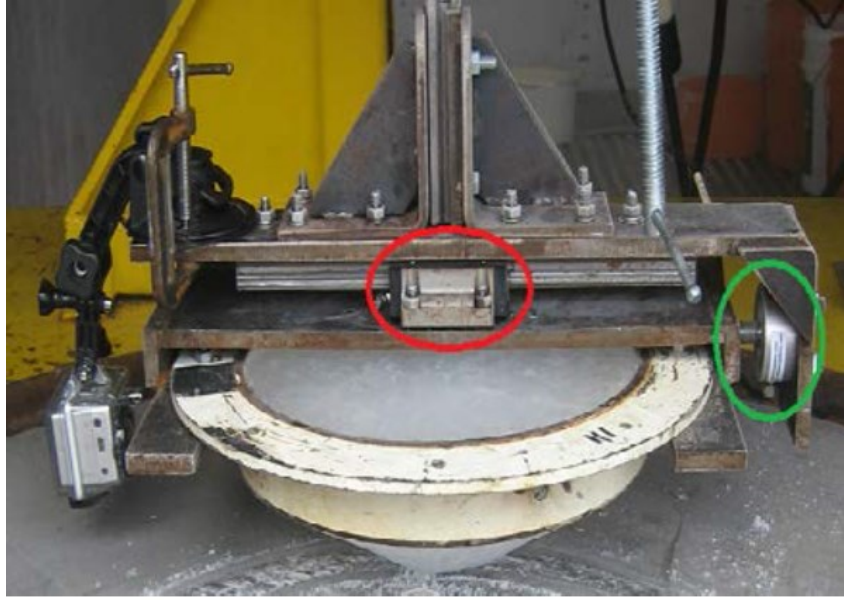


Figure 3.7: Bottom setup holding an ice sample with bearing 2 (red circle) and sensor (green circle). (Dagenais, 2013)

3.1.4 Data Acquisition and Control System

The two force sensors are connected to a data acquisition system to record the data (Figure 3.8).

Every 0.01 second (100Hz), a value is recorded on each channel.



Figure 3.8: Data Acquisition and Control System. (Dagenais, 2013)

3.2 Ice Sample Preparation

Ice sample preparation procedures were designed to produce consistently uniform and repeatable ice samples. As mentioned in the section 2.2, the closest natural ice the test samples represent would be multi-year or iceberg ice, in terms of impurities and micro-structure.

Figure 3.9 shows the thin section of a conical ice sample which prepared following the same procedure as this study.

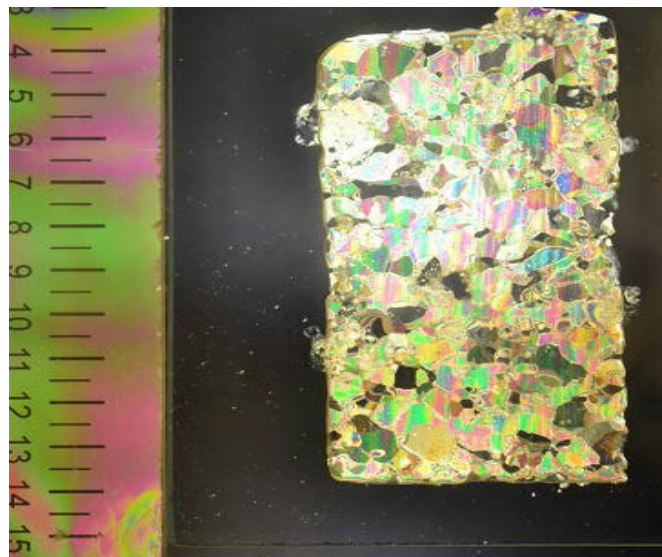


Figure 3.9: Thin section of conical ice sample. (Dragt, 2013)

Producing the ice samples required a number of steps, e.g. water preparation: i.e., distillation, deionization, de-aerating, etc. and preparation of ice seeds, which help to obtain the required micro-structure. Sample production methods are detailed below.

3.2.1 Water preparation

As mentioned before, an iceberg consists of layers of snow formed under very high pressure over thousands of years, this pressure compresses the air in the ice and the ice of icebergs is quite

pure. Multi-year ice contains relatively small levels of impurity due to partial melting and re-freezing cycles. In order to minimize impurities and maintain repeatable and consistent ice samples, the aim of water preparation is to obtain clean, pure water with low air density. In this step, the water was first distilled, then deionized, then de-aerated and finally refrigerated (Manuel, 2012).

3.2.2 Making ice seeds

As mentioned in section 2.2, grained structure is one of the common structures formed in natural ice. Store-bought bags of ice with low mineral count are chopped into ice seeds of proper size (2mm-10mm) in order to simulate the grained structure in natural ice. Figure 3.10, 3.11 shows the ice seeds.



Figure 3.10: Chipped ice prior to sieving. (Manuel, 2012)



Figure 3.11: Chipped ice after sieving. (Manuel, 2012)

3.2.3 Mixing and Freezing the Ice

After the preparation of water and ice seeds is finished, the buckets for the freezing process are prepared and filled, following the "STePS²: Manual of Laboratory Procedures" (Manuel, 2012).

Following figures 3.12-3.16 show the steps of freezing process.



Figure 3.12: Prepared bucket. (Manuel, 2012)



Figure 3.13: Modified freezer cover with insulators. (Manuel, 2012)

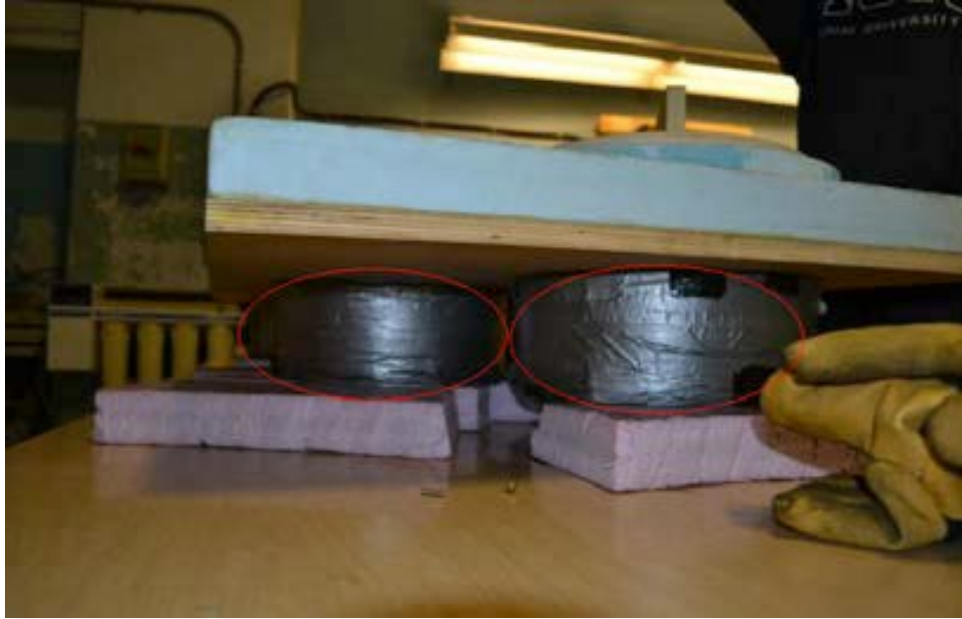


Figure 3.14: Side view of modified freezer cover and insulators (circled in red). (Manuel, 2012)



Figure 3.15: Bucket filled with ice seeds. (Manuel, 2012)



Figure 3.16: Water pouring into the bucket filled with ice seeds. (Manuel, 2012)

3.2.4 Sample Shaping

After the cylindrical ice samples are prepared and fully frozen, they are shaped into cones with a designed angle of 30 degrees, following the procedures of the "STePS²: Manual of Laboratory Procedures". The shaper used for the preparation is shown in Figure 3.17.



Figure 3.17: Shaper including jack (circled in red), blade (circled in black), ice sample (circled in green) and plug (circled in orange). (Manuel, 2012)

3.3 Ice plate preparation

An ice plate was specifically made in this study to provide one of the contacting ice surfaces in the tests. The preparation of the ice plate is introduced in this section.

3.3.1 Mixing and freezing the ice

The same water and chipped ice seeds which are used for preparing samples are used to form an ice plate on the turntable so that the ice plate and samples would have the same micro-structure for the ice-ice friction experiments.

The de-aerated water is cooled down to 0 degrees Celsius before the chipped ice seeds were laid on the ice plate in a layer about 2 cm thick. The surface is flattened using a bubble-level as screed. Then at an ambient temperature of -10°C , water is poured slowly into the ice seed layer until the space between ice seeds is filled. After that the ice plate is allowed to freeze in the cold room at -10°C .

3.3.2 Ice plate surface smoothing

The surface of the ice plate was smoothed in order to minimize the effect of surface roughness on the frictional coefficient. After the plate was formed, a steel panel was warmed up by an iron to melt the rough surface of the formed ice plate. About a third thickness of the surface layer of ice seeds were melted and the melt water filled the rough surface. The warmed steel smoothing plate was moved manually and continuously on the surface to make sure the whole plate surface was smoothed evenly. Failure to move the steel smoothing plate continuously would cause the steel smoothing plate to sink into the ice plate, which leads to an unusable ice surface. After smoothing, the ice plate is left in the cold room to let the surface refreeze. Finally, the surface of

the smoothed ice plate was examined with a level to make sure that the surface was flat. Figure 3.18 shows the prepared ice plate ready for testing.



Figure 3.18: Prepared Ice Plate and Ice Sample Ready for testing.

Chapter 4 EXPERIMENTAL METHOD

Design of experiment method is used for this study to collect data at different levels of different controlled variables and analyze the results. Multilevel categorical full factorial design was chosen for experimental design. The following elements of the research are introduced in this section: the chosen range of the studied factors, testing plan and testing procedures.

4.1 Factors Studied

In conducting the experiments, certain variables were controlled as part of the study and other variables were not controlled but were monitored as part of the experiments. The primary controlled variables were velocity and normal force. Velocity was varied between tests but held constant for each test. Normal force was either held constant or varied during a test. The range of velocity varied from 0.47m/s to 0.8m/s and the range of normal forces varied from 526N to 1888N with pressure as high as to 6MPa. Other factors such as the ice surface roughness and the contact area that developed as the ice was abraded were observed during or after the tests.

4.1.1 Velocity

The turntable has an average turning speed of 20.5 rpm. The normal force apparatus was located at 3 locations along the radial direction away from the center of the rotating ice plate, in order to achieve the three linear speed levels. They were 0.47 m/s, 0.63 m/s and 0.8 m/s.

4.1.2 Normal force

Normal force was applied by filling the hopper located above the conical ice sample with steel pellets. Taking into consideration the load limit of the apparatus and the practicality of carrying out the tests, four levels of weight, from 454N (100lb), 908N (200lb), 1362N(300lb) to 1816N (400lb) of the pellet ballast, were chosen. The normal force includes the steel pellets in the

hopper, the weight of ice sample holder and sample and the supported apparatus, therefore, 100lb of weight in the hopper corresponds to approximately 526N of normal force applied at the contact face, and 400lb corresponds to 1888N.

4.1.3 Tests with Changing Normal Force

Additional tests were carried out at each speed and weight level by adding 2lb weight every 10 seconds to the bucket over the duration of the test, in order to find out if increasing weight would have an effect on the ice sample crushing and ice friction.

4.2 Experimental Design

A test plan was made according to the design of the experiment to provide suitable variations and combinations of each level of each factor:

- Velocity: Low (0.47m/s), Medium (0.63m/s), High (0.8m/s) within the available range
- Initial normal force: 454N, 908N, 1362N, 1816N
- Changing weight: Yes, No

One level of each factor is selected to combine with one level of other factors including all the possibilities. A set of 24 tests experiment was designed. One replicate test was planned for each test in case of failure and for the sake of comparison. As shown in Table 4.1, 48 tests in total were planned for the experiment.

Table 4.1: Test plan.

Test number(#)	Initial normal force (N)	Normal force change (y/n)	Velocity level(m/s)
1	454	n	0.47
2	454	n	0.47
3	454	y	0.47
4	454	y	0.47
5	454	n	0.63
6	454	n	0.63
7	454	y	0.63
8	454	y	0.63
9	454	n	0.8
10	454	n	0.8
11	454	y	0.8
12	454	y	0.8
13	908	n	0.47
14	908	n	0.47
15	908	y	0.47
16	908	y	0.47
17	908	n	0.63
18	908	n	0.63
19	908	y	0.63

Table 4.1: Test plan. (Continued from previous page)

Test number(#)	Initial normal force (N)	Normal force change (y/n)	Velocity level(m/s)
20	908	y	0.63
21	908	n	0.8
22	908	n	0.8
23	908	y	0.8
24	908	y	0.8
25	1362	n	0.47
26	1362	n	0.47
27	1362	y	0.47
28	1362	y	0.47
29	1362	n	0.63
30	1362	n	0.63
31	1362	y	0.63
32	1362	y	0.63
33	1362	n	0.8
34	1362	n	0.8
35	1362	y	0.8
36	1362	y	0.8
37	1816	n	0.47
38	1816	n	0.47

Table 4.1: Test plan. (Continued from previous page)

Test number(#)	Initial normal force (N)	Normal force change (y/n)	Velocity level(m/s)
39	1816	y	0.47
40	1816	y	0.47
41	1816	n	0.63
42	1816	n	0.63
43	1816	y	0.63
44	1816	y	0.63
45	1816	n	0.8
46	1816	n	0.8
47	1816	y	0.8
48	1816	y	0.8

4.3 Testing Procedures

Each test was performed using the same standardized procedure. The steps in the procedure were:

Record weight of shaped ice sample

The weight of the cone shaped ice sample is measured on an electronic scale, and recorded for use in later calculations.

Connect sensors to DAC (Data Acquisition System)

5 meter long cables are used to connect the apparatus sensors in the cold chamber to the DAC in the laboratory outside the cold chamber.

Start reading data from both sensors

Start reading data from the sensors to make sure the test is set properly. Adjust the weight of the bucket to the required weight level of the test as measured by the bucket sensor and confirm that the reading of the friction force sensor is zero.

Set test ready

Set up the sample and the camera. Lower the lifting apparatus slowly until full weight of the bucket is pressing the sample against the ice plate.

Check reading on DAC

After setting up the test, the frictional force should be 0 and the normal force should be the weight level that is planned for the test.

Start testing

Start recording data on DAC and turn on the camera before turning on the turntable.

During testing

Lower the lifting apparatus as ice sample is crushed so that the full weight of the bucket continues on the ice sample. Add a 2lb weight every 10 seconds (for the changing normal weight tests). The weight is added manually by putting the pellets gently into the bucket.

Ending testing

Turn off the turntable after 5 minutes of testing. For changing weight tests, 60lb of weight is added to the total weight in the end. Stop and remove the camera. Stop recording data and lift the bucket up. Take off the sample. Save data and video recorded during tests.

Preparing for next test

The ice plate surface needs to be smoothed for the next test, because the crushing of sample leaves a track on the plate and the initial roughness of the surface needs to be set same for each

test. Before smoothing the surface, ice chips from ice sample crushing need to be cleaned off the surface of the ice disk to aid in smoothing the ice plate surface.

4.4 Calculations

The data collected for all the tests are the normal force from the weight bucket and the frictional force at every 0.01s. Calculation of the basic results from the tests is introduced in this section.

The calculation of data is adapted from methods presented in Dagenais (2012), because the test is carried out on the same apparatus. In order to illustrate the calculation procedure we can take test 24 (which is changing weight, with 908N bucket normal force, at 0.8m/s) as an example. The cone ice sample weight is initially measured as 7.464kg. At 200.01 seconds the readings from the bucket sensor is 232.659 (lb), and 8.316124 (lb) from the friction force sensor. The friction coefficient of test 24 at 200.01seconds is calculated in the following sections to illustrate the method applied to all tests in the study.

4.4.1 Conversion of DAC output

The results from DAC output are two time series waves of data measured from the bucket and friction force sensor in pound force (lbf). The data from the “bucket sensor” is converted to kilogram force (kgf) in order to calculate the total normal force applied on the ice sample. The data from the “friction force sensor” is also converted to newton (N) accordingly in order to calculate the frictional coefficient. For the ice sample of test 24 at 200.01 seconds:

Bucket sensor 232.659 lbf = 105.754 kgf

Friction force sensor 8.316124 lbf = 81.6 N

4.4.2 Ice loss weight

Figure 4.1 is a snapshot from the video recording of a test. As shown, the top of ice sample is crushed and rubbed off, and the amount of the ice loss varies due to the changing of the parameters.

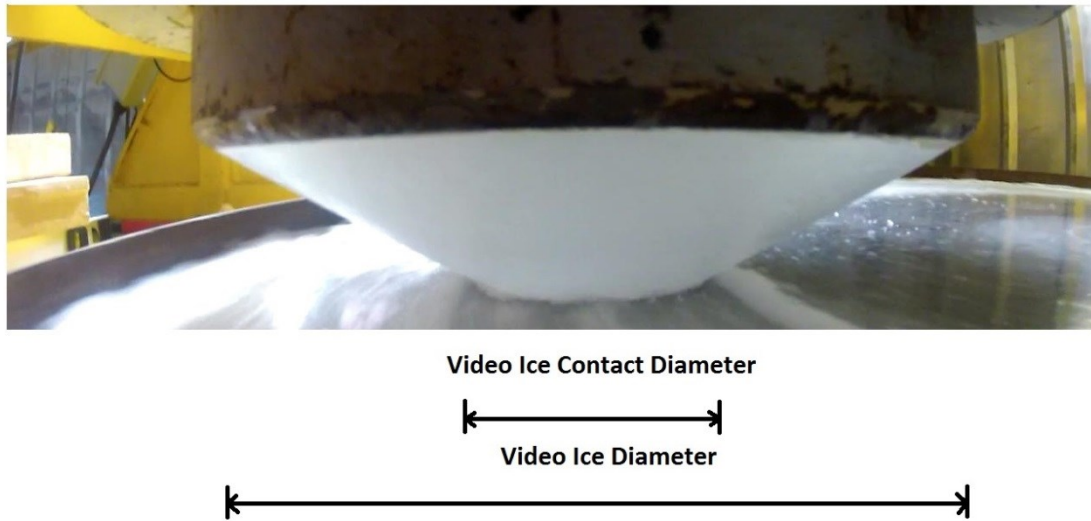


Figure 4.1: Video ice contact diameter and video ice diameter.

Since the image of the ice sample from the video is proportional to the object, with the diameter measured from video image, the diameter of the contact area can be calculated as follows.

$$D_C = D_S \frac{D_{Cv}}{D_{Sv}} \quad (1)$$

D_C = Real Ice Contact Diameter

D_S = Real Ice Sample Diameter

D_{Cv} = Video Ice Contact Diameter

D_{Sv} = Video Ice Sample Diameter

While the ice sample weight changes with time due to grinding, and it is possible to calculate this change from the video record of the contact. It was found that the change in weight was an insignificantly small portion of the total weight applied to the contact face. On this basis it was

decided to just use the average weight of the ice sample with the mean calculated at 180 seconds chosen as the effective ice sample weight.

For Test 24:

$$D_C = 0.26 \times 7.9 / 24.5 = 0.08387 \text{ m}$$

Ice Lost Mass = Ice density \times Ice Lost Volume

$$\begin{aligned} &= \rho \times \quad \quad \quad (2) \\ &= 916.76 \times \frac{1}{3} \times 0.57735 \times 0.08387 \times 0.08387 \times 0.08387 \times 3.1415926 \\ &= 0.327 \text{ kg} \end{aligned}$$

4.4.3 Extra mass calculation

Extra mass besides the bucket and ice sample weight needs to be summed up to calculate the total normal force applied on the ice sample. These weights which are constant in the tests are shown below.

Mass of Camera: $m_1 = 0.397 \text{ kg}$

Mass of C-Clamp Holding Camera in Place: $m_2 = 0.198 \text{ kg}$

Mass of Railing and L-Shaped Part: $m_3 = 8.669 \text{ kg}$

Mass of Forklift Part: $m_4 = 5.673 \text{ kg}$

Extra Mass = $m_1 + m_2 + m_3 + m_4 = 0.397 \text{ kg} + 0.198 \text{ kg} + 8.669 \text{ kg} + 5.673 \text{ kg} = 14.937 \text{ kg}$

4.4.4 Ice sample's real normal force

The ice sample's real normal force is calculated as the total weight (kgf). For test 24:

Total Mass = Bucket Mass + Extra Mass + Ice Sample Mass - Ice Lost Mass

$$\begin{aligned} &= 105.754 \text{ kg} + 14.937 \text{ kg} + 7.464 \text{ kg} - 0.327 \text{ kg} \\ &= 126.52 \text{ (kgf)} = 1240.7 \text{ (N)} \end{aligned}$$

4.4.5 Ice sample friction coefficient

After the total normal force is calculated, with the frictional force, the frictional coefficient of the ice sample against ice plate at every 0.01 second can be calculated as follows:

Friction Coefficient=Frictional force (N) / Total normal force (N)

Accordingly the friction coefficient of test 24 at 200.01 seconds is calculated as:

$$81.6\text{N}/1240.7\text{N} = 0.02988$$

4.4.6 Rotational velocity conversion

As mentioned previously the turning table is turning at an unregulated speed averaging 2.15 rad/sec. According to the radius chosen for each speed level, the relative linear speed of the ice sample against the ice plate can be calculated as follows:

$$v = \omega \times r \tag{3}$$

Where: v is the linear velocity in m/s

ω is the angular velocity in radians per second = $2\pi * \text{rpm}/60$

r is the radius in meters

Figure 4.2 shows the radius that is chosen for each speed level.

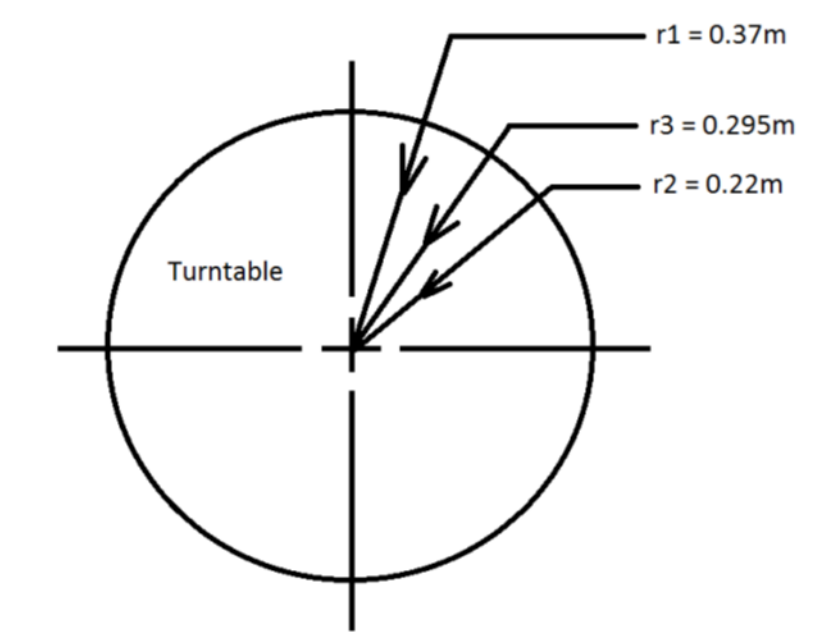


Figure 4.2: Radiuses for Different Velocity Level. (Dagenais, 2013)

Accordingly, the average linear velocity of test 24 is:

$$v = \omega \times r = 2.15 \times 0.37 = 0.8 \text{ m/s}$$

Chapter 5 RESULTS

As introduced in the previous section, after the friction coefficient was calculated, raw data of the results of each test was ready to be analyzed. The technical graphing and data analysis were performed with the software Igor Pro.

5.1 Smoothing method

As all the ice experiment data show considerable oscillation at relatively high frequencies, the test results shows some level of randomness and unsteadiness. Much of this is thought to arise from vibrations in the experimental apparatus. Figure 5.1 and 5.2 show the raw data from two tests.

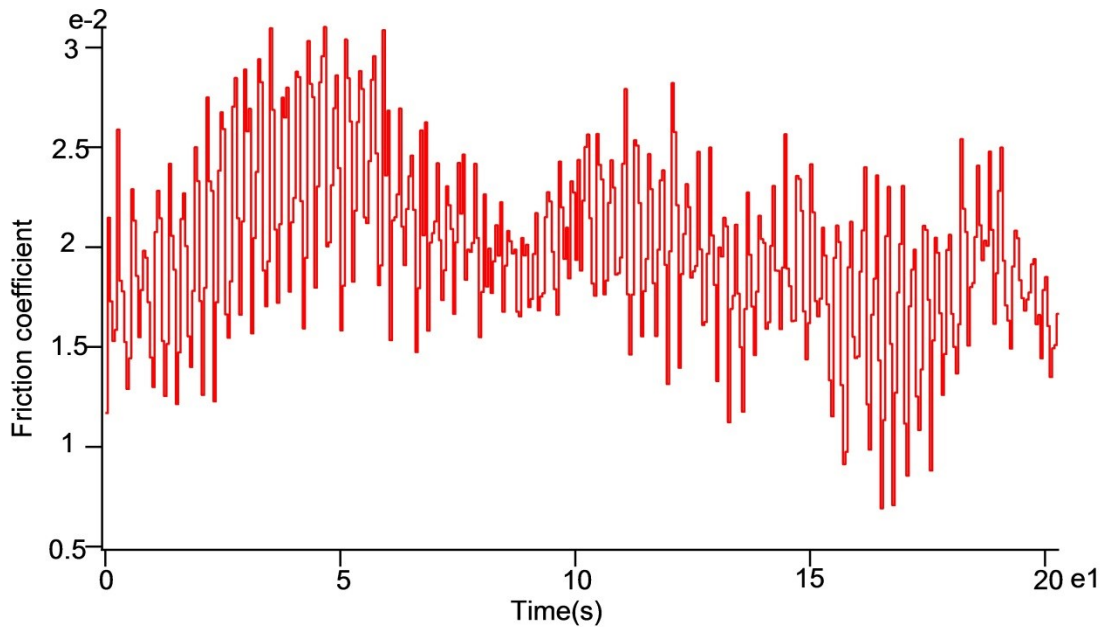


Figure 5.1: Raw data plotting of test 9.

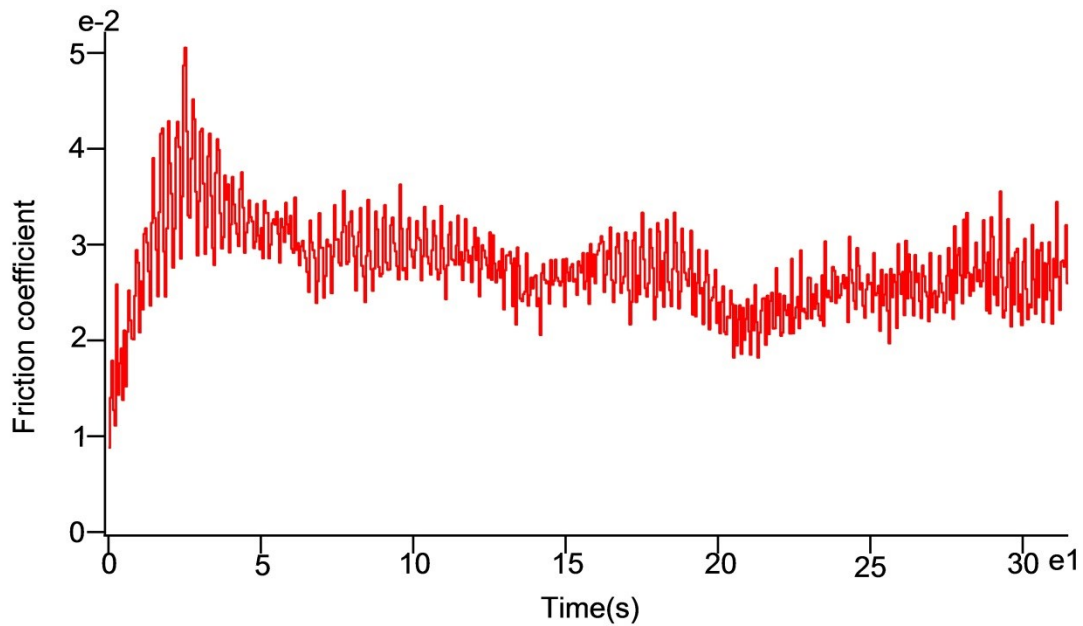


Figure 5.2: Raw data plotting of test 31.

As shown in the raw data, the friction coefficient varies through the test with both high frequency oscillations and lower frequency trends. “Box” smoothing method is used to smooth the raw data. Box smoothing is similar to a moving average, except that an equal number of points before and after the smoothed value are averaged together with the smoothed value. The advantages of the method are that it provides a clearer visual picture of the data curve trend and it can show what the trend is.

As shown in Figures 5.3 and 5.4, maximum and minimum of the ice friction coefficient, and the trends are easier to identify from the results after smoothing. And generally, the curves can be separated into 3 stages according to the trends. In stage 1, the friction coefficient rises to the peak value, and then decreases in stage 2; and then vibrates and decreases to a certain range in stage 3.

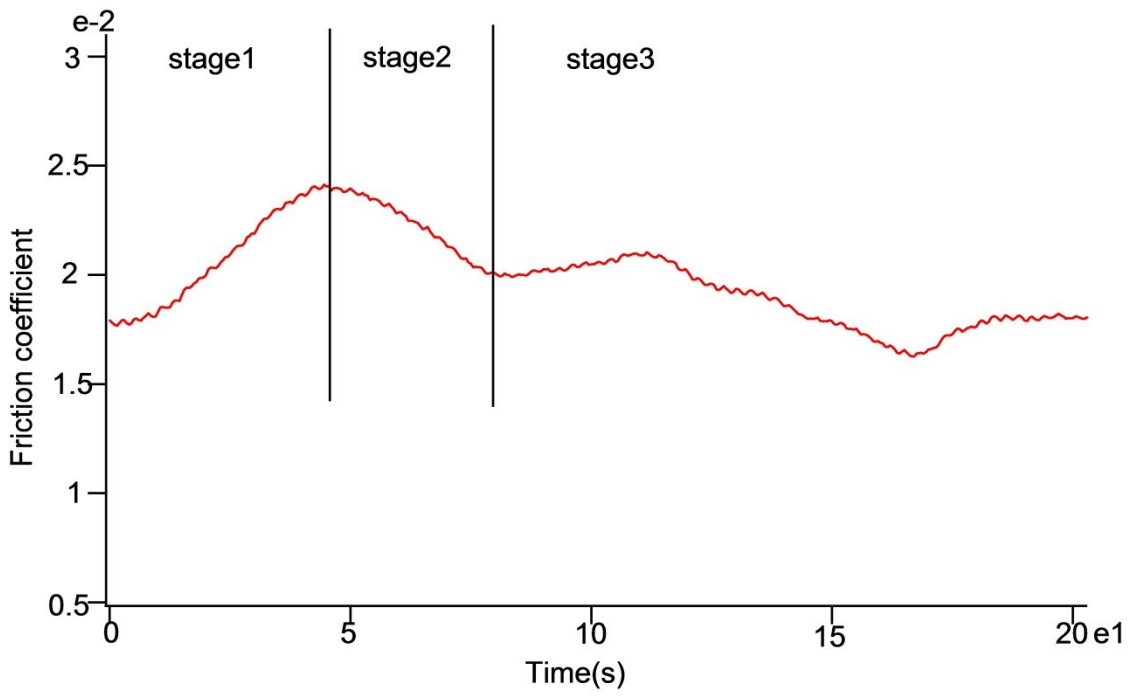


Figure 5.3: Smoothed raw data plotting of test 9.

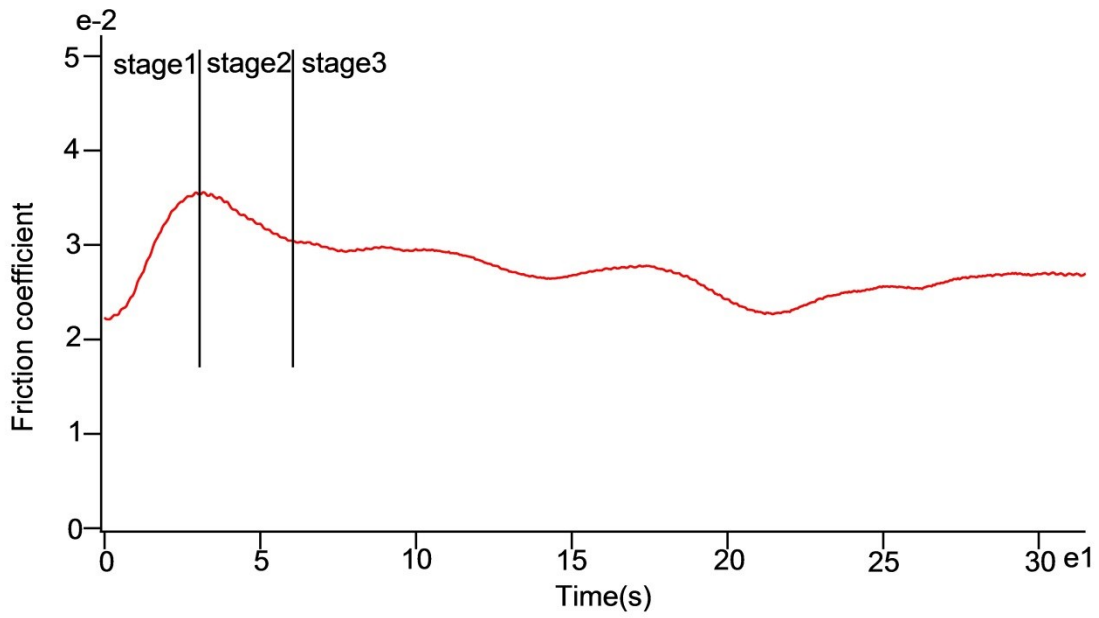


Figure 5.4: Smoothed raw data plotting of test 31.

5.2 Plotting of the results

Although the results vary among tests, certain general trends can be identified. For each test, the ice frictional coefficient first rises sharply to the peak, then decreases and settles down to within a certain range of values.

If we compare the evolution of friction coefficient to the corresponding video records of the tests, we can identify 3 stages, the initial stage, the peak and the post-peak stage. Each stage corresponds to a different physical mechanism. At the initial stage, the friction coefficient rises as the ice cone is both crushed and abraded under relatively high pressure. At this stage the friction is thought to be increasing, because of the rapid ice crushing increases the roughness of contact surface. The slope of the curve at this stage indicates how quickly the contact surface roughness increases.

The second stage of the frictional behavior is where the friction coefficient reaches a maximum. At this peak stage, the friction coefficient reaches maximum and subsequently starts to decrease. As the contact area increases, the normal pressure decreases. The peak is thought to represent the point at which the pressure falls below the crushing pressure and the ice is no longer generating a lot of ice chips and rubble in the contact area. The roughness of the contact surface starts to decrease and the lubricant effects of conventional non-crushing ice friction are introduced in between the surfaces (i.e. effects of frictional heating and the disordered surface layer). The maximum friction coefficient indicates the peak of the roughness of the ice surface when ice friction is combined with ice crushing.

For the post-peak steady state stage, the friction coefficient decreases and settles down within a certain range. The roughness of the contact surfaces decreases as the contact surfaces continue a lower rate of abrading combined with the known lubricant effects at the contact interface.

Eventually it is expected that the friction coefficient would settle in a certain range when the temperature of the contact surface reaches equilibrium and the abrasion effects at the contact surface settle down to a very low rate. For some tests, the friction coefficient settled within the test; for others, the friction coefficient was still decreasing at the end of the test reflecting that equilibrium of temperature or abrasion or both had not been reached.

The following figure (5.5) is extracted from the video. It shows the ice sample at the peak friction coefficient point which marks the transition from the stage of peak to the stage of settling from the smoothed data. Although the contact area continues growing afterward, the rate of increase is much slower and the ice friction coefficient starts to decrease. Figure 5.6 shows the ice contact at the later stage. Figure 5.7 shows the sequence pictures of 30s testing duration around the peak friction point.



Figure 5.5: Ice cone of test 29 at 45s (Peak stage).



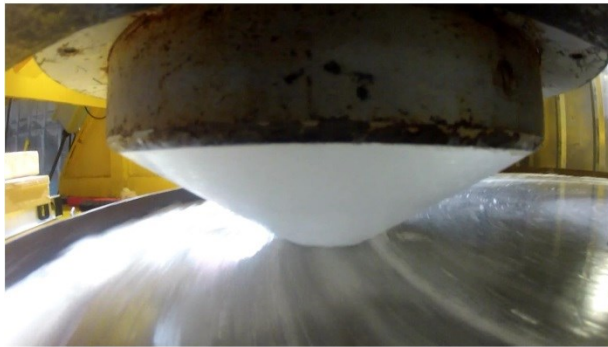
Figure 5.6: Ice cone of test 29 at 270s (Steady state stage).



Ice cone of test 29 at 25s



Ice cone of test 29 at 35s



Ice cone of test 29 at 45s



Ice cone of test 29 at 55s

Figure 5.7: Sequence picture of test 29 around peak stage.

If we compare the contact area of ice cone at 55s and 270s to the contact area at 25s, we can see that: approximately, in the first 30s, the contact area increased 100%, but for 245s the contact area only increased 300%. That means the rate of contact area increase is much higher in the early stage of testing.

5.2.1 Deriving Significant Parameters

Rather than just look at the ice-ice friction coefficient as a single dependent variable of interest, it was decided to take the three parameters that defined the common characteristics of each of the test data traces and assess how each of these parameters changed with the changes in the independent variables. The three defined dependent variables were then: a) the slope of the friction coefficient curve during the initial crushing stage, b) the peak measured friction coefficient that defined the transition from ice crushing to non-crushing friction and c) the post-crushing average of the ice friction coefficient. The method of derivation of each of these is described in the following sections.

5.2.1.1 Slope of the coefficient change

The following figure (5.8) shows the initial stage of one of the tests. All the data are similar for the initial stage, in that the slope of the coefficient change would increase at the beginning and decrease as the friction coefficient approaches the peak value. In between the beginning and the end phase of the initial stage, the rate of increasing of the frictional coefficient is relatively stable.

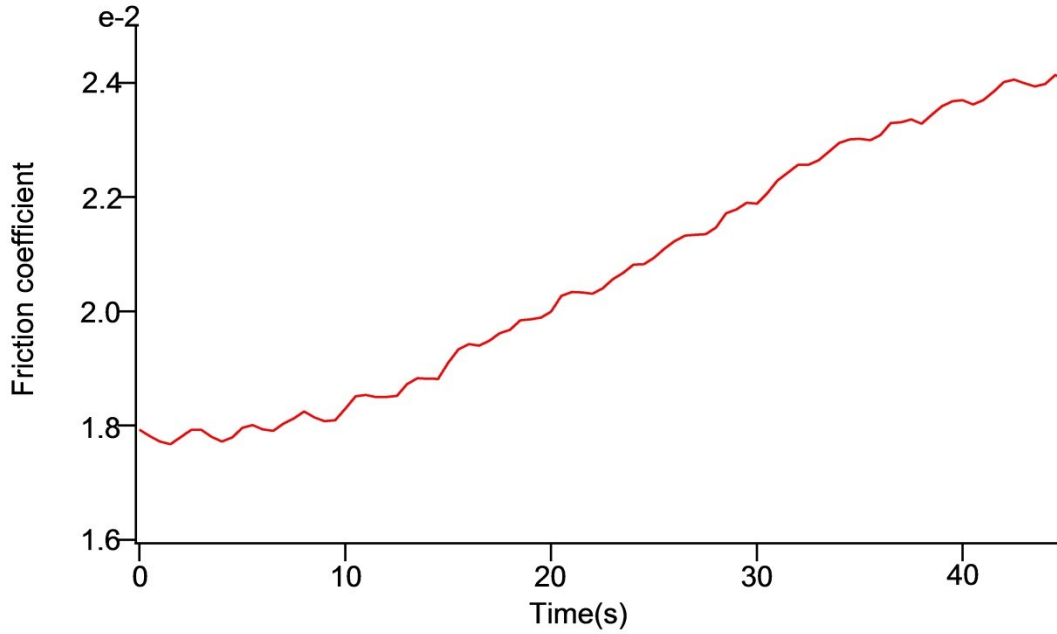


Figure 5.8: *The initial stage of test 9.*

As shown in the following figure (5.9), the beginning and the end phase of the initial stage are edited out before fitting the stable phase of slope of changing (red) with a line (blue). The slope of the fitted line is used to represent the relatively steady increasing of the friction coefficient in the initial stage. This slope indicates how the crushing mechanism causes the ice surface roughness to increase under the different conditions of test velocity and applied normal force, or pressure.

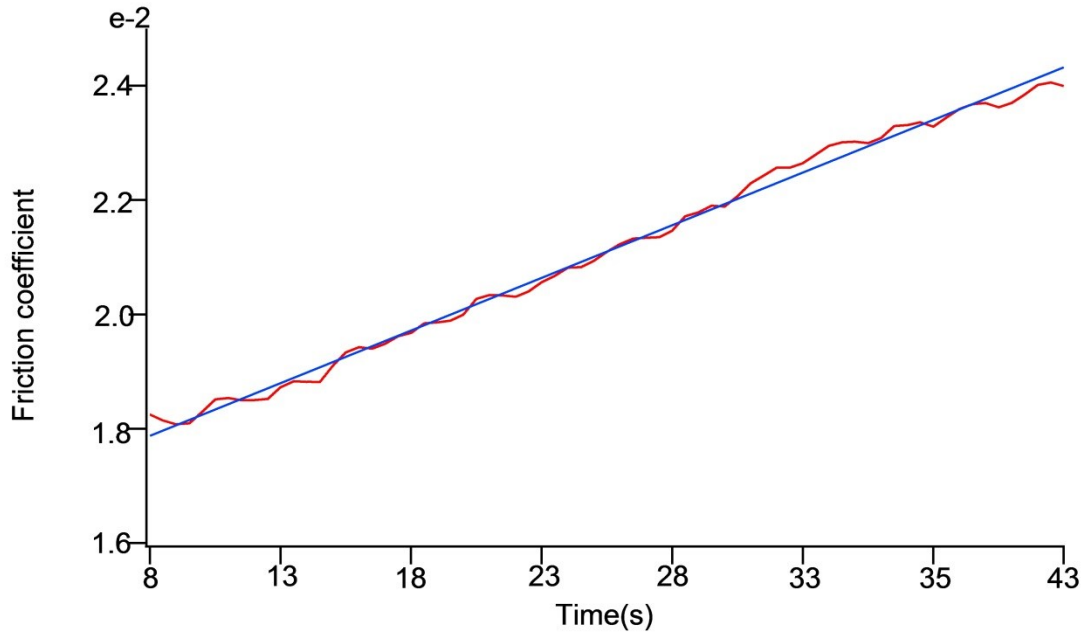


Figure 5.9: Slope of changing fitted with a line (in blue)

5.2.1.2 Peak friction coefficient

The peak friction coefficient is the peak value of the ice friction coefficient in the testing process. It can be easily obtained through the software, i.e. Igor Pro (See Figure 5.10). The peak value indicates how high the ice friction coefficient can reach as the crushing mechanism roughens the surface.

5.2.1.3 Settled friction coefficient

The post-crushing settled friction coefficient is a value derived from the later stage of the tests to show how the ice friction coefficient decreases as the abrading mechanism smoothens the surfaces. In the steady state stage, the ice friction is either settled in a certain range, or in many cases it is decreasing but still varies due most probably to not reaching equilibrium. Figure 5.10 shows the trend for most of the tests: the friction coefficient drops to a point then rises a bit and

then oscillates in a certain range. In this case, the lowest value of the ice friction coefficient in the steady state stage is derived as settled friction coefficient.

In the case of the initial rise of friction coefficient, and the identified peak value, these characteristics were reasonably consistent and evident in each of the experiments. The later stage where the friction coefficient was either steady with oscillations or declining with oscillations was not consistent in each experimental case. Thus the analysis and conclusions for this phase are not as strongly based as that for the other two outputs.

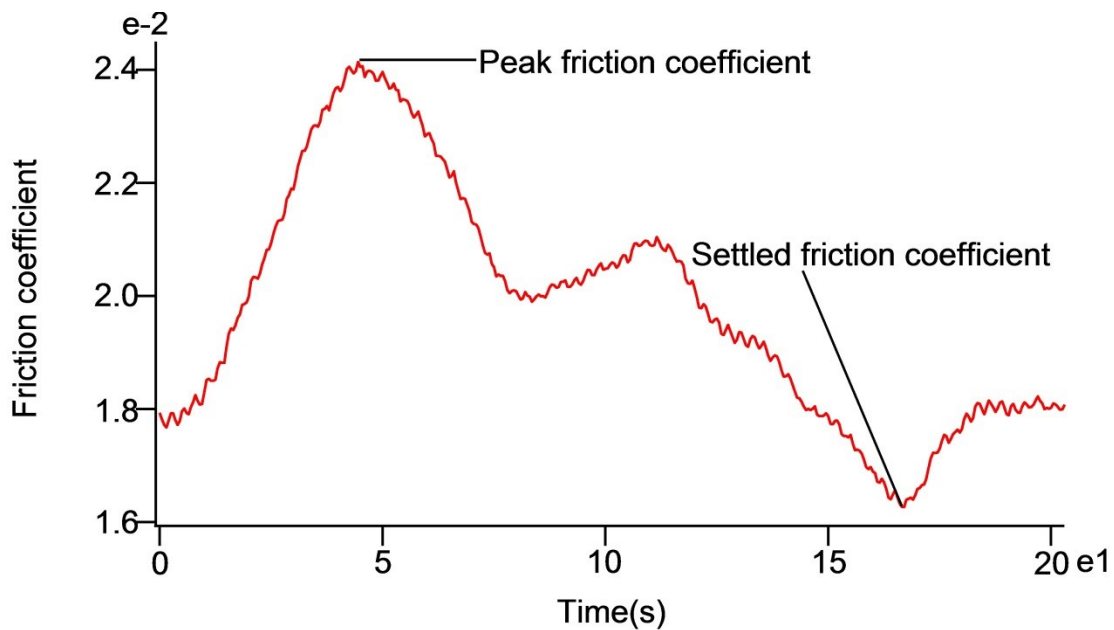


Figure 5.10: General case of deriving Peak FC and Settled FC.

In a few tests the friction coefficient behaved differently as in Figures 5.11: the friction coefficient was still decreasing by the end of the test. In these cases, the settled friction coefficient is derived manually based on the trend of the data get a reasonable value to represent the steady-state stage.

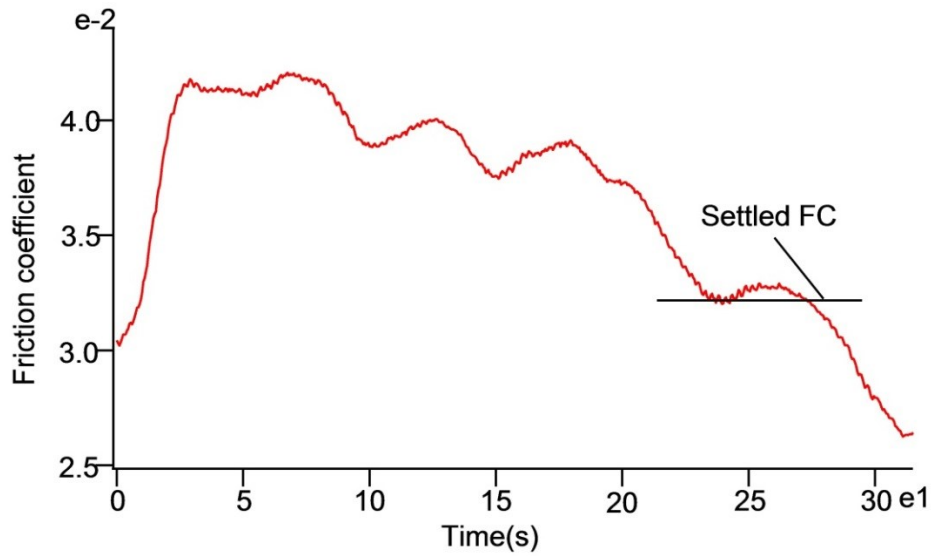


Figure 5.11: Deriving of settled FC for one of irregular cases

Table 5.1 is the data of three derived parameters rounded to three significant figures.

Table 5.1: The value of three derived parameters for all the tests.

Test (#)	Initial normal force(N)	Normal force change(y/n)	Velocity (m/s)	Changing slope(1/s)	Peak FC	Settled FC
1	454	n	0.47	5.00E-004	2.95E-002	1.60E-002
2	454	n	0.47	6.45E-004	3.02E-002	1.50E-002
3	454	y	0.47	4.92E-004	3.00E-002	1.72E-002
4	454	y	0.47	6.78E-004	3.39E-002	1.75E-002
5	454	n	0.63	6.21E-004	3.79E-002	2.60E-002
6	454	n	0.63	3.15E-004	3.13E-002	1.95E-002

Table 5.1: The value of three derived parameters for all the tests. (Cont'd from previous page)

Test (#)	Initial normal force(N)	Normal force change(y/n)	Velocity (m/s)	Changing slope(1/s)	Peak FC	Settled FC
7	454	y	0.63	4.54E-004	4.27E-002	2.60E-002
8	454	y	0.63	5.08E-004	3.99E-002	2.40E-002
9	454	n	0.8	1.84E-004	2.41E-002	1.63E-002
10	454	n	0.8	4.75E-004	2.69E-002	1.89E-002
11	454	y	0.8	2.65E-004	2.55E-002	1.58E-002
12	454	y	0.8	3.69E-004	2.29E-002	1.34E-002
13	908	n	0.47	3.41E-004	4.13E-002	2.30E-002
14	908	n	0.47	6.10E-004	3.78E-002	2.68E-002
15	908	y	0.47	6.43E-004	4.17E-002	3.33E-002
16	908	y	0.47	4.82E-004	3.51E-002	2.15E-002
17	908	n	0.63	7.35E-004	4.25E-002	2.96E-002
18	908	n	0.63	6.30E-004	4.11E-002	2.32E-002
19	908	y	0.63	5.13E-004	3.47E-002	2.20E-002
20	908	y	0.63	5.97E-004	3.77E-002	2.53E-002
21	908	n	0.8	2.39E-004	3.07E-002	1.81E-002
22	908	n	0.8	1.80E-004	2.80E-002	1.72E-002
23	908	y	0.8	4.06E-004	3.29E-002	2.23E-002
24	908	y	0.8	1.91E-004	3.50E-002	1.87E-002

Table 5.1: The value of three derived parameters for all the tests. (Cont'd from previous page)

Test (#)	Initial normal force(N)	Normal force change(y/n)	Velocity (m/s)	Changing slope(1/s)	Peak FC	Settled FC
25	1362	n	0.47	5.59E-004	4.48E-002	2.60E-002
26	1362	n	0.47	5.85E-004	4.43E-002	3.35E-002
27	1362	y	0.47	6.90E-004	4.21E-002	3.20E-002
28	1362	y	0.47	5.08E-004	3.58E-002	2.85E-002
29	1362	n	0.63	4.07E-004	5.00E-002	3.91E-002
30	1362	n	0.63	3.80E-004	3.93E-002	1.94E-002
31	1362	y	0.63	1.09E-004	3.59E-002	2.56E-002
32	1362	y	0.63	7.12E-004	3.56E-002	2.28E-002
33	1362	n	0.8	1.52E-004	3.24E-002	2.10E-002
34	1362	n	0.8	4.52E-004	3.02E-002	2.03E-002
35	1362	y	0.8	4.71E-004	2.96E-002	2.04E-002
36	1362	y	0.8	4.32E-004	2.63E-002	1.82E-002
37	1816	n	0.47	2.70E-004	4.33E-002	2.80E-002
38	1816	n	0.47	6.65E-004	4.02E-002	2.80E-002
39	1816	y	0.47	5.15E-004	4.96E-002	2.70E-002
40	1816	y	0.47	5.40E-004	4.02E-002	3.23E-002
41	1816	n	0.63	5.30E-004	3.83E-002	2.55E-002

Table 5.1: The value of three derived parameters for all the tests. (Cont'd from previous page)

Test (#)	Initial normal force(N)	Normal force change(y/n)	Velocity (m/s)	Changing slope(1/s)	Peak FC	Settled FC
42	1816	n	0.63	5.55E-004	4.10E-002	3.00E-002
43	1816	y	0.63	6.91E-004	4.17E-002	3.04E-002
44	1816	y	0.63	5.52E-004	3.87E-002	2.63E-002
45	1816	n	0.8	3.17E-004	3.07E-002	2.11E-002
46	1816	n	0.8	3.10E-004	3.32E-002	2.41E-002
47	1816	y	0.8	3.70E-004	3.09E-002	1.96E-002
48	1816	y	0.8	2.75E-004	2.66E-002	1.45E-002

5.2.2 Constant force tests

Figures 5.12-5.15 show results of constant force tests in different weight levels. Different velocity levels are shown in different colors. For each test condition, there were two tests planned for comparison and in case of failure. Because there are some irregular cases, the better one of each test condition is chosen for display.

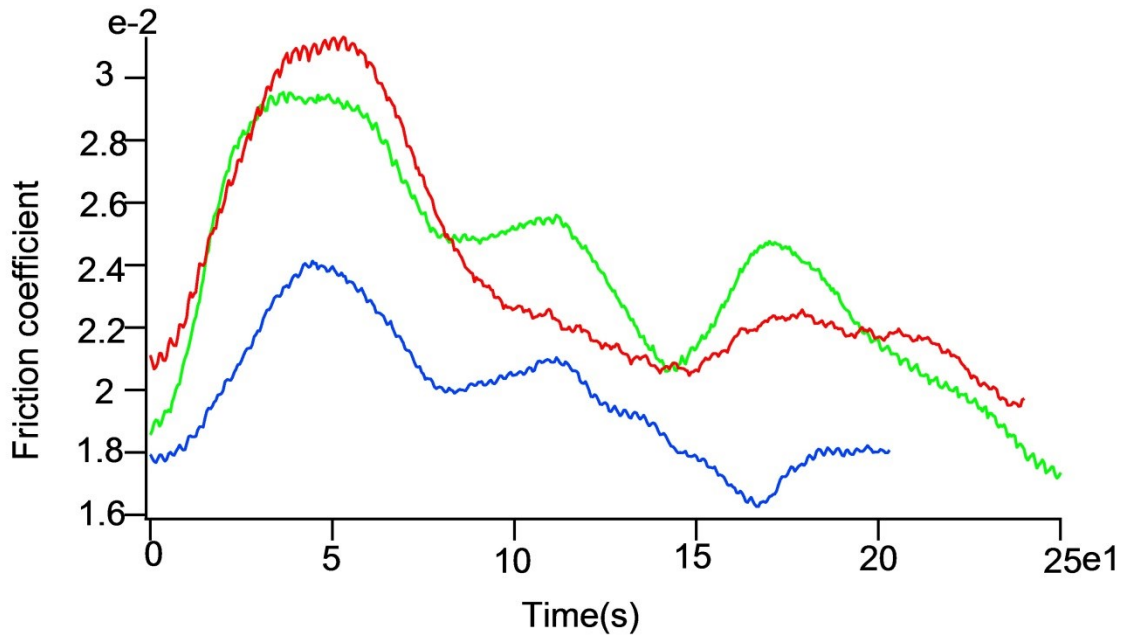


Figure 5.12: FC of 454N normal force tests. Green, low velocity (0.47m/s); red, medium velocity (0.63m/s); blue, high velocity (0.8m/s).

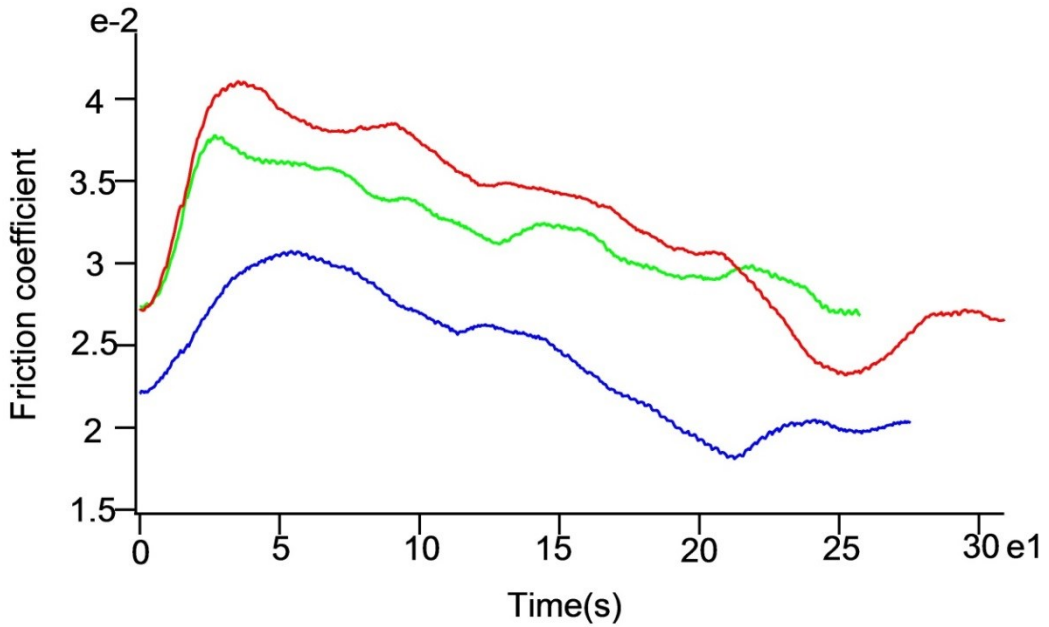


Figure 5.13: FC of 908N normal force tests. Green, low velocity (0.47m/s); red, medium velocity (0.63m/s); blue, high velocity (0.8m/s).

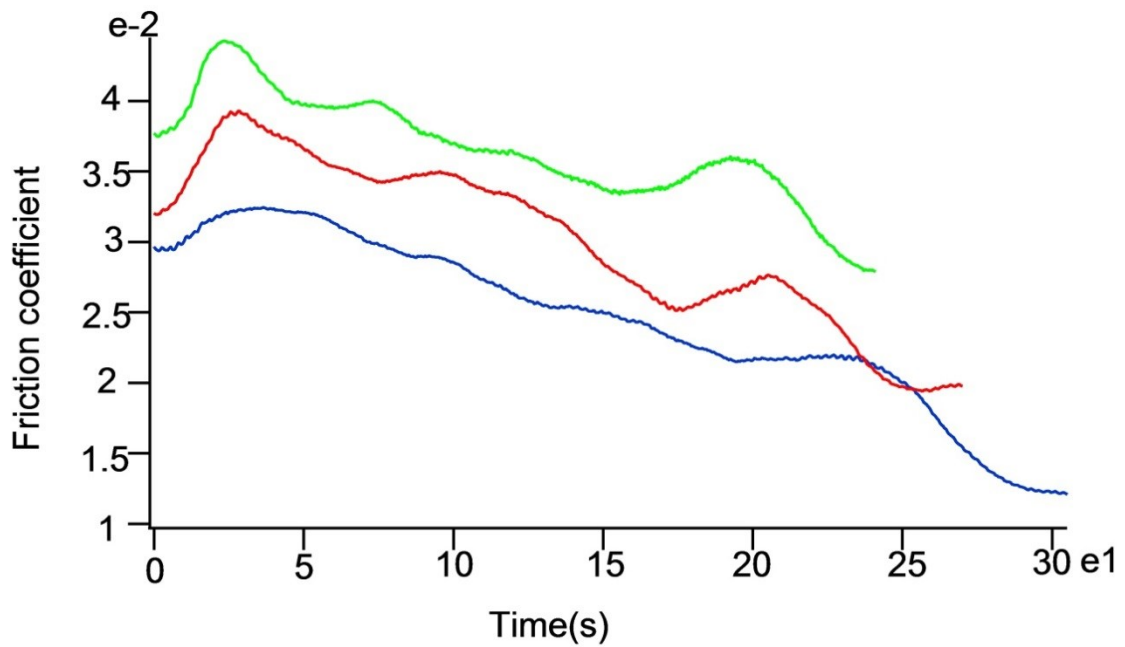


Figure 5.14: FC of 1362N normal force tests. Green, low velocity (0.47m/s); red, medium velocity (0.63m/s); blue, high velocity (0.8m/s).

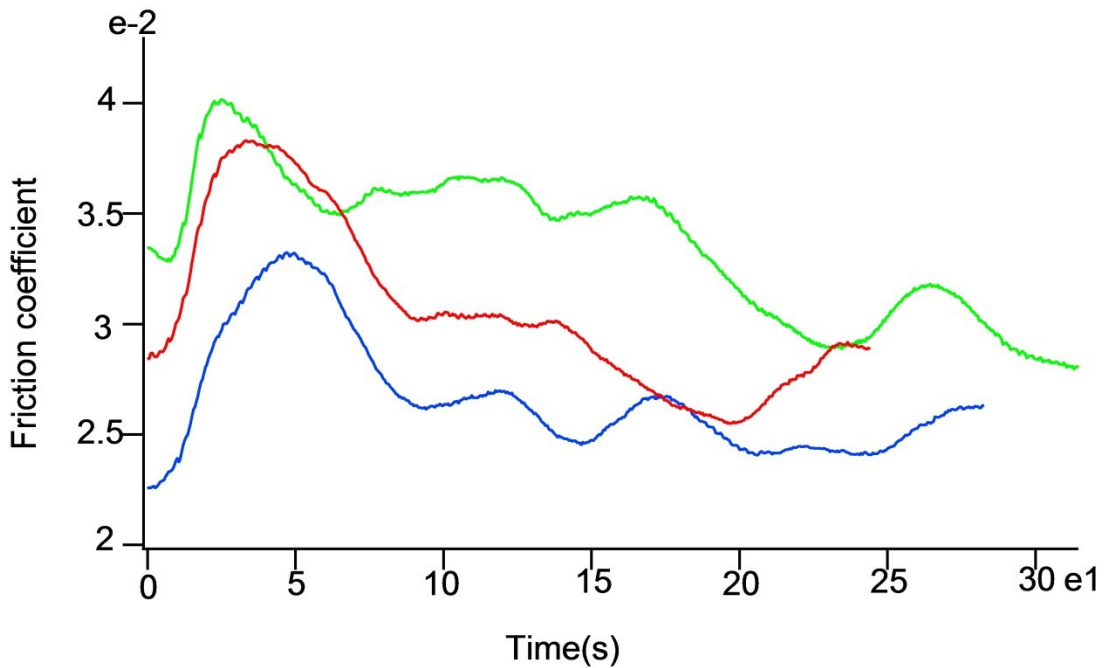


Figure 5.15: FC of 1816N normal force tests. Green, low velocity (0.47m/s); red, medium velocity (0.63m/s); blue, high velocity (0.8m/s).

The form of the results is the same for all speeds. There is no consistent trend in the magnitude of low and medium speed results but the high speed tests consistently show lower magnitudes throughout.

5.2.3 Changing normal force tests

The following figures (5.16-5.19) show results of changing force tests in different weight levels. Different velocity levels are shown in different colors. For each test condition, there were two tests for comparison and in case of failure. Because there are some irregular cases, the better one of each test condition is chosen for display.

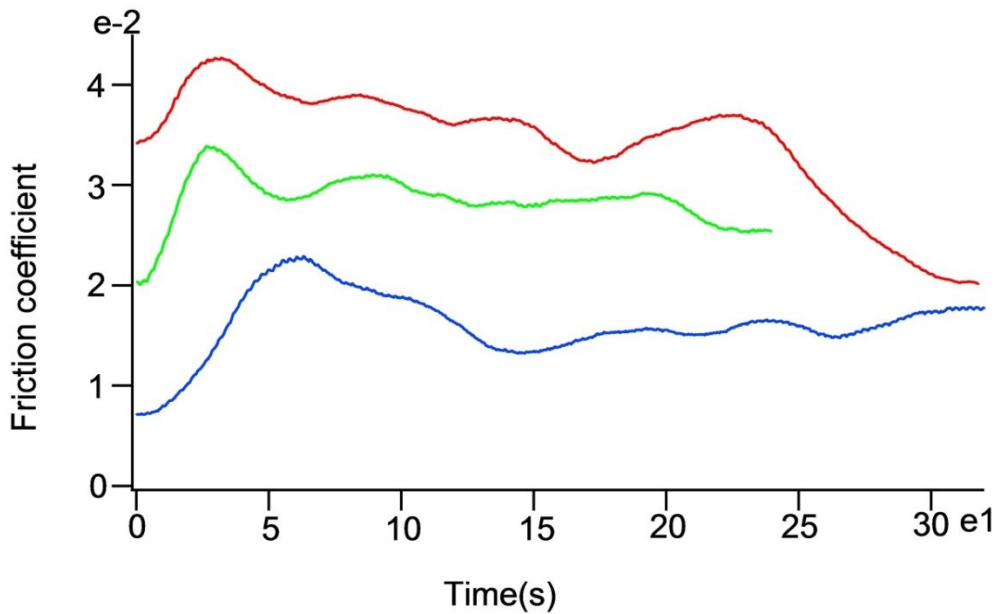


Figure 5.16: FC of 454N normal force tests. Green, low velocity (0.47m/s); red, medium velocity (0.63m/s); blue, high velocity (0.8m/s).

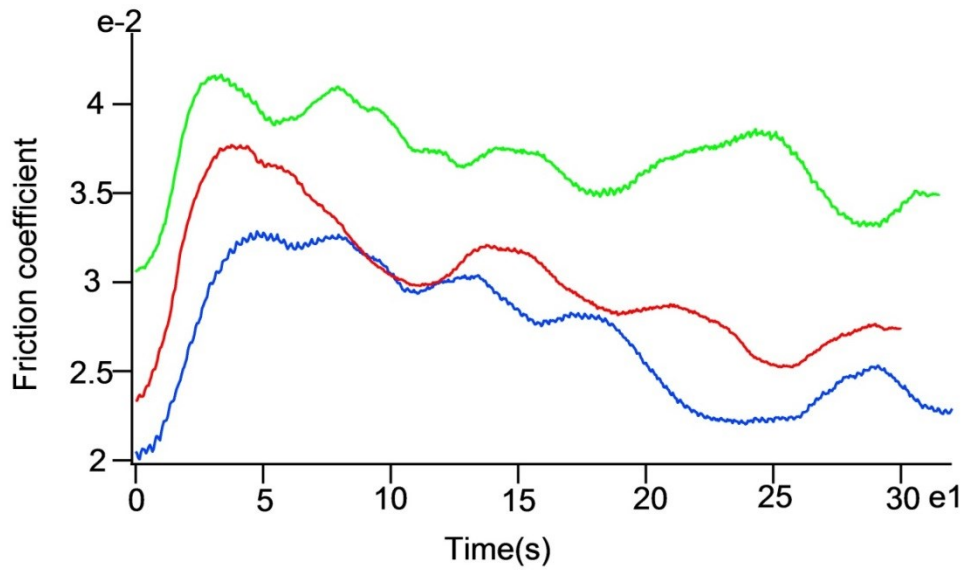


Figure 5.17: FC of 908N normal force tests. Green, low velocity (0.47m/s); red, medium velocity (0.63m/s); blue, high velocity (0.8m/s).

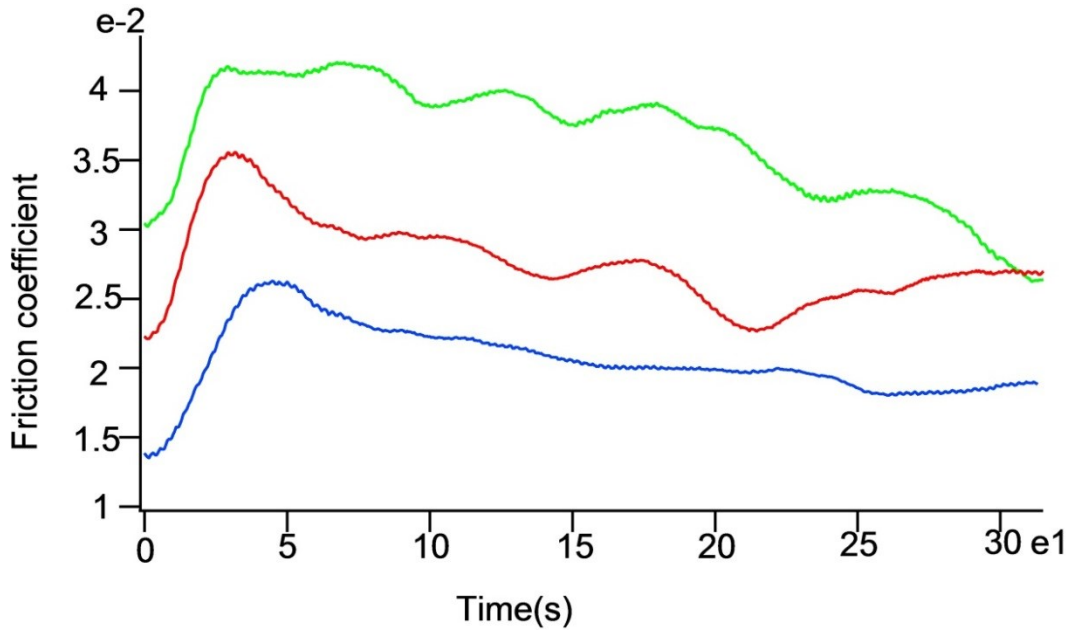


Figure 5.18: FC of 1362N normal force tests. Green, low velocity (0.47m/s); red, medium velocity (0.63m/s); blue, high velocity (0.8m/s).

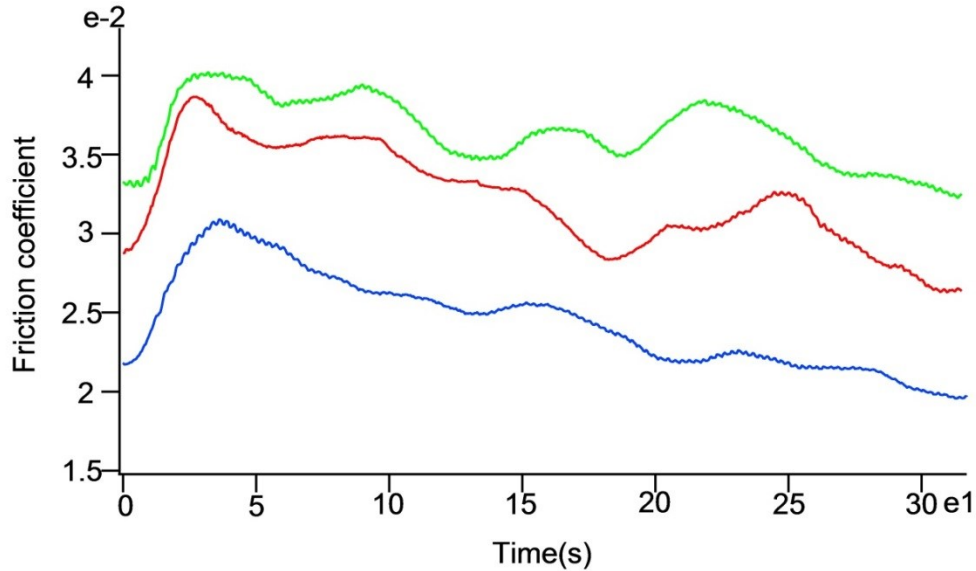


Figure 5.19: FC of 1816N normal force tests. Green, low velocity (0.47m/s); red, medium velocity (0.63m/s); blue, high velocity (0.8m/s).

Comparing the smoothed curves of friction coefficient of the test, it can be concluded that as the normal force increases, the peak is reached faster and is less pronounced. Over all there are not big differences between changing force tests and steady force tests. For the changing force tests, 272N force in total was added to the normal force over the test duration. The reason for the small difference between changing force tests and constant force tests may be because 272N additional force is relatively small compared to total normal force. Additionally, it may be that normal force is not a significant factor.

5.3 Summary

From the results plotting, there is no significant difference between changing normal force tests and constant normal force tests. This is most probably due to the relatively small change in normal force and to the fact that the contact area increased during a test in either event. Thus the pressure was always reducing during the course of a given test and adding to the normal force

only slowed the rate of pressure reduction. As velocity increases, the maximum and minimum friction coefficient value and the slope of the initial rising in the friction coefficient decreases. Effects of changing weight level on the maximum and minimum friction coefficient value and the slope of rising in the beginning of the test are not obvious.

In calculating the normal force, the normal weight at 180s for each test is used as the normal force through the test. This simplification results a difference between real value and calculated value at other time points. The difference is at its maximum in the beginning. The difference decreases to zero as it approach to 180s and then increases afterward. As the example given in calculations, the ice loss weight at 180s is 0.981kg. At the starting point, the difference can be calculated as following:

$$0.327 / (0.327 + 126.52) = 0.00257790881$$

It is means that the calculated value is lower than the theoretical real value by 0.26% at the starting point.

Chapter 6 DISCUSSION AND ANALYSIS

As explained in the previous section, the recorded results tended to show similar characteristics in terms of the change of friction coefficient as each experiment proceeded. In analyzing the data derived from the experiments, it was decided to take the three prominent characteristics from the raw friction coefficient curves as dependent outputs, namely the initial slope of the curve, the peak measured friction coefficient and settled friction coefficient, and try to determine how these characteristics changed with the independent variables of the experimental program. Based on analysis of the progress of each test, these three parameters corresponded roughly as shown in Table 6.1 below.

Table 6.1: Three sections of test correspond with parameters and assumed mechanisms.

Section of test	Parameters	Mechanisms
Initial stage	Slope of coefficient change	Initial crushing, abrading of sample
Peak stage	Maximum friction coefficient	Transition from crushing to steady state abrading
Settling stage	Average settled friction coefficient	No crushing but sample abrasion

Using these three parameters as indices, further analysis was performed to see how these changed with the controlled variables of the test, namely, normal force, velocity and changes in normal force.

In the following section, how each of these parameters (slope of the coefficient change, peak friction coefficient, steady state friction coefficient) changes with the varied factors (normal force, changing normal force, sliding velocity) are discussed. Subsequently, how the factors cause the changes in the test is discussed. Finally, the variability of the results is reviewed.

6.1 Plotting of Significant Parameters

In this section, the significant parameters are plotted against the factors studied in this research, namely normal force and velocity, to discuss the effect of the factors on the changing of ice friction coefficient.

6.1.1 Slope of the coefficient change

The following figure (6.1) shows the average value of the slope of the initial rising of the friction coefficient plotted against weight level. Lines connected marks with the same condition regarding to velocity level and if force changed, however, they are not to show the trend between normal force levels.

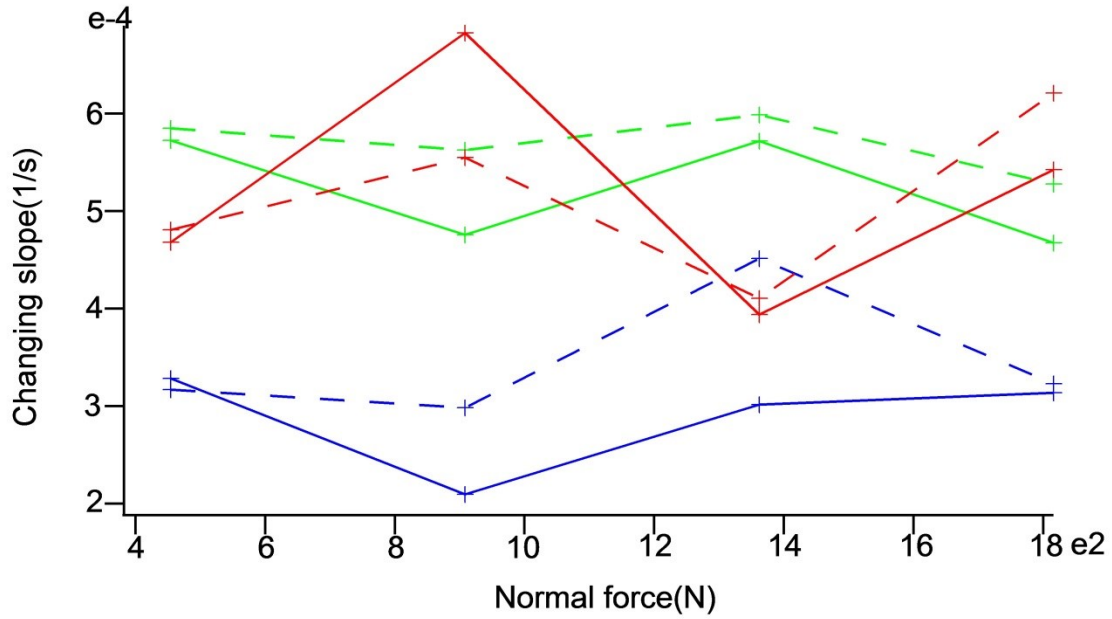


Figure 6.1: Slope of changing plotted against initial normal force. Green, low velocity (0.47m/s); red, medium velocity (0.63m/s); blue, high velocity (0.8m/s). Dots connected by a dashed line indicate changing normal force tests and dots connected by solid line indicate constant normal force tests.

The following figure (6.2) shows the average value of the slope of initial rising of the friction coefficient plotted against velocity. Lines connected marks with the same condition regarding to velocity level and if force changed, however, they are not to show the trend between normal force levels.

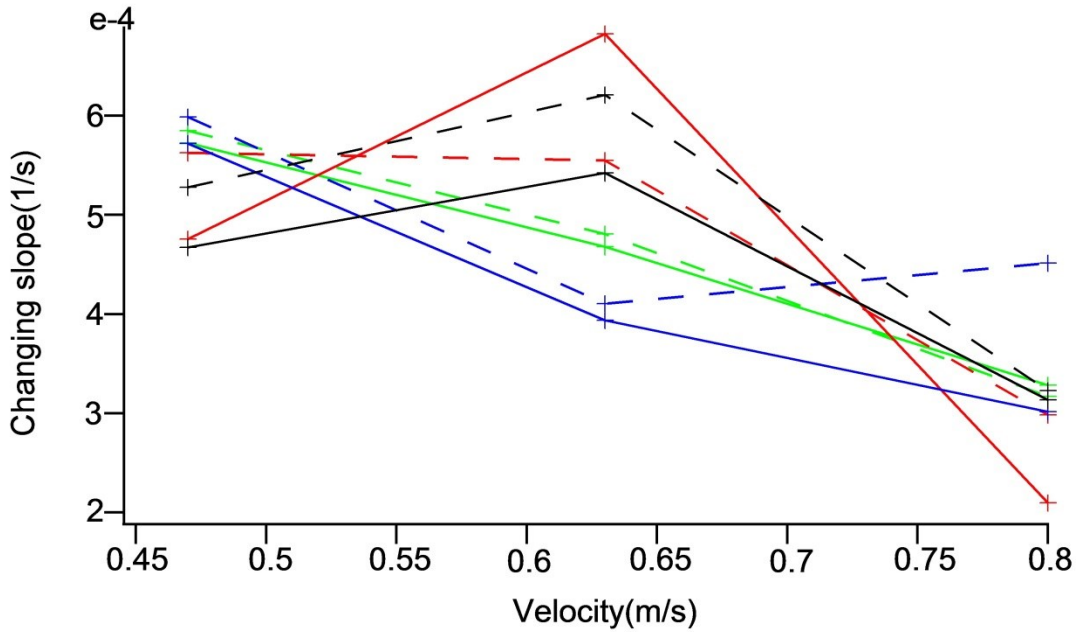


Figure 6.2: Slope of changing plotted against velocity. Green, 454N initial normal force; red, 908N initial normal force; blue, 1362N initial normal force; black, 1816N initial normal force. Dots connected by a dashed line indicate changing normal force tests and dots connected by solid line indicate constant normal force tests.

According to the results, it is easy to conclude that the slope of the coefficient change decreases as sliding velocity increases, especially at a high speed level (0.8m/s); however, it appears that the slope or rate of change in friction coefficient is independent of the normal force or of any change in normal force.

The implication of a lower change in friction coefficient associated with higher velocities is that both the friction coefficient and the increase in friction coefficient is lower/slower at higher velocity under conditions where the ice is actively crushing. This implies that the two mechanisms of crushing and abrading are probably dominated by the abrasion as it is expected that the abrasion mechanism (or shear failure at the interface) would be accelerated for higher velocities whereas the crushing mechanism would be accelerated for higher normal forces.

Another mechanism may be that the higher velocity extrudes broken ice at a higher rate thus reducing the friction mechanism.

6.1.2 Peak friction coefficient

The peak friction coefficient is the peak value of the ice friction coefficient in the testing process. It can be easily obtained through the software. The peak value indicates how high the ice friction coefficient can reach as the crushing mechanism roughs the surface.

Figure 6.3 shows the average value of the peak friction coefficient for each level of test. Lines connected marks with the same condition regarding to velocity level and if force changed, however, they are not to show the trend between normal force levels.

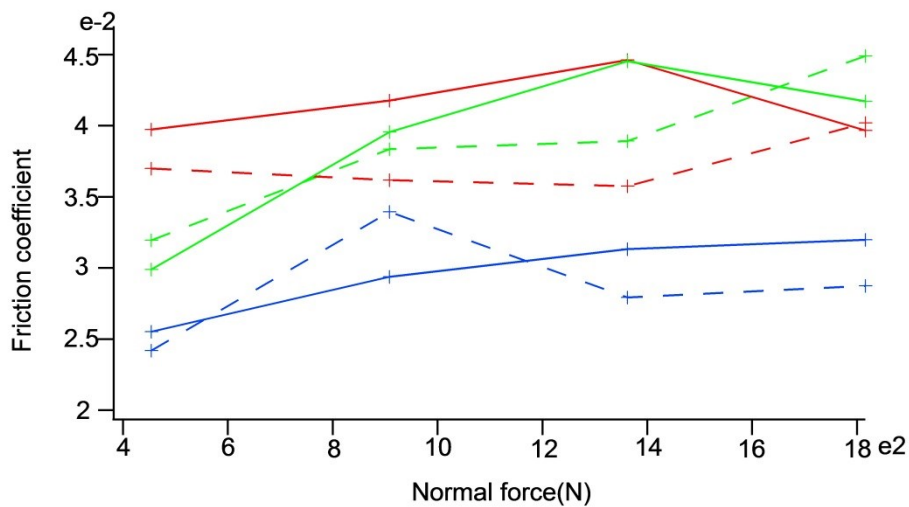


Figure 6.3: Peak friction coefficient plotted against initial normal force. Green, low velocity (0.47m/s); red, medium velocity (0.63m/s); blue, high velocity (0.8m/s). Dots connected by a dashed line indicate changing normal force tests and dots connected by solid line indicate constant normal force tests.

Figure 6.4 shows the average value of the peak friction coefficient plotted against velocity. Lines connected marks with the same condition regarding to velocity level and if change force, however, they are not to show the trend between normal force levels.

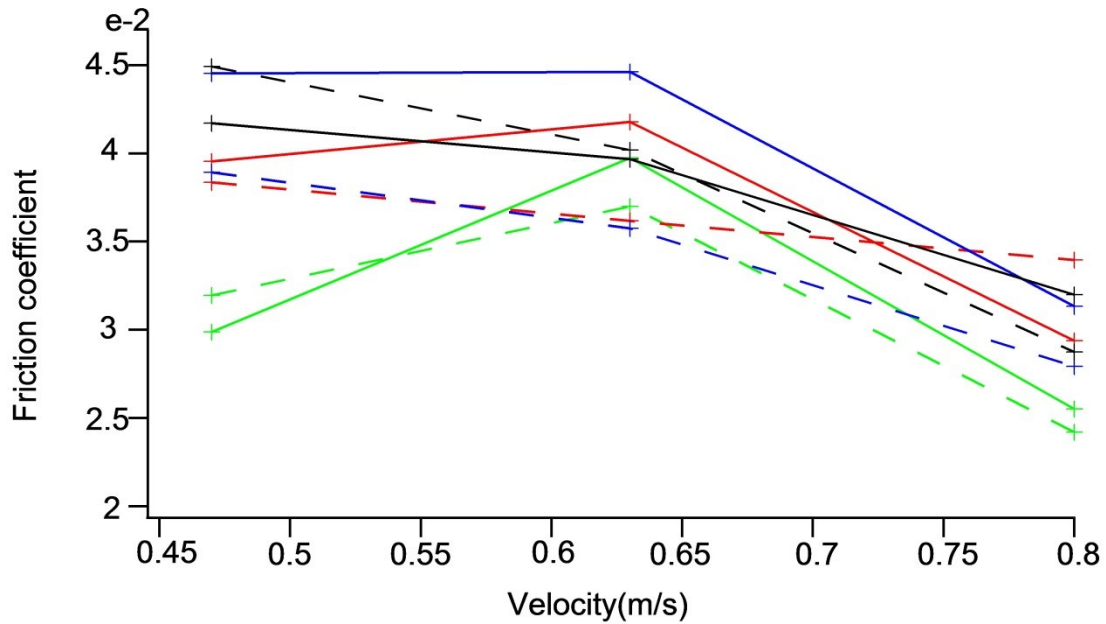


Figure 6.4: Peak friction coefficient plotted against velocity. *Green, 454N initial normal force; red, 908N initial normal force; blue, 1362N initial normal force; black, 1816N initial normal force. Dots connected by a dashed line indicate changing normal force tests and dots connected by solid line indicate constant normal force tests.*

It is obvious from the results that the peak friction coefficient is lower with higher velocity; but the effect of sliding velocity is not significant at lower speeds. The effect of normal force on the friction coefficient is not significant from the plots; although there is a slight increasing trend in peak friction coefficient with increasing normal force.

6.1.3 Settled friction coefficient

Figure 6.5 shows the average value of the settled friction coefficient for each level of test. Lines connected marks with the same condition regarding to velocity level and if force changed, however, they are not to show the trend between normal force levels.

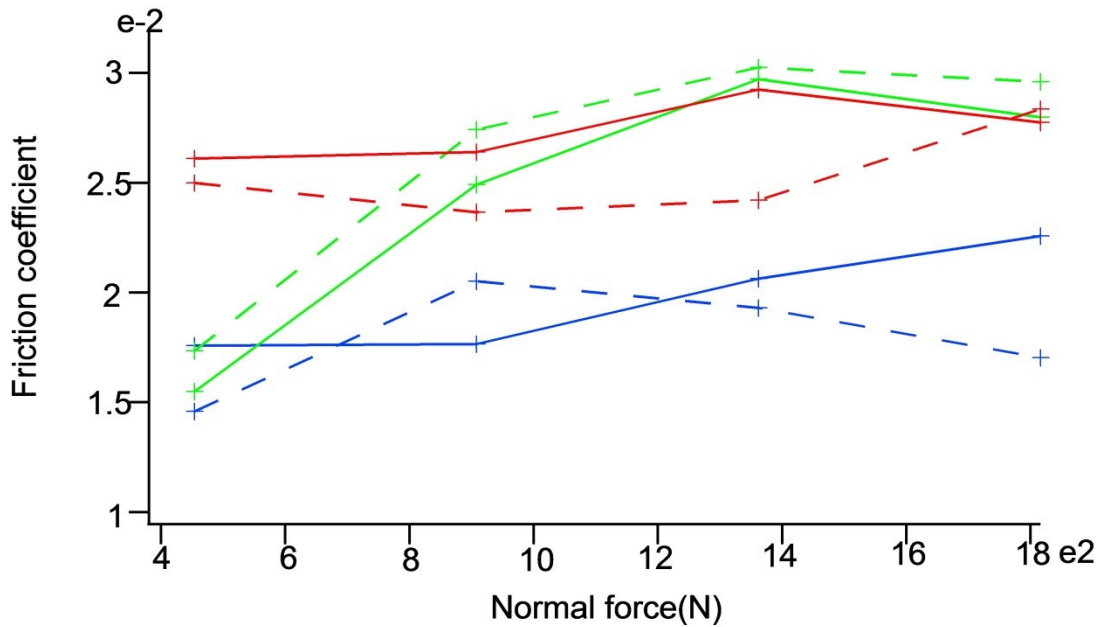


Figure 6.5: Settled friction coefficient plotted against initial normal force. Green, low velocity (0.47m/s); red, medium velocity (0.63m/s); blue, high velocity (0.8m/s). Dots connected by a dashed line indicate changing normal force tests and dots connected by solid line indicate constant normal force tests.

Figure 6.6 shows the average value of settled friction coefficient plotted against velocity. Lines connected marks with the same condition regarding to normal force level and if force changed, however, they are not to show the trend between velocity levels.

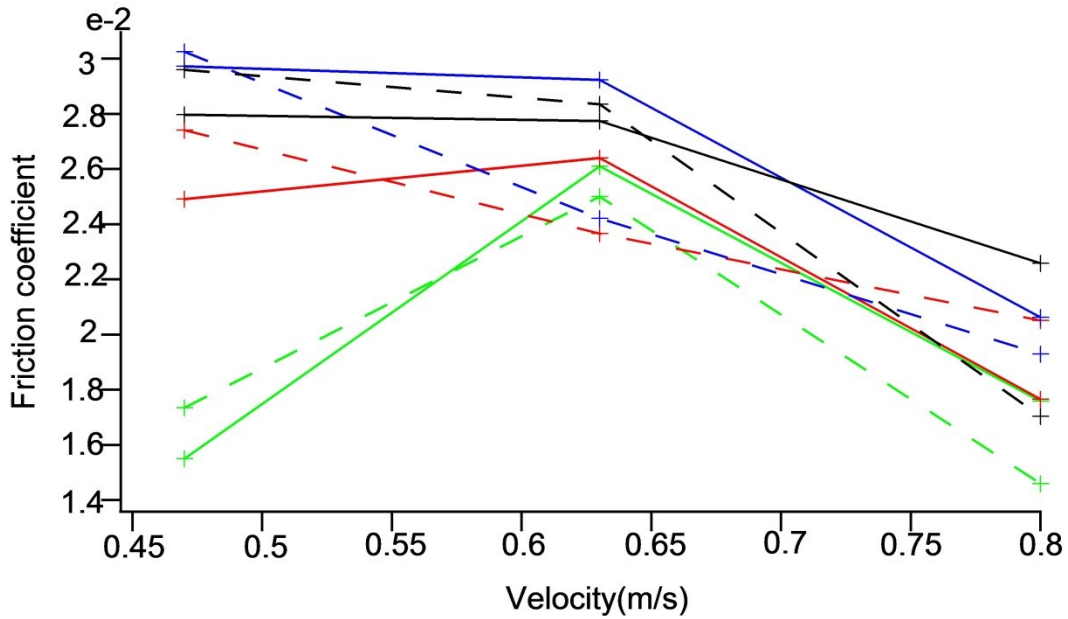


Figure 6.6: Settled friction coefficient plotted against velocity. Green, 454N initial normal force; red, 908N initial normal force; blue, 1362N initial normal force; black, 1816N initial normal force. Dots connected by a dashed line indicate changing normal force tests and dots connected by solid line indicate constant normal force tests.

According to the results, the settled friction coefficient is generally lower with higher velocity; but the effect of sliding velocity is not significant at lower speeds. The effects of normal force and changing normal force are not significant; although again there is a slight upward trend in the friction coefficient with increasing normal force. It can be concluded that settled friction coefficient increases as normal force increases comparing 454N weight level and 1816N weight level. The effect of varied factors on settled state friction coefficient is similar with peak friction coefficient. The results show that the settled friction coefficient at low velocity level is as low as it is at high velocity level.

According to the experiment, the peak value of ice-ice friction coefficient varies in range from 0.0229 to 0.0499; the settled state value of ice-ice friction coefficient varies in range from 0.0134

to 0.0335. These values are consistent with, but somewhat lower than, many of the values reported in the references covered in the literature review. The mechanisms that cause the variations are discussed in next section.

6.2 Mechanisms

The differences in friction coefficient characteristics between constant normal force and changing normal force are insignificant; but with a larger normal force difference, there is a change in the ice friction coefficient. It is shown that the high pressure causes crushing and pulverization of the ice. It is possible that at the initial stage, crushing is the main mechanism that influences the changing of the friction coefficient. Although both crushing and abrading were happening at the same time, the roughness of the contact surface may be increased by the presence of ice rubble rather than lubricated by melted ice. Figure 6.7 shows the ice plate after testing. Ice chips are accumulated beside the sliding track on the ice plate. If we take a close look in Figure 6.8, we can see that the ice chips produced in the earlier stage of testing, which was pushed away from the track, are bigger than the ice chips closer to the track, which was produced in the later stage of testing.

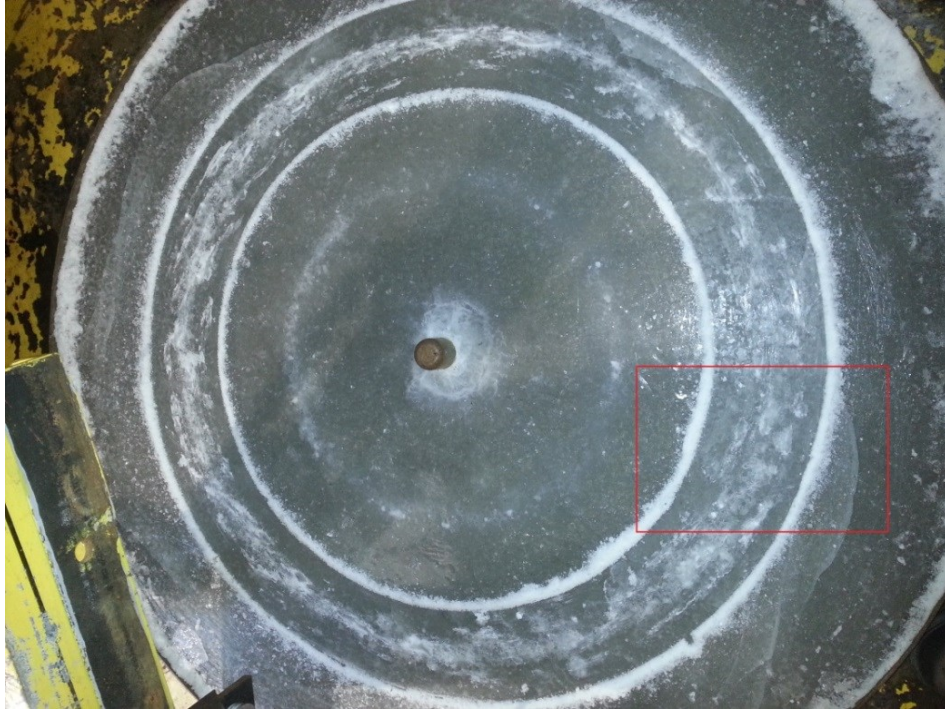


Figure 6.7: Ice plate after testing. Ice chips beside the sliding track in red rectangle.

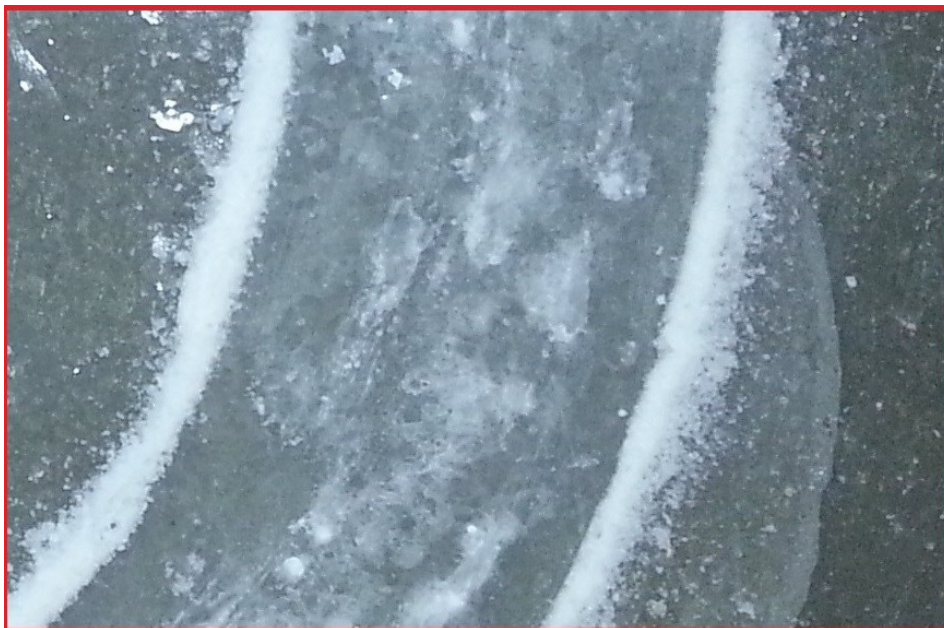


Figure 6.8: Close picture of the red rectangle in Figure 82.

Different from most of former studies, the friction coefficient in the tests rises before decreasing. The reason may be that, in this study, the contact surface was damaged in crushing as it was under relatively high normal pressure, so the roughness of the contact surface increased. An interesting observation from the test is that the slope of the coefficient change decreases as sliding velocity increases. This was not as expected. Additionally, there is little difference in the contact area for tests of same weight level at 60 seconds, yet the friction coefficient and the slope of the coefficient change varies as the velocity changes. The conclusion we can draw from this is that higher velocity causes smaller surface roughness by grinding finer ice pieces off the ice cone. The reason could be that before fracture, there is deformation on the surface, and higher velocity leads to fracture of smaller chips before the deformation is accumulated to yield larger pieces. This indicates that ice shows elastic characteristics as its deformation is more influenced by velocity rather than normal stress. Another reason for the lower friction at higher velocities may be the increased action of the relative motion removing broken ice rubble from the contact area at the higher speeds.

6.3 Analysis in Design Expert

As a check on the statistical validity of the conclusions, the results are analyzed in the software Design Expert to check the variability and the statistical validity of the observations. Design Expert analyzes which factor is significant to the changing of the response and if there is interaction in between the factors, using ANOVA (analysis of variance). ANOVA is a statistical method used to analyze the difference between group means and the variation between and among the groups. The assumptions of ANOVA are: 1. the distribution of sample means is normally distributed; 2. Errors between cases are independent of one another; 3. Outliers have

been removed from the data set; 4. Population variances in different levels of each independent variable are equal.

The factors are normal force, velocity level and whether normal force changes during the test.

The responses are Peak FC, Settled FC and Changing Slope.

6.3.1 Diagnostics

Residuals vs. Run figures indicate if all the responses the cases are independent. Following are the Residuals vs. Run figures for the three responses: Changing slope (Figure 6.9), Peak FC (Figure 6.10) and Settled FC (Figure 6.11). As shown, the data are randomly scattered, except there is one extreme value in Settled FC. However, because the tests are not carried out exactly in the run sequence, this might not be a proper interpretation.

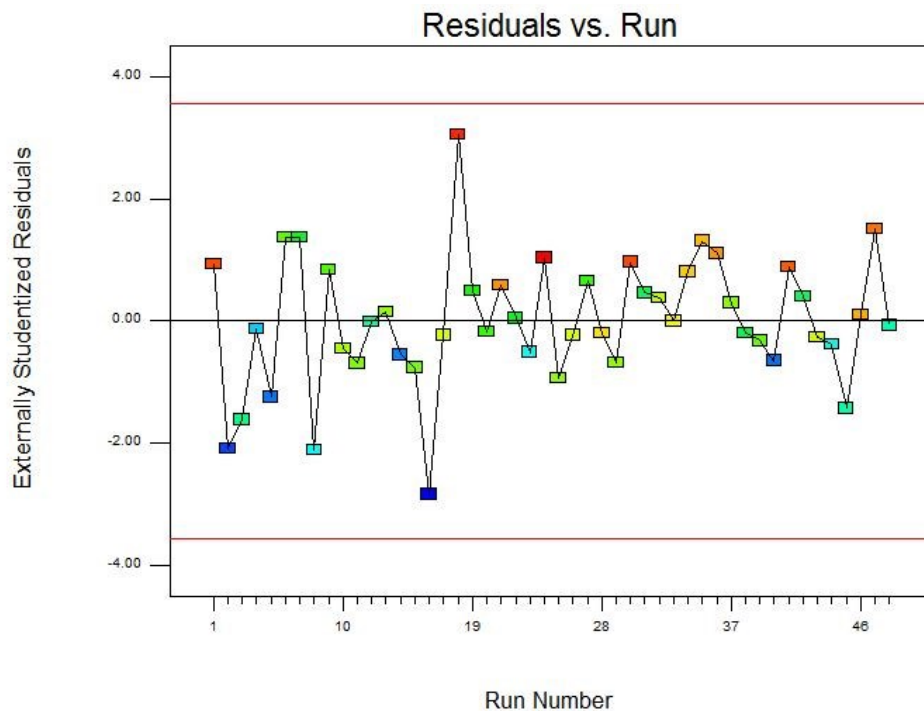


Figure 6.9: Residuals vs. run plot for Changing slope. Different colors indicate different tests.

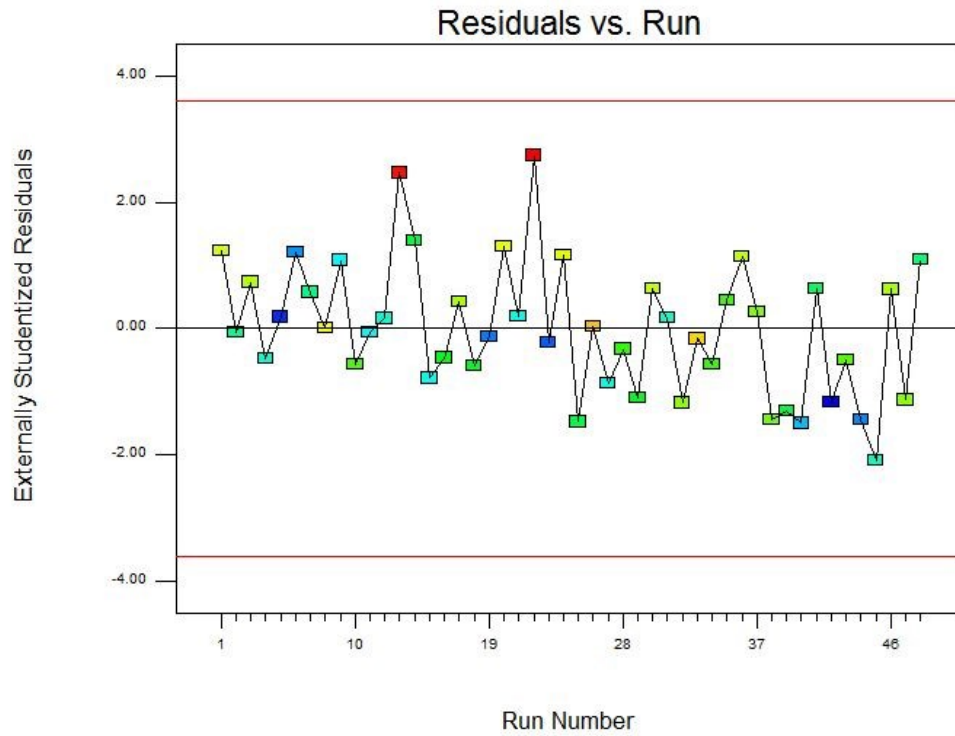


Figure 6.10: Residuals vs. run plot for Peak FC. Different colors indicate different tests.

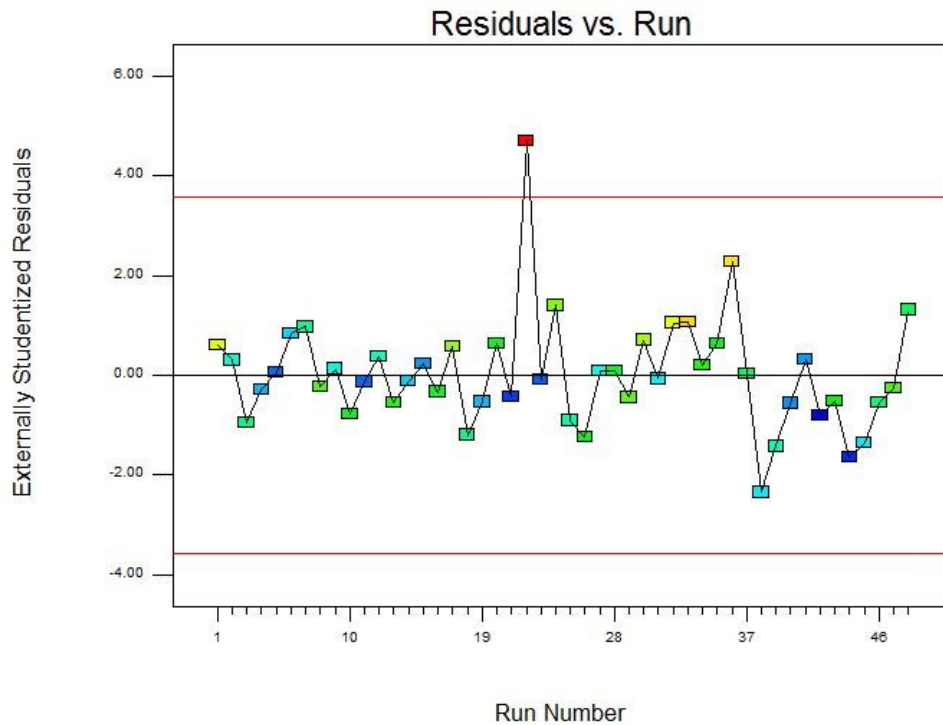


Figure 6.11: Residuals vs. run plot for Settled FC. Different colors indicate different tests.

“Normal plot of residuals” shows the normality of the results of the responses. Following are the “Normal plot of residuals” figures for changing slope (Figure 6.12), peak FC (Figure 6.13) and settled FC (Figure 6.14). According to the plots, the results are generally in keeping with normal distribution for all three responses, except for several tests away from the red line.

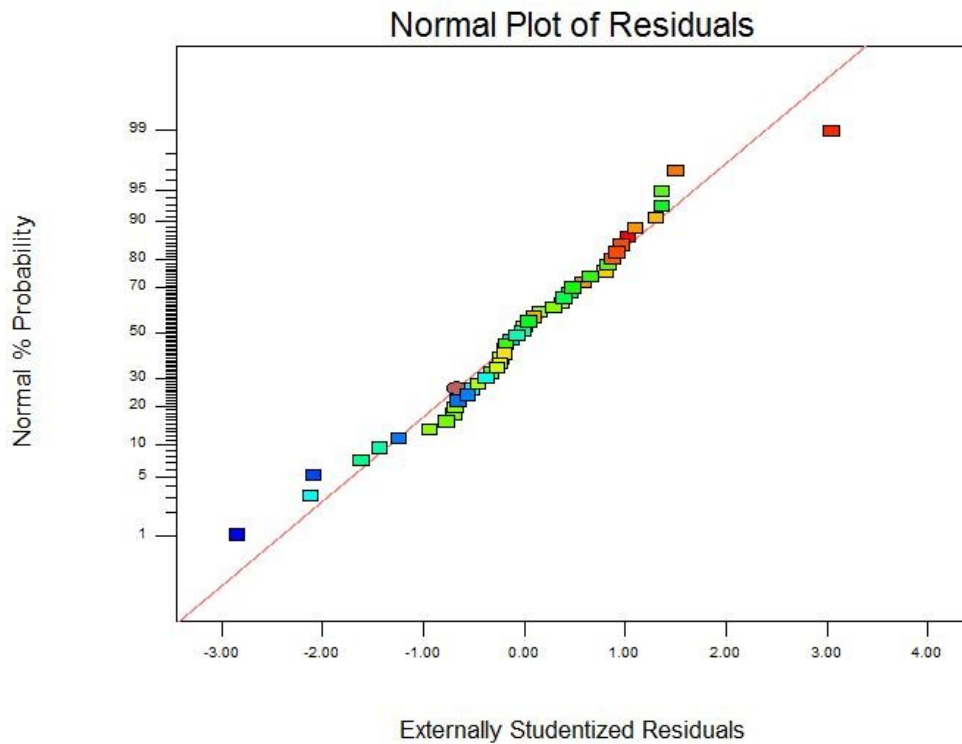


Figure 6.12: Normal plot of residuals for changing slope. Different colors indicate different tests.

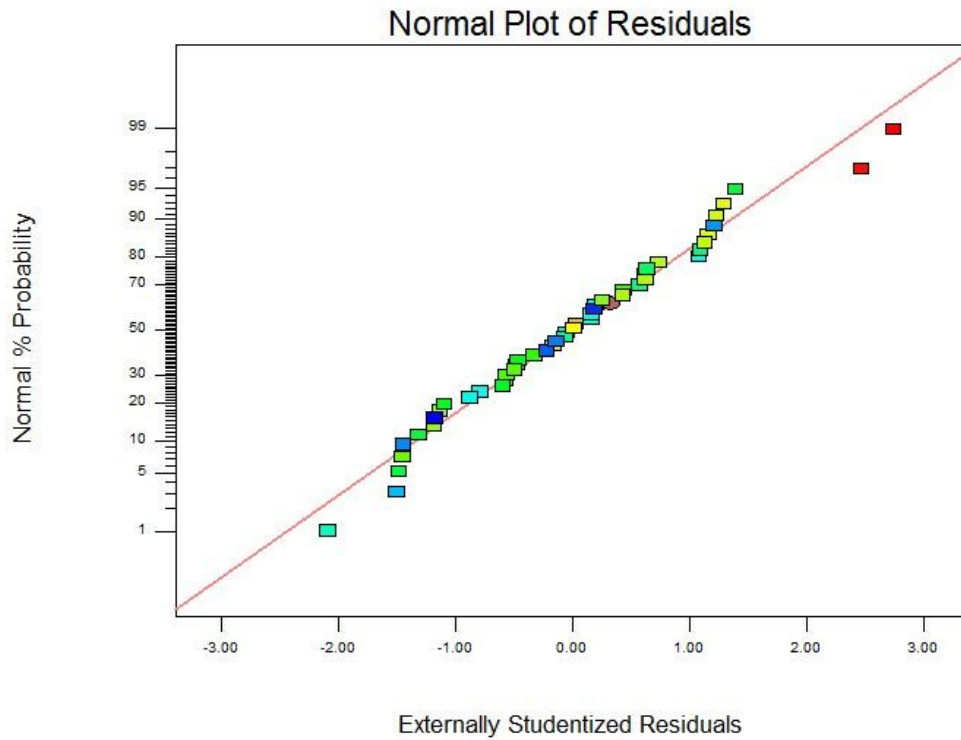


Figure 6.13: Normal plot of residuals for Peak FC. Different colors indicate different tests.

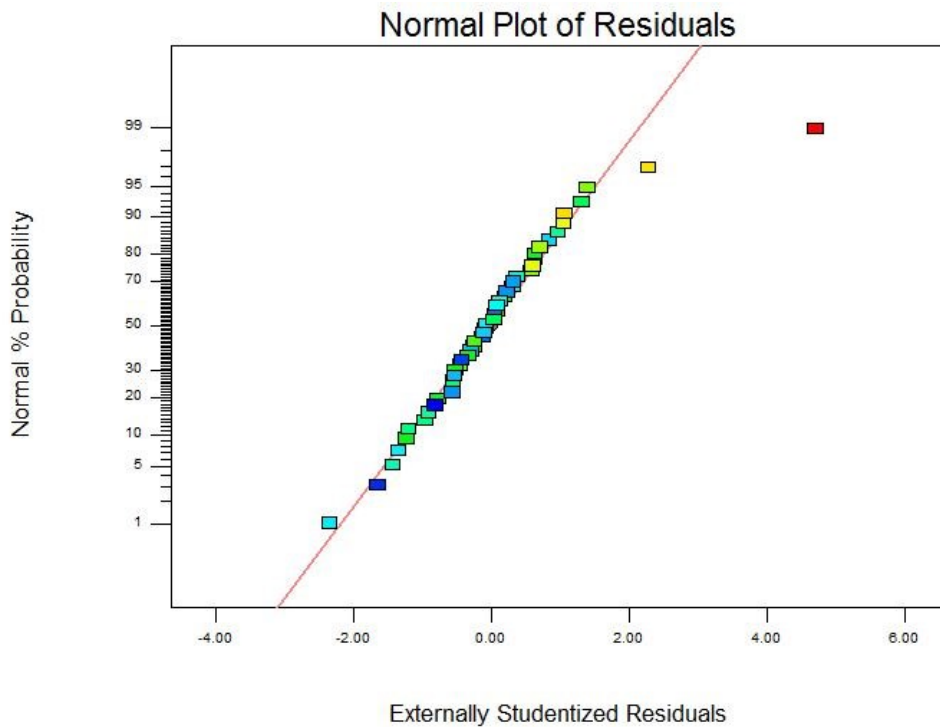


Figure 6.14: Normal plot of residuals for Settled FC. Different colors indicate different tests.

“Residuals vs. Predicted” plot shows if the models chosen for ANOVA maintain the assumption of constant variance in the groups. Following are the “Residuals vs. Predicted” plot for changing slope (Figure 6.15), Peak FC (Figure 6.16) and Settled FC (Figure 6.17). As shown, the data are within the two red lines, except one test for settled FC.

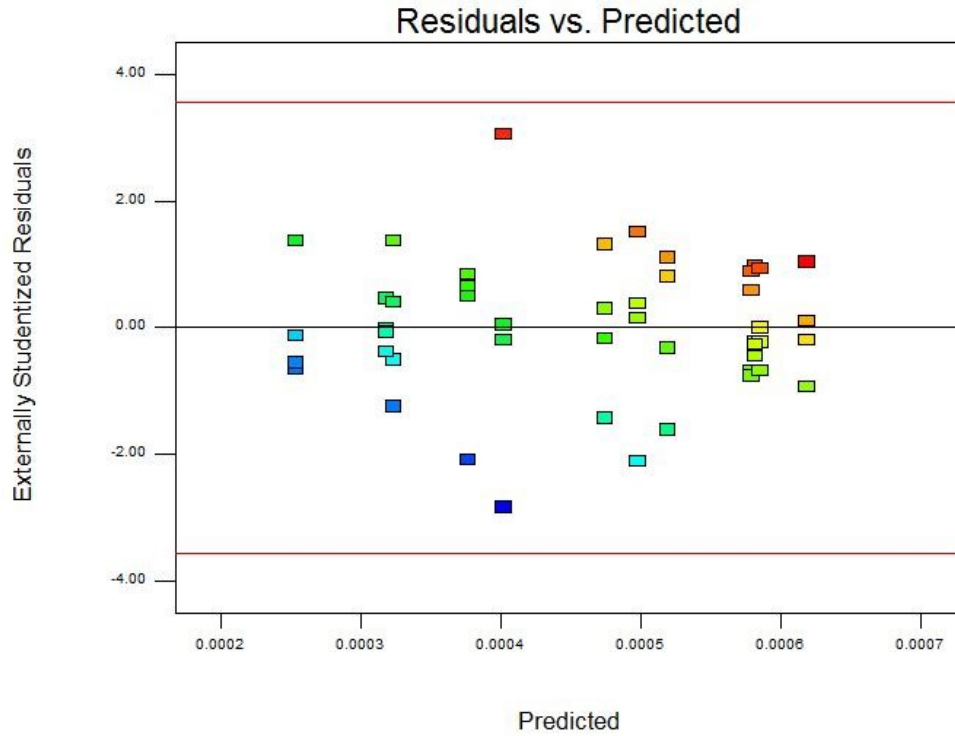


Figure 6.15: Residuals vs. predicted plot for changing slope. Different colors indicate different tests.

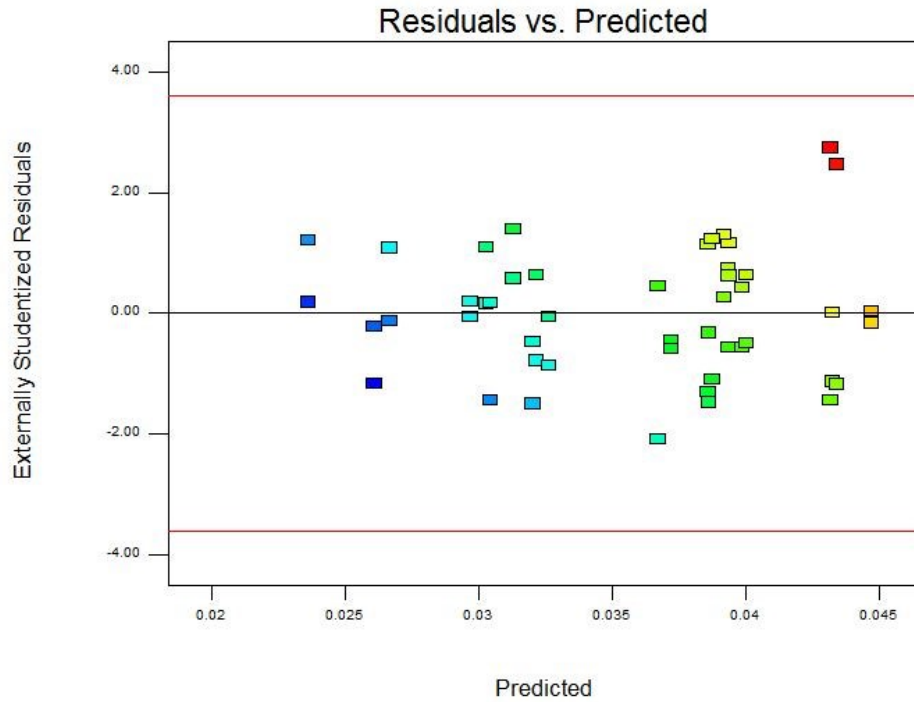


Figure 6.16: Residuals vs. predicted plot for Peak FC. Different colors indicate different tests.

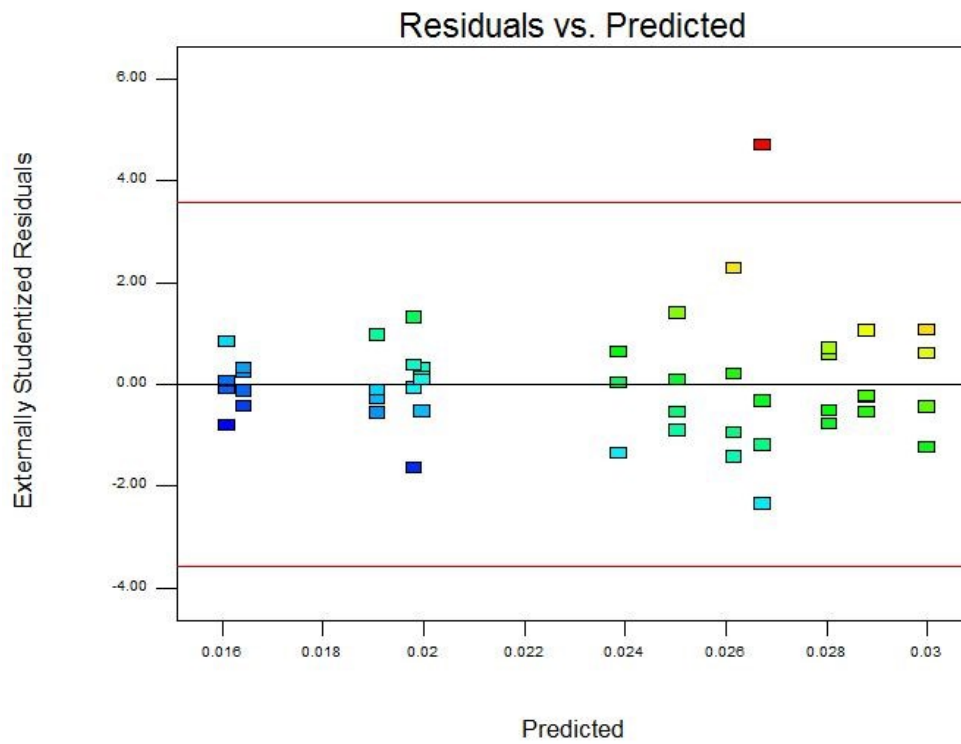


Figure 6.17: Residuals vs. predicted plot for Settled FC. Different colors indicate different tests.

The conclusion from these three plots is that the experiments as conducted did not show any bias or abnormal results except in a limited number of cases where external factors may have caused the results of those particular tests to exceed the limits imposed by the program. The results generally maintain the assumptions for ANOVA for all three responses.

6.3.2 Effects and interactions

The factors and interactions between the factors for each response are analyzed in Design Expert to see if they are significant. The results are presented and discussed in this section.

6.3.2.1 Peak friction coefficient

Figure 6.18, the half-normal plot show which factors or the interaction of factors influence the response significantly. The results from ANOVA are shown: Normal force and velocity are the significant factors for peak friction coefficient, and also the interaction between them. “If change force” is not a significant factor. It is shown in the half-normal plot because the interaction between “normal force” and “if change force” is considered significant. A factor needs to be shown if its interaction with other factor is considered significant, even though it is not significant itself.

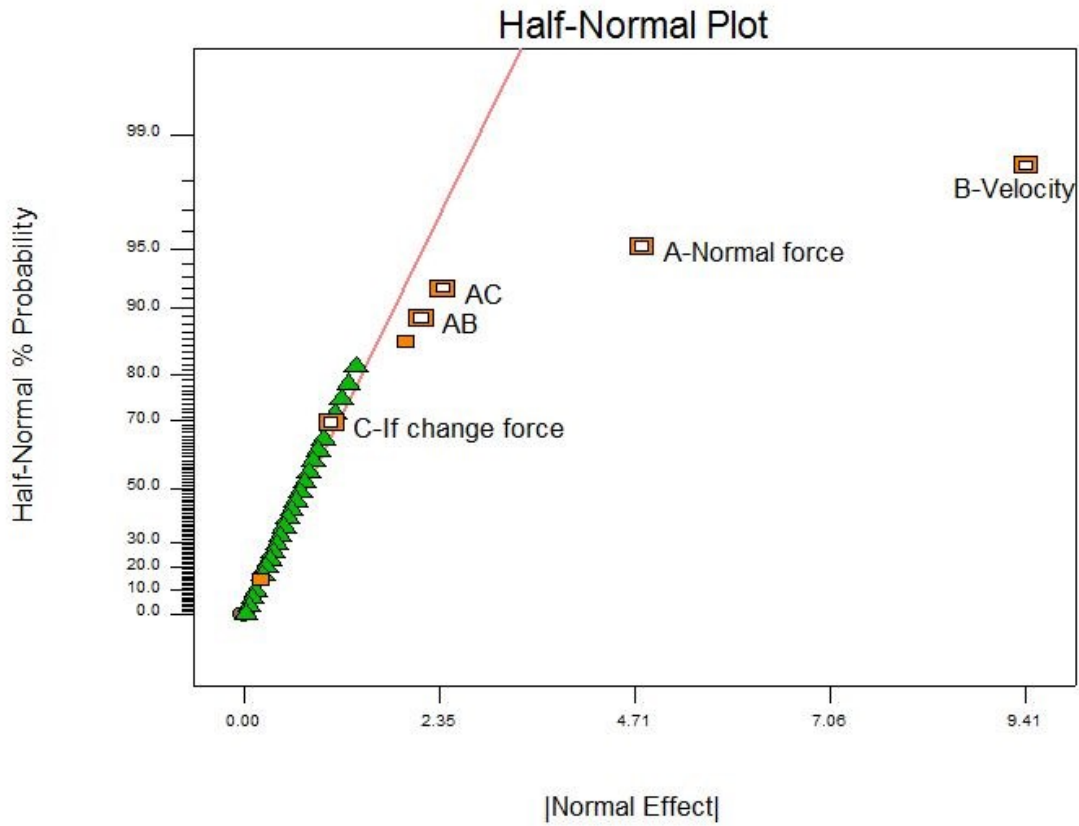


Figure 6.18: Half-normal plot for Peak FC

Figure 6.19 is the ANOVA table for Peak FC. F values indicate how significant the factors are.

As shown, velocity is the most significant factor on Peak FC.

Response	2	Peak FC				
ANOVA for selected factorial model						
Analysis of variance table [Classical sum of squares - Type II]						
Source	Sum of Squares	df	Mean Square	F Value	p-value Prob > F	
Model	1.649E-003	15	1.099E-004	9.89	< 0.0001	significant
A-Normal force	3.295E-004	3	1.098E-004	9.88	< 0.0001	
B-Velocity	1.040E-003	2	5.201E-004	46.80	< 0.0001	
C-If change force	1.246E-005	1	1.246E-005	1.12	0.2977	
AB	1.529E-004	6	2.548E-005	2.29	0.0593	
AC	1.141E-004	3	3.802E-005	3.42	0.0288	
Residual	3.556E-004	32	1.111E-005			
Lack of Fit	1.202E-004	8	1.502E-005	1.53	0.1989	not significant
Pure Error	2.355E-004	24	9.812E-006			
Cor Total	2.005E-003	47				

Figure 6.19: ANOVA table for Peak FC

Interaction figures show how the factors affect the effect of other factors on the responses.

Figures 6.20, 6.21 are the interaction figures of AB (normal force and velocity) and AC (normal force and if changing force). As shown in Figure 6.20, the peak friction coefficient increases as weight increases, however, the impact of weight on ice friction coefficient changing decreases as velocity increase.

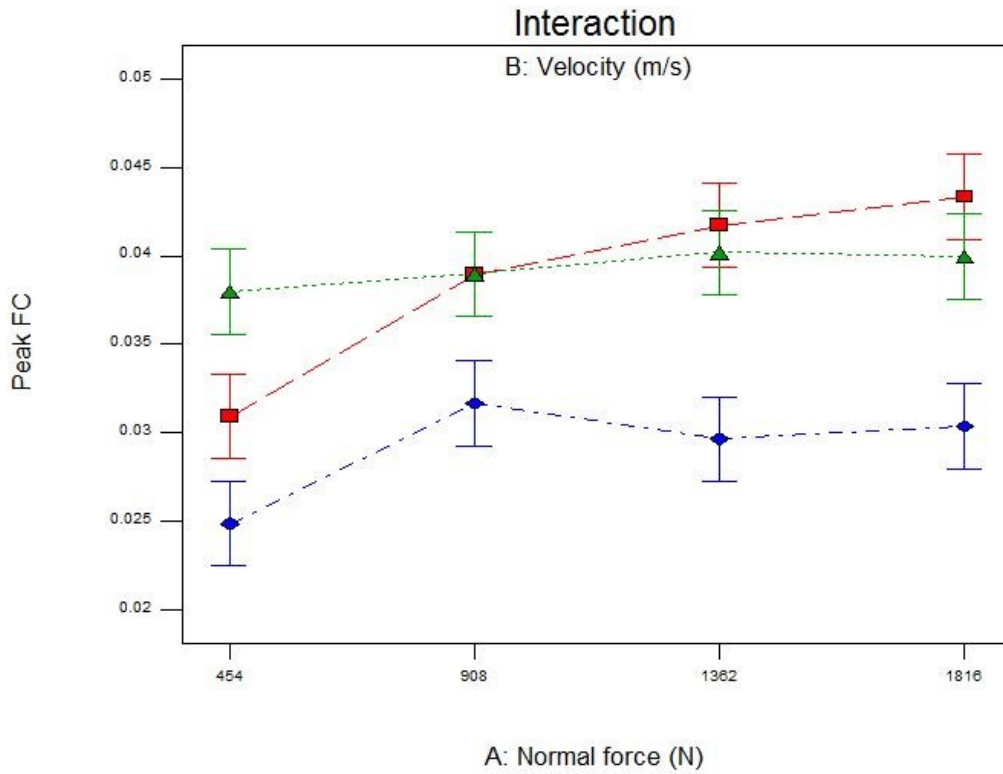


Figure 6.20: Interaction between velocity and normal force on Peak FC. Red, low velocity (0.47m/s); green, medium velocity (0.63m/s); blue, high velocity (0.8m/s).

Figure 6.21 is the interaction between normal force and if change force. Although ANOVA considers interaction between normal force and whether force changes to be significant, how the two factors interact cannot be concluded due to the error and randomness of the results.

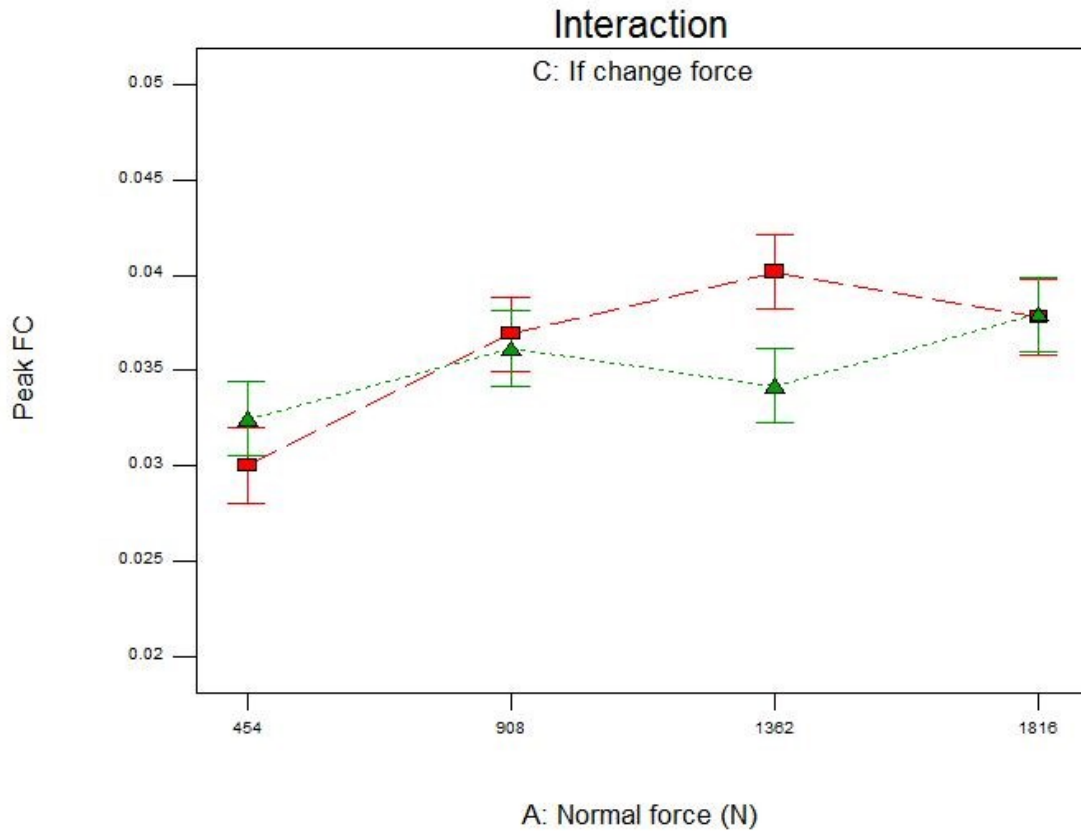


Figure 6.21: Interaction between normal force and if change force on Peak FC. Red, constant normal force; green, change normal force.

6.3.2.2 Settled friction coefficient

Figure 6.22 is the half-normal plot for settled friction coefficient. The results from ANOVA are shown: Normal force and velocity are the significant factors for peak friction coefficient, and also the interaction between them.

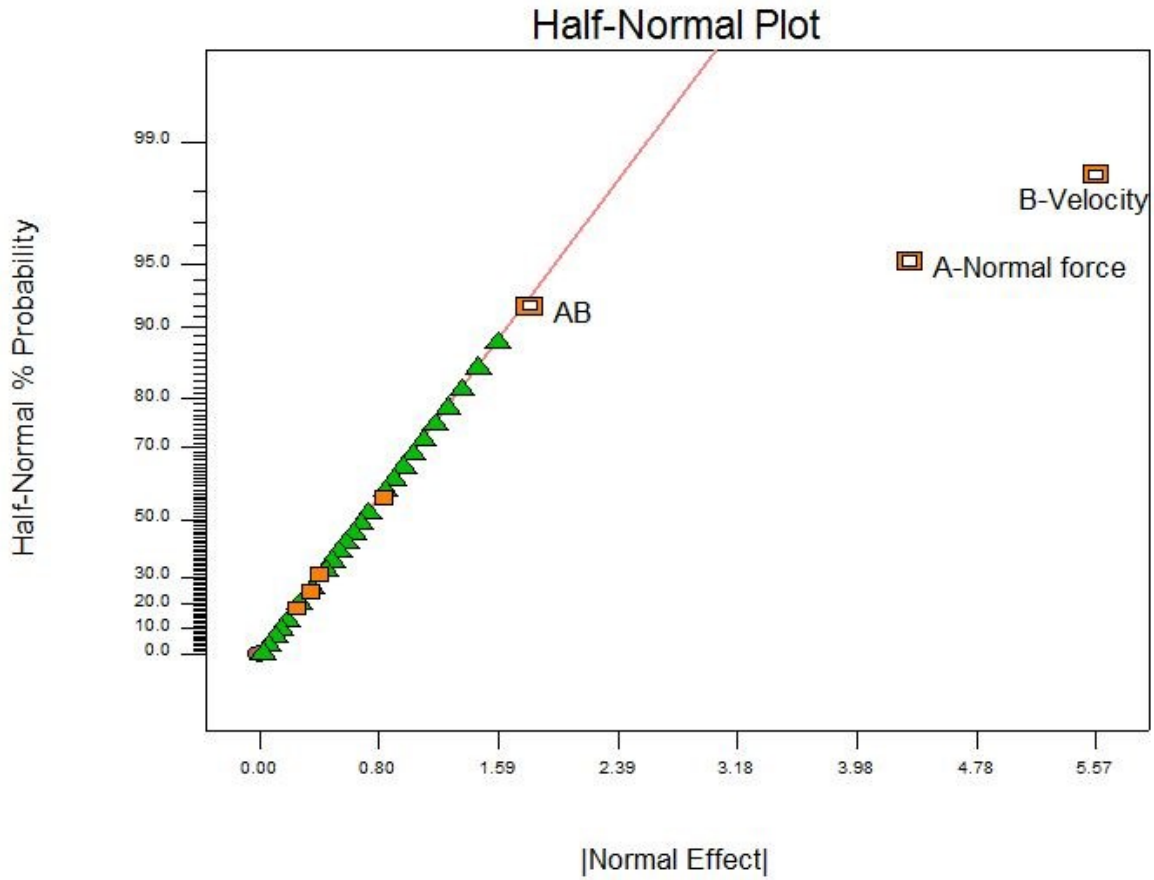


Figure 6.22: Half-normal plot for Peak FC

Figure 6.23 is the ANOVA table for Settled FC. As shown, velocity is the most significant factor on Peak FC.

Response	3	Settled FC				
ANOVA for selected factorial model						
Analysis of variance table [Classical sum of squares - Type II]						
Source	Sum of Squares	df	Mean Square	F Value	p-value	Prob > F
Model	1.044E-003	11	9.490E-005	6.52	< 0.0001	significant
A-Normal force	3.657E-004	3	1.219E-004	8.37	0.0002	
B-Velocity	5.094E-004	2	2.547E-004	17.49	< 0.0001	
AB	1.689E-004	6	2.814E-005	1.93	0.1020	
Residual	5.242E-004	36	1.456E-005			
Lack of Fit	1.005E-004	12	8.372E-006	0.47	0.9105	not significant
Pure Error	4.237E-004	24	1.766E-005			
Cor Total	1.568E-003	47				

Figure 6.23: ANOVA table for settled FC.

The interaction of normal force and velocity figure (6.24) shows that settled friction coefficient decreases as velocity increases, however, the impact of velocity decreases as normal force increases.

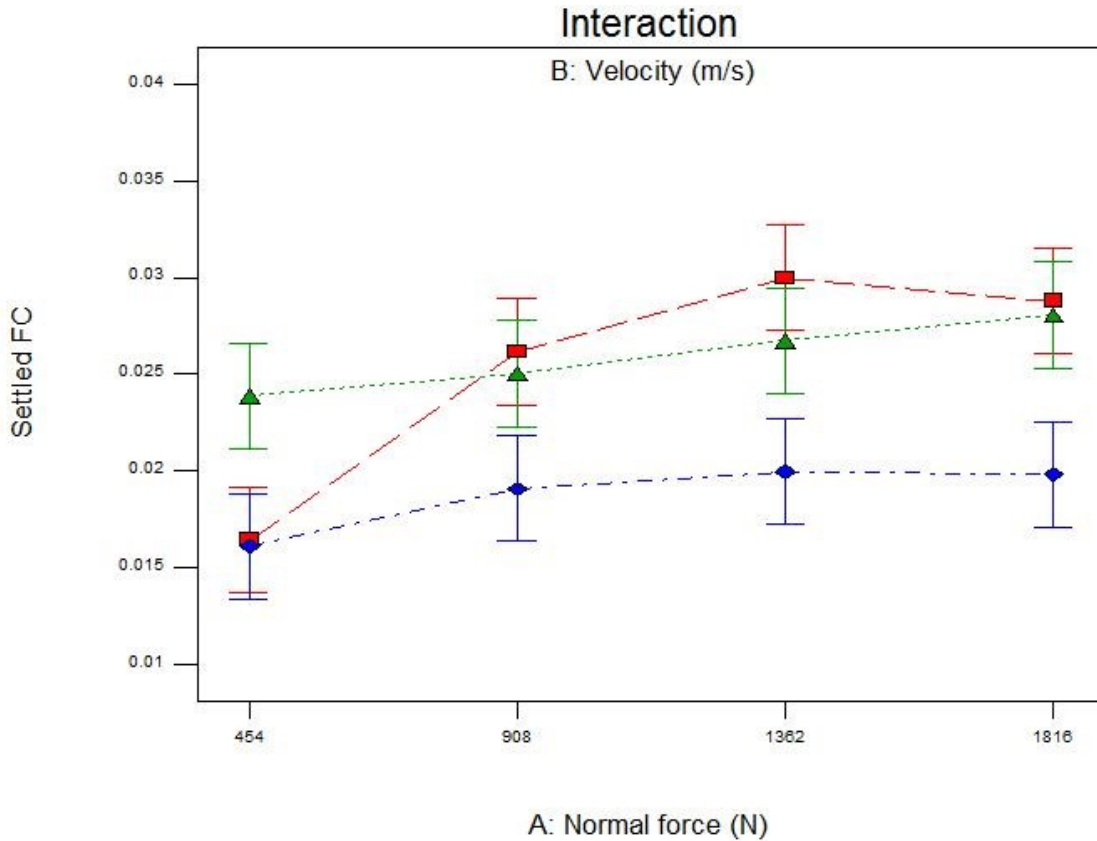


Figure 6.24: Interaction between velocity and normal force on Settled FC. Red, low velocity (0.47m/s); green, medium velocity (0.63m/s); blue, high velocity (0.8m/s).

6.3.2.3 Initial changing slope

According to the ANOVA, normal force and velocity are the significant factors for the initial slope, as well as the interaction between them (Figure 6.25). From the ANOVA table we can see how significant the factors are, according to the F values (Figure 6.26).

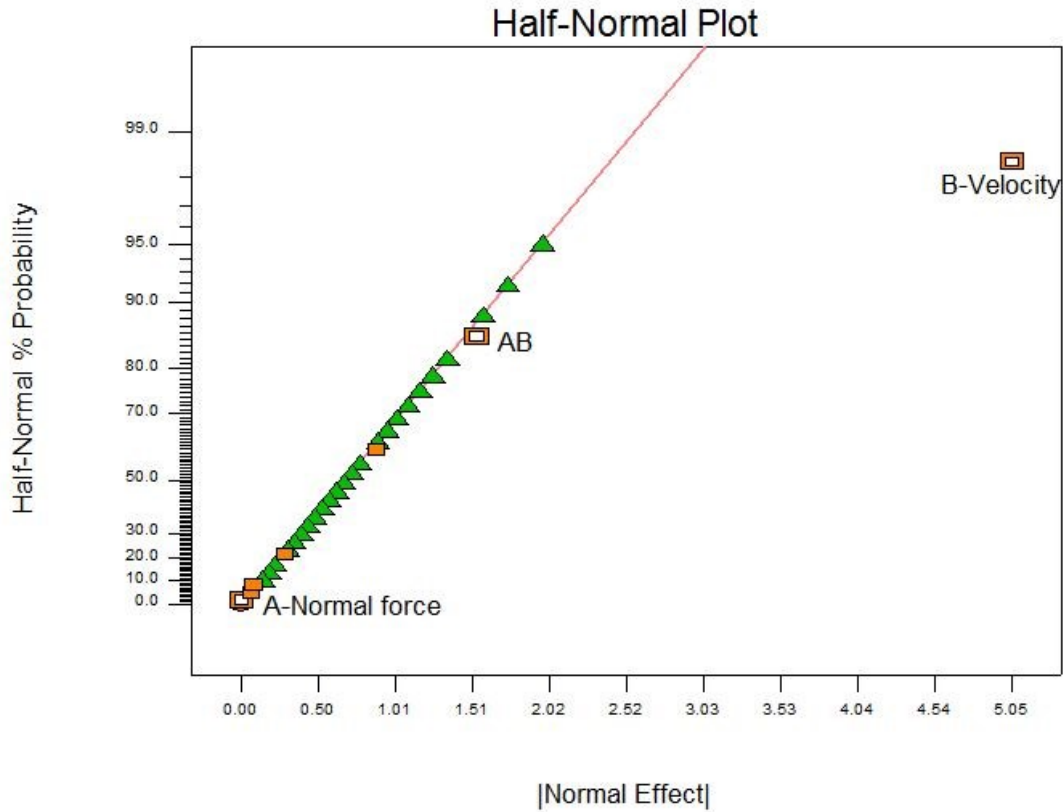


Figure 6.25: Half-normal plot for changing slope

Response	1	Changing slope				
ANOVA for selected factorial model						
Analysis of variance table [Classical sum of squares - Type II]						
Source	Sum of Squares	df	Mean Square	F Value	p-value	
Model	6.660E-007	11	6.055E-008	3.58	0.0018	significant
A-Normal force	9.154E-010	3	3.051E-010	0.018	0.9966	
B-Velocity	4.948E-007	2	2.474E-007	14.61	< 0.0001	
AB	1.703E-007	6	2.838E-008	1.68	0.1553	
Residual	6.097E-007	36	1.694E-008			
Lack of Fit	6.565E-008	12	5.471E-009	0.24	0.9933	not significant
Pure Error	5.441E-007	24	2.267E-008			
Cor Total	1.276E-006	47				

Figure 6.26: ANOVA table for changing slope

Figure 6.27 is the interaction figure of AB (weight and velocity). As shown in the figure, velocity is the main factor affecting the value of the initial slope. The initial slope decreases as the velocity increases, however, increasing normal force would abate this effect.

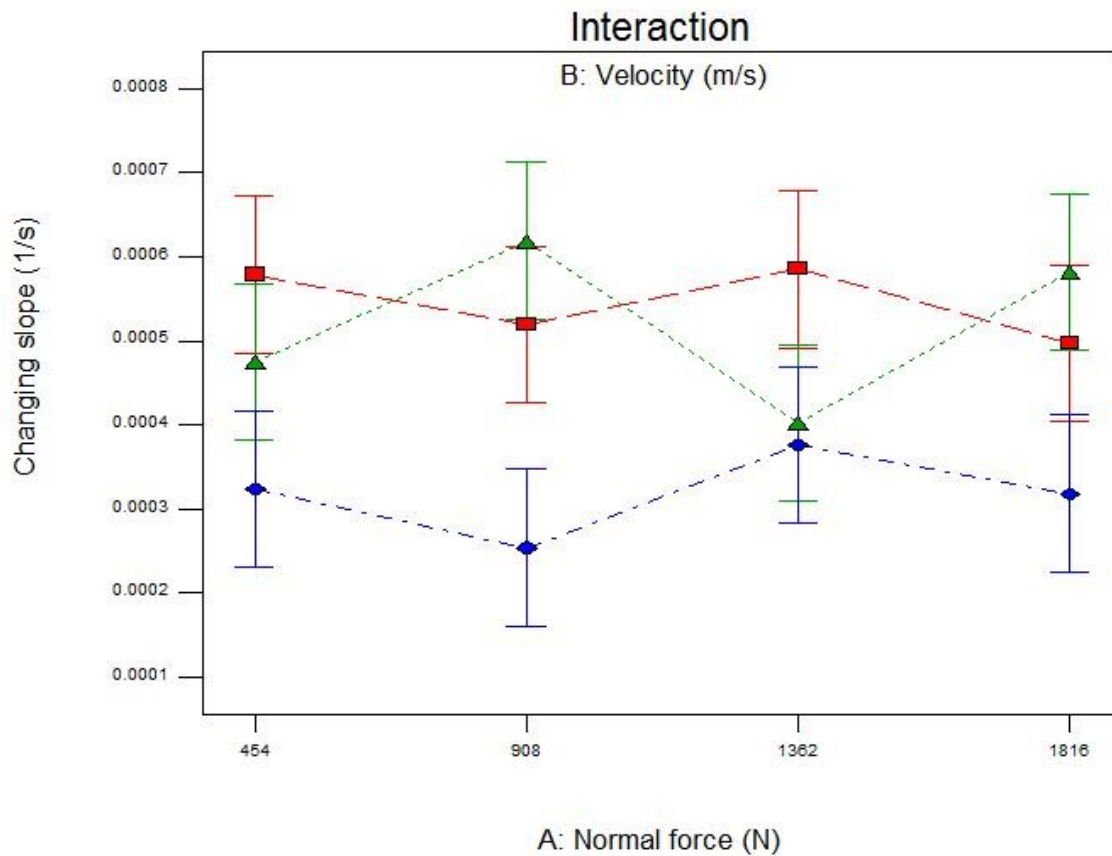


Figure 6.27: Interaction of velocity and weight on initial changing slope. *Red*, low velocity (0.47m/s); *green*, medium velocity (0.63m/s); *blue*, high velocity (0.8m/s).

6.4 Summary

In this section, the experiment results were plotted directly and analyzed with Design Expert. In analyzing with Design Expert, according to the diagnostic plots, over all the models chosen for ANOVA provide good fit for the three responses statistically.

In summary of the plotting of results and the analysis in Design Expert, velocity is certainly a significant factor that has effect on the changing of the ice friction coefficient. Whether normal force is a significant factor cannot be easily concluded from plotting of results, however, according to the statistical analysis, normal force and the interaction between normal force and velocity are considered significant.

The peak friction coefficient decreases when velocity increases, and it increases slightly when normal force increases. Increasing normal force reinforces the effect of increasing velocity on decreasing the friction coefficient. The situation of the settled friction coefficient is similar to the peak friction coefficient.

The slope of the changing friction coefficient decreases when velocity increases. The effect of normal force on the changing slope is difficult to determine due to the randomness of the data, however, the results show that increasing normal force would decrease the effect of increasing velocity on decreasing the slope of the changing friction coefficient.

The results show that: for ice friction under high normal pressure, in which the contact surface of ice is damaged by crushing, the normal force contributes to the roughening of the contact surfaces of ice rather than pressure melting effect; velocity affects the crushing at the initial stage and plays a role in the smoothing of the contact surface and may also generate heat to lubricate the surface, either by melting the ice or increasing the disordered surface layer.

Chapter 7 CONCLUSIONS

The objectives of the study were improving the knowledge of ice friction influences on vessels or structures, to study the effects of temperature, pressure, velocity and some other parameters on the ice-ice friction coefficient in relatively high pressure and velocity scenarios. This was done specifically to improve understanding of how the ice friction changes when crushing and abrading are involved.

This study discovered under relatively high interface pressure, how the roughness of the surface increases with surface deformation. Abrading and crushing were found have a significant influence on the ice-ice friction coefficient. The friction coefficient would increase under high normal pressure as crushing roughens the ice contact surfaces. When the normal pressure decreases and abrading becomes the dominant mechanism at the surfaces, the ice friction coefficient decreases as the contact surfaces are smoothed, and keeps decreasing because of the special characteristics of ice surface, until it settles in a certain range (if the duration of abrasion is long enough).

Ice friction varies due to many factors, such as temperature, normal pressure, sliding velocity, ice microstructure etc. Taking mechanisms of ice friction changing into consideration would improve the simulation and prediction of ice interaction load, i.e., during ice impact, when developing ice related numerical models.

7.1 Experimental Error

Some errors in the experiment are inevitable due to design of the research. They are discussed in this section for future reference.

Human error is a major error. When the ice cone crushed in the tests, the crane needs to be lowered manually with the descending bucket. If it is not done properly, the crane would reduce

the normal force applied on the ice surface. Additionally, in the changing weight tests, ideally, the weights should be added steadily without impulse. However, adding weight manually inevitably causes error.

There is error in experimental material. The ice plate was reused several times by smoothing after tests. The structure of the ice surface layer lost the original grain structure after it was smoothed several times. The ice chips and powder from the ice surface crushing and abrading that accumulated on the ice plate may have functioned as lubricant and caused the decrease of the ice friction coefficient in the later phase of the tests.

Due to the setup of the experiment, normal pressure is not constantly controlled as a factor; however, it provided continuous changing pressure within the expected range for analysis.

Finally, in calculations, contact area at one point of time was used as the contact area all though the test. The calculated ice friction coefficient value was a bit higher than the theoretical real value before the chosen point and a bit lower after the chosen point.

7.2 Future Study

Former research on ice friction did not consider abrading and crushing very much, because most of the tests were carried out under relatively low pressure and low velocity. This research was carried out under relatively high pressure, and all the results indicated that the phenomenon of pressure melting does exist; however, deformation of the surface influenced the ice friction coefficient to change more significantly. For ice friction, one thing that needs to be mentioned is that crushing in ice friction is different from crushing in direct compression. In ice friction, ice is crushed by normal stress combining with shear stress. If this is the case, to study the mechanical characteristic of ice as material would improve the understanding of ice friction under various circumstances. To understand the mechanical characteristic of ice as material, one of the areas of

future study would be the micro-structure of the ice. Air density, salinity and the ice forming process (maybe more) are the factors affecting the micro-structure of ice which leads to different mechanical characteristic of ice. The knowledge of deformation of the bulk material can be adapted into ice friction studies. Further experiments need to be designed to see how the special characteristics of ice behavior, together with general bulk material characteristics, affect deformation mechanisms. Additionally, when predicting ice movement or ship interaction with ice, the ice behavior is better modeled probabilistically. Because the randomness of ice behavior is inevitable, but it can be narrowed down to a certain range. A numerical model that can take all the mentioned elements into consideration would be more likely to meet the need of the industry.

REFERENCES

- AKIMOTO, K., 2009. Power games in the Arctic Ocean. *October*, **20**, pp. 12-13.
- ALBRACHT, F., REICHEL, S., WINKLER, V. and KERN, H., 2004. On the influences of friction on ice. *Materialwiss. Werkstofftech*, **35**(10/11), pp. 620-625.
- ANDERSSON, S. and NINHAM, B.W., 2003. Why ice floats on water. *Solid State Sciences*, **5**(5), pp. 683-693.
- BARNES, P., TABOR, D. and WALKER, J., 1971. The friction and creep of polycrystalline ice. *Proceedings of the Royal Society of London, .Series A. Mathematical and Physical Sciences*, **324**(1557), pp. 127-155.
- BÄURLE, L., SZABÓ, D., FAUVE, M., RHYNER, H. and SPENCER, N., 2006. Sliding friction of polyethylene on ice: tribometer measurements. *Tribology Letters*, **24**(1), pp. 77-84.
- BEEMAN, M., DURHAM, W. and KIRBY, S., 1988. Friction of ice. *Journal of Geophysical Research*, **93**(B7), pp. 7625-7633.
- BISHOP, C., PAN, D., LIU, L., MICHAELIDES, A., WANG, E. and SLATER, B., 2009. On thin ice: Surface order and disorder during pre-melting. *Faraday discussions*, **141**, pp. 277-292.
- BJERKAS, M., 2006. Ice actions on offshore structures. PhD Thesis, Norwegian University of Science and Technology, Trondheim, Norway.
- BOWDEN, F. P., and HUGHES, T. P., 1939. The mechanism of sliding on ice and snow. *Proceedings of the Royal Society of London. Series A. Mathematical and Physical Sciences*, **172**(949), PP.280-298.
- BOWDEN, F.P., 1953. Friction on snow and ice. *Proceedings of the Royal Society of London. Series A. Mathematical and Physical Sciences*, **217**(1131), pp. 462-478.

- BUHL, D., FAUVE, M. and RHYNER, H., 2001. The kinetic friction of polyethylene on snow: the influence of the snow temperature and the load. *Cold Regions Science and Technology*, **33**(2), pp. 133-140.
- CALABRESE, S., BUXTON, R. and MARSH, G., 1980. Frictional characteristics of materials sliding against ice. *Lubrication Engineering*, **36**(5), 283.
- COLBECK, S.C., 1995. Pressure melting and ice skating. *American Journal of Physics*, **63**, pp. 888-890.
- COLBECK, S.C., NAJARIAN, L. and SMITH, H., 1997. Sliding temperatures of ice skates. *American Journal of Physics*, **65**, pp. 488.
- COLE, D. M., 2000. The microstructure of ice and its influence on mechanical properties. *Engineering Fracture Mechanics*, **68**, pp. 1797-1822.
- DAGENAIS, J.S., 2014. Effects of normal force, velocity and lubrication on ice. Memorial University of Newfoundland.
- DE KONING, J.J., DE GROOT, G. and INGEN SCHENAU, G.J.V., 1991. Coordination of leg muscles during speed skating. *Journal of Biomechanics*, **24**(2), pp. 137-146.
- DUCRET, S., ZAHOUANI, H., MIDOL, A., LANTERI, P. and MATHIA, T., 2005. Friction and abrasive wear of UHMWPE sliding on ice. *Wear*, **258**(1), pp. 26-31.
- EVANS, D., NYE, J. and CHEESEMAN, K., 1976. The kinetic friction of ice. *Proceedings of the Royal Society of London. A. Mathematical and Physical Sciences*, **347**(1651), pp. 493-512.
- FREDERKING, R. and BARKER, A., 2002. Friction of sea ice on steel for condition of varying speeds, *Proc. 12th International Offshore and Polar Engineering Conference 2002*, pp. 26-31.

- FREDERKING, R. and BARKER, A., 2001. Friction of sea ice on various construction materials. PERD/CHC Report 3-49, HYD-TR-067. Ottawa, Canada.
- FORTT, A.L., SCHULSON, E.M., 2009. Velocity-dependent friction on Coulombic shear faults in ice. *Acta Mater*, 57, 4382–4390.
- GAUTIER, D.L. et al, 2009. Assessment of undiscovered oil and gas in the Arctic. *Science Magazine*, Vol. 324 no. 5931 pp. 1175-1179
- GOLECKI, I. and JACCARD, C., 1978. Intrinsic surface disorder in ice near the melting point. *Journal of Physics. C: Solid state physics*, 11(20), pp. 4229.
- HOPKINS, M., 1996. On the mesoscale interaction of lead ice and floes. *Journal of Geophysical Research*, vol. 101, No. C8, pp. 18315-18326
- ITAGAKI, K., 1987. Discussion: “Parameters affecting the kinetic friction of ice” (Akkok, M., Ettles, CM McC., and Calabrese, SJ, 1987, ASME J. Tribol., 109, pp. 552–559). *Journal of Tribology*, 109, pp. 560.
- JISKOOT, H., 2014. Dynamics of glaciers. *Encyclopedia of Earth Sciences Series*, pp. 245-256.
- JORDAAN, I., FREDERKING, R. and LI, C., 2006. Mechanics of ice compressive failure, probabilistic averaging and design load estimation, *Proceedings 18th International Symposium on Ice, IAHR'06*, pp. 223-230.
- KENNEDY, F., SCHULSON, E. and JONES, D., 2000. The friction of ice on ice at low sliding velocities. *Philosophical Magazine A*, 80(5), pp. 1093-1110.
- KIETZIG, A.M., HATZIKIRIAKOS, S.G. and ENGLEZOS, P., 2010a. Ice friction: the effect of thermal conductivity. *Journal of Glaciology*, 56(197), pp. 473-479.

- KIETZIG, A.M., HATZIKIRIAKOS, S.G. and ENGLEZOS, P., 2010b. Physics of ice friction. *Journal of Applied Physics*, **107**(8), pp. 081101-081101-15.
- KIETZIG, A.M., HATZIKIRIAKOS, S.G. and ENGLEZOS, P., 2009. Ice friction: The effects of surface roughness, structure, and hydrophobicity. *Journal of Applied Physics*, **106**(2), pp. 024303-024303-7.
- KOZLOV, I. and SHUGAI, A., 1991. Experimental study of high-speed friction on ice. *Fluid dynamics*, **26**(1), pp. 145-147.
- LEHTOVAARA, A., 1987. Influence of vibration on the kinetic friction between plastics and ice. *Wear*, **115**(1), pp. 131-138.
- LI, Y. and SOMORJAI, G.A., 2007. Surface premelting of ice. *The Journal of Physical Chemistry C*, **111**(27), pp. 9631-9637.
- LIANG, H., MARTIN, J. and MOGNE, T., 2003. Experimental investigation of friction on low-temperature ice. *Acta materialia*, **51**(9), pp. 2639-2646.
- LISHMAN, B., SAMMONDS, P., FELTHAM, D. and WILCHINSKY, A., 2009. The rate- and state- dependence of sea ice friction. POAC 09-66.
- LISHMAN, B., SAMMONDS, P., FELTHAM, D. and WILCHINSKY, A., 2010. Sea ice friction and arctic sea ice dynamics. *Proceedings of the HYDRALAB III Joint User Meeting, Hannover*.
- MAENO, N., ARAKAWA, M., YASUTOME, A., MIZUKAMI, N. and KANAZAWA, S., 2003. Ice-ice friction measurements and water lubrication and adhesion-shear mechanisms. *Canadian Journal of Physics*, **81**(1-2), pp. 241-249.
- MAENO, N. and ARAKAWA, M., 2004. Adhesion shear theory of ice friction at low sliding velocities, combined with ice sintering. *Journal of Applied Physics*, **95**(1), pp. 134-139.

- MANUEL, A., 2012. STePS2: Manual of laboratory procedures. Memorial University of Newfoundland: STePS2, St. John's, NL.
- MARMO, B.A., BLACKFORD, J.R. and JEFFREE, C.E., 2005. Ice friction, wear features and their dependence on sliding velocity and temperature. *Journal of Glaciology*, **51**(174), pp. 391-398.
- MIZUKAMI, N. and MAENO, N., 2000. Normal stress dependence of ice-ice friction coefficients. *Seppyo*, **62**(6), pp. 515-521.
- MONTAGNAT, M. and SCHULSON, E.M., 2003. On friction and surface cracking during sliding of ice on ice. *Journal of Glaciology*, **49**(166), pp. 391-396.
- OKSANEN, P. and KEINONEN, J., 1982. The mechanism of friction of ice. *Wear*, **78**(3), pp. 315-324.
- ROSENBERG, R., 2005. Why is ice slippery? *Physics Today*, **58**, pp. 50.
- SCHULSON, E. and FORTT, A., 2012. Friction of ice on ice. *Journal of Geophysical Research*, Vol. 117, B12204
- SLOTFELDT-ELLINGSEN, D. and TORGENSEN, L., 2000. Water on ice; influence on friction. *Journal of Physics D: Applied Physics*, **16**(9), pp. 1715.
- Strategic importance of the Arctic in U.S. Policy. 2009. *Special Hearing*. 111-259
- STRAUSKY, H., KRENN, J., LEITNER, A. and AUSSENEK, F., 1998. Sliding plastics on ice: fluorescence spectroscopic studies on interfacial water layers in the μm thickness regime. *Applied Physics B: Lasers and Optics*, **66**(5), pp. 599-602.
- SUKHORUKOV, S., 2013. Ice-ice and ice-steel friction in field and in laboratory. PhD Thesis, Norwegian University of Science and Technology, Trondheim, Norway.

TAN, X., RISKI, K. and MOAN, T., 2014. Effect of dynamic bending of level ice on ship's continuous-mode icebreaking. *Cold Regions Science and Technology*, 106-107, 82-95

TANAKA, H., 2001. Hydrogen bonds between water molecules: thermal expansivity of ice and water. *Journal of Molecular Liquids*, **90**(1-3), pp. 323-332.

TIMCO and WEEKS, 2010. A review of the engineering properties of sea ice. *Cold Regions Science and Technology*, 60, pp. 107-129.

TUSIMA, K.T., 1977. Friction of a steel ball on a single crystal of ice. *Journal of Glaciological*, **19**(81), pp.225-235.

TUSIMA, K., 2011. Adhesion theory for low friction on ice. *University of Toyama, Japan*.

WEBER, T.A. and STILLINGER, F.H., 1984. Pressure melting of ice. *The Journal of chemical physics*, **80**, pp. 438.

YASUTOME, A., ARAKAWA, M. and MAENO, N., 1999. Measurements of ice-ice friction coefficients. *Seppyō*, **61**(6), pp. 437-443.